Università degli Studi di Padova

Dipartimento dei Beni Culturali: Archeologia,
Storia dell'Arte, del Cinema e della Musica

Master's degree in ARCHAEOLOGICAL SCIENCES

Curriculum in
APPLIED SCIENCES TO CULTURAL HERITAGE MATERIALS AND SITES

# Tracing the provenance of the amphorae from underwater sites by archaeometric analysis: The case of Torre Santa Sabina (Apulia, southern Italy)

Supervisor: Prof. Lara Maritan
Co-supervisor: Dott. Maria Emanuela Mascaro

Master Candidate
Hasti Pezeshkanjalili
2039383

ACADEMIC YEAR 2023/2024

# List of content

# Acknowledgment

I would like to express my sincere gratitude to my supervisors, Professor Lara Maritan and Maria Emanuela Mascaro, for their invaluable guidance, encouragement, and patience. Their unwavering support has given me the incredible opportunity to develop my skills and knowledge throughout this thesis. Working alongside them has been an inspiring and enriching experience, for which I am genuinely thankful.

I would also like to extend my heartfelt thanks to my wonderful parents, Shohreh and Fattah, my amazing and supportive partner, Sina, and my beloved family and friends, who have always been there for me, supporting and believing in me.

# Abstract

This thesis deals with the archaeometric study of ceramic materials and in particular of a set of amphorae, from the underwater archaeological site of Torre Santa Sabina (Apulia region, Southern Italy), dating back to the Republican period (late 2nd century BCE).

The main aim of this study is to define the provenance of the amphorae found in the underwater shipwrecks and to verify their possible local origin. For this purpose, the amphorae fragments form Torre Santa Sabina underwater site was compared with a set of amphorae fragments recovered from the ancient local production centers of Apani and Giancola (defined as reference groups).

Petrographic, mineralogical, and chemical analyses were carried out on 19 samples from Torre Santa Sabina and 11 samples from Apani and Giancola. All the specimens were analyzed by polarized-light microscopy, X-ray Powder Diffraction (XRPD), X-ray fluorescence (XRF) and Scanning Electron Microscope (SEM). The polarized-light microscope analysis provides information on the textural features of the ceramic bodies and the nature and type of inclusions allowing the characterization of the different fabrics. The underwater samples showed heterogeneity both in terms of amphora forms and the textural characteristics of the ceramic bodies. Overall, two macro-groups were identified: one characterized by groundmass of a more carbonate nature and the other one rich in the terrigenous component. This subdivision is also reflected by the mineralogical and chemical composition of the potsherds. XRPD analysis was used to determine the mineralogical composition of the ceramic bodies. Quartz, K-feldspar, muscovite/illite, plagioclase, hematite, pyroxenes, and calcite are the main phases detected; gehlenite was detected in some samples from Apani and Giancola, while sulfur-based mineral phases, as pyrite, were detected only in underwater samples as post-depositional alteration phases. XRF results showed a fairly similar chemical composition among the underwater samples, although they represent amphorae of different types. Some trace elements, like sulfur, show greater variability as they are linked to the precipitation of post-depositional secondary phases, especially pyrite ($FeS_2$). A more in-depth observation by SEM was performed on some representative samples, allowing us to better analyze the microstructural features of the ceramic bodies and also confirm the occurrence of pyrite in the underwater samples.

The results revealed compositional similarities between marine and terrestrial fragments suggesting Apani and Giancola as potential production centers of some of the underwater amphorae found on the TSS seabed. In particular, the “Ovoidal Adriatic” type shows the greatest similarity to the products from these local centers, mainly for grain-size distribution of inclusions and the presence of fossil traces. However, a few fragments differ significantly from the others in both mineral-petrographic and chemical characteristics, indicating different places of origin in Mediterranean areas such as Italian Tyrrhenian side (probably Campania region) and North Africa. These outcomes shed light on the nature of the submerged cargo and enhance our knowledge of the site and its role in ancient maritime trade routes across the Mediterranean.

# Riassunto

Questa tesi riguarda lo studio archeometrico dei materiali ceramici e in particolare delle anfore provenienti dal sito archeologico subacqueo di Torre Santa Sabina (TSS) in Puglia, Italia sud-orienatle, risalente al periodo repubblicano (fine II secolo a.C.).

L'obiettivo principale di questo studio è quello di definire la provenienza dei campioni rinvenuti nel contesto subacqueo ed in particolare di andare a esplorare l'ipotesi di una loro possibile produzione locale. A tal fine, è stato effettuato un confronto con frammenti di anfore recuperati dai centri di produzione di Apani e Giancola (definendo quindi i campioni da tali contesti come a formare i rispettivi come gruppi di riferimento dei due siti produttivi). 19 campioni ceramici rinvenuti dal sito subacqueo di Torre Santa Sabina e 11 campioni dai siti di Apani e Giancola sono stati sottoposti ad uno studio multi analitico, tramite analisi petrografica, mineralogica e geochimica utilizzando la microscopia a luce polarizzata, la diffrazione a raggi X delle polveri (XRPD), la fluorescenza ai raggi X (XRF) e il microscopio elettronico a scansione (SEM). L'analisi al microscopio a luce polarizzata ha fornito informazioni sulle caratteristiche tessiturali dei corpi ceramici e sulla natura e il tipo di inclusi, permettendo di caratterizzare i diversi impasti. I campioni subacquei mostrano eterogeneità sia in termini di forme delle anfore sia di tessitura dei corpi ceramici. Complessivamente, sono stati identificati due macro-gruppi basati sulle caratteristiche della matrice, uno caratterizzato da una matrice più carbonatica, contenente anche microfossili calcarei, e l'altro con una matrice terrigena ricca di ferro. L'analisi XRPD è stata utilizzata per determinare le fasi mineralogiche presenti nei campioni, che sono risultate essere date da quarzo, K-feldspato, muscovite/illite, plagioclasio, ematite, pirosseno e calcite; la gehlenite è stata rilevata solo in alcuni campioni di Apani e Giancola, mentre fasi minerali a base di zolfo, come la pirite, sono presenti solo nei campioni provenienti dal contesto subacqueo. L'analisi tramite XRF ha mostrato una composizione chimica abbastanza simile dei campioni subacquei, sebbene rappresentino anfore di diversi tipi. Alcuni elementi in traccia, come lo zolfo, mostrano una maggiore variabilità poiché sono legati alla precipitazione di fasi secondarie post-deposizionali, come la pirite ($FeS_2$). Un'osservazione più approfondita in microscopia elettronica, eseguita solo su alcuni campioni rappresentativi, ha permesso di analizzare meglio le caratteristiche microstrutturali dei corpi ceramici confermando anche la presenza di pirite nei campioni subacquei.

I risultati hanno rivelato somiglianze composizionali tra frammenti marini e terrestri suggerendo Apani e Giancola come potenziali centri di produzione di alcune delle anfore subacquee trovate sul fondale di Torre Santa Sabina. In particolare, le anfore di tipo “Ovoidale Adriatico” mostrano la maggiore affinità con i prodotti di questi due centri produttivi principalmente per la distribuzione granulometrica delle inclusioni e la presenza di tracce fossili. Tuttavia, alcuni frammenti differiscono significativamente dagli altri sia per caratteristiche minero-petrografiche sia chimiche, indicando origini da diverse aree del Mediterraneo, come il versante tirrenico italiano (probabilmente regione Campania) e il Nord Africa. Questi risultati fanno luce sulla natura del carico sommerso e migliorano la nostra conoscenza del sito e del suo ruolo nelle antiche rotte commerciali marittime attraverso il Mediterraneo.

# 1 Introduction

Seas are among the most enigmatic environments on Earth where life begins, and in their depths hold even more wonders than we imagine. These environments hide a huge quantity of cultural heritage that can help us trace the development of human civilization, for example, by reconstructing the maritime trade routes of our past. After a shipwreck, most of the ship's materials and equipment sink to the seabed, becoming partly or fully buried by sand and on the remains of the ships themselves. Despite the strong hydrodynamics that characterize the maritime environment, ceramic materials are strong enough to be the best-preserved underwater remains (Ruppe, Barstad 2002).

This makes them the most abundant materials found in archaeological excavations worldwide. Therefore, ceramic artifacts are considered important sources of information of the archaeological context to which they belong, (Gliozzo, 2020) especially in underwater contexts. Ceramics are the result of clay processing through many actions, from the selection of the raw materials to the firing of the final object (Maritan, 2024). The study of ancient pottery, through the characterization of ceramic body composition and mineralogical and chemical alterations that ceramics undergo during their life cycle, provides us with important data on raw material, provenance and production technologies. (Maggetti, 1982; Maritan, 2024).

Among different types of ceramics that can still be found near ancient submerged wrecks, amphorae are often the most abundant, since they were used to transport and store a large variety of foodstuffs and other goods, such as wine and oil, in a large scale of commercial activities by sea, especially during the Roman Empire when the economy and trades became more complex (Opdebeeck, 2005).

In this context, an archaeometric investigation of amphora’s fragments from the underwater archaeological site of Torre Santa Sabina (Camerini Bay, province of Brindisi, Apulia region, south-eastern Italy) and from the terrestrial sites of Apani and Giancola (Apulia region, south-eastern Italy) was carried out within this thesis projects. Optical and spectroscopic techniques were used to analyze the petrographic, mineralogical, and geochemical features of their ceramic bodies in order to characterize and classify the samples. The archaeometric investigation of pottery from these sites highlights important traces of cultural and technological identity, supporting the

interpretation of maritime trade dynamics and helping in the further understanding of the ancient seafaring history of the bay.

# 2 Aims and scope

The main purpose of this study is to define the provenance of the underwater samples of Torre Santa Sabina and verify a possible local production by detecting the compositional correspondence with sherds found in Apani and Giancola sites. From the moment of their fabrication to the time of their discovery during archaeological excavations (underwater at Torre Santa Sabina, and in land at Apani and Giancola) after centuries, ceramic materials underwent various microstructural, chemical, and mineralogical transformations. These transformations are the result of a combination of various factors such as the primary clay composition, the firing conditions, the intended use, and the chemical and physical characteristics of the environment in which they were buried for a long time (Maritan, 2020, 2024). Therefore, in the study of ancient pottery, the analysis of the paste composition and the alterations phenomena offers important insights into its provenance.

Comparison with reference ceramic groups, typical of particular workshops or geographical regions, helps to determine the origin of the ceramic samples under examination, finding compositional and typological similarities through the study of discarded ceramic materials that match unique clay sources, playing an essential role in revealing the provenance of the pottery (Maritan, 2024).

For underwater ceramics, especially when they come from diverse discovery contexts with a variety of forms/types (and in some cases also with specific stamps), comparing them with 'terrestrial' samples from production centers of the same type, also from those regionally occurring with respect to the shipwreck location is essential to address the issue of provenance. This comparison covers both scientific and archaeological perspectives including typological and petrographic observations, geochemical and mineralogical analysis and the study of the geological characteristics of the territory of interest, in order to identify outcrops that could potentially be exploited for the supply of clay raw materials.

Moreover, the discrimination of microstructural and compositional changes occurring in submerged ceramics due to interactions with the underwater environment from those that are

indicators of production technology or provenance is a useful tool to properly tune the archaeometric data avoiding misinterpretations.

# 3 Historical and archaeological background

## 3.1 The underwater site of Torre Santa Sabina

The site of Torre Santa Sabina (40°45'26"N 17°42'13" E), located in the Camerini Bay in the province of Brindisi (Apulia region, south-eastern Italy), is one of the most important underwater archaeological sites in the Mediterranean. Since the early 1970s, underwater excavation campaigns brought to light important archaeological evidence, including several shipwrecks and a large quantity of fired clay wares relevant in terms of types, shapes, and chronology.

Figure 1. – Iconic tower of Torre Santa Sabina

This, linked to the stratigraphy of the seabed, confirms a long history of continuous occupation from the Bronze Age to the Medieval period (Auriemma, 2014), documenting the intense life of the harbor and its relations to the surrounding area and inland centers.

Over the centuries, the site of Torre Santa Sabina (hereafter TSS) has witnessed exchanges between different peoples, and its seabed is now characterized by a precious stratigraphic sequence formed by materials from wrecked ships' cargoes and equipment on board, along with other materials from port dumping activities. This makes TSS an exceptional archaeological deposit offering important insights into ancient maritime networks in the Mediterranean.

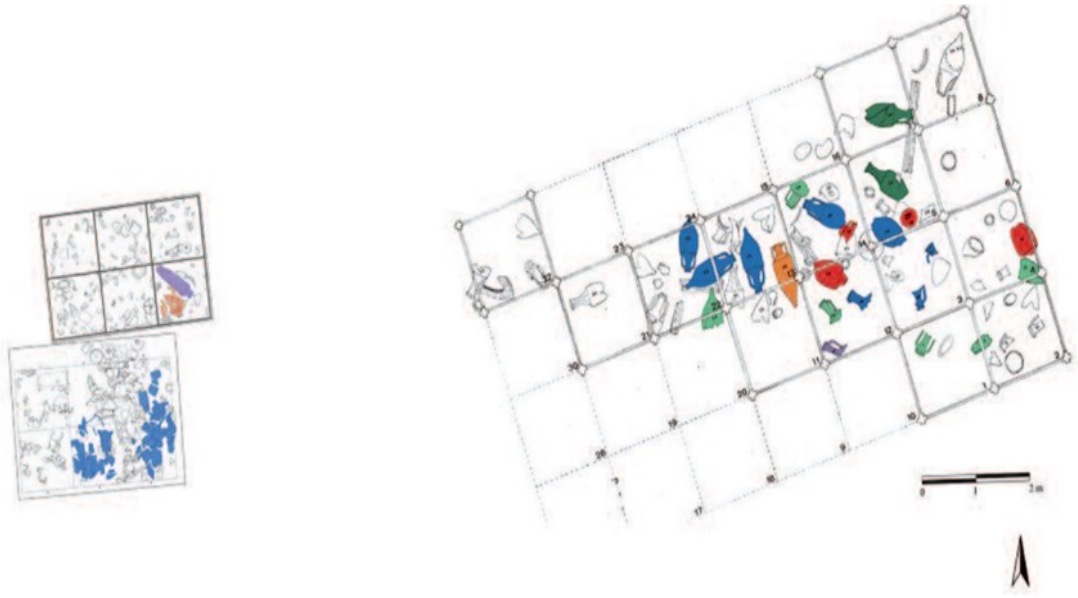

Figure 2. — The overall plan of the interventions in 1987, 2007, and 2009. The late republican load (Torre S. Sabina 4) (source: Auriemma, 2014).

In the rich submerged deposit identified as Area B, located at the foot of the western rocky bank close to the tower of Santa Sabina (Figure 1.), a large quantity of transport containers, dated, on the basis of the ceramic shapes and types, between the end of the Archaic period and Late Antiquity (late 6th century BCE - 5th-6th century CE), were found. The majority of them were attributed to Adriatic and Tyrrhenian production and, to a lesser extent, to the Aegean and African ones. From 1972 to 1983 systematic research carried out on TSS seabed led to the discovery of numerous ceramic artifacts heterogeneous in type, chronology (4th to 1st century BCE), and form, supporting the hypothesis of the existence of several different shipwrecks in the bay (Antonazzo, 2014).

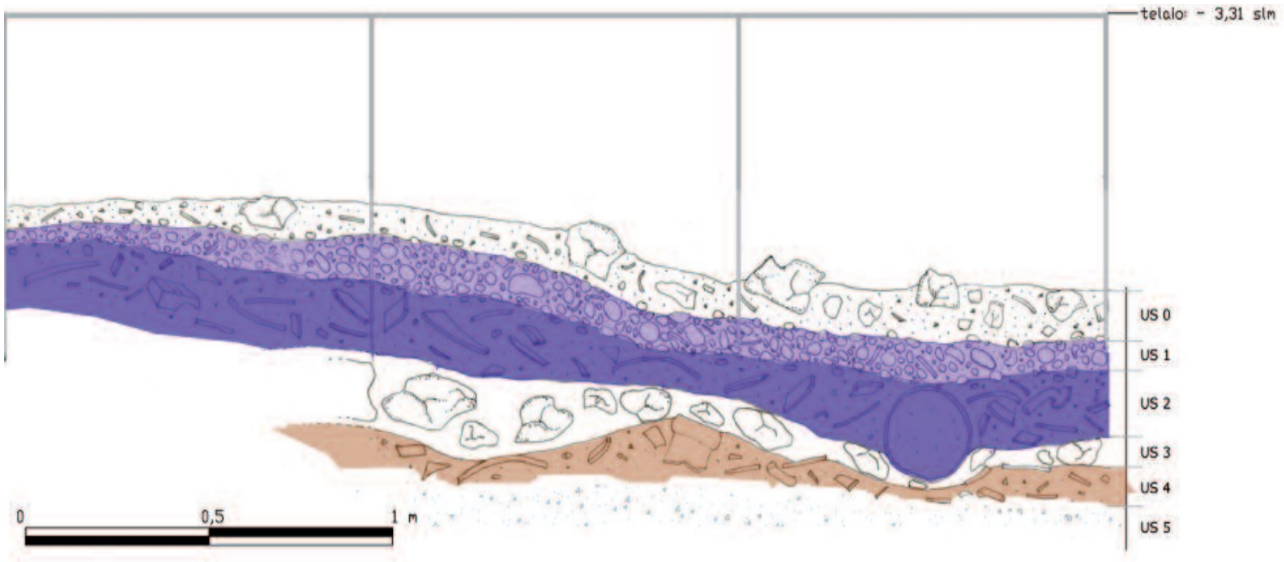


Figure 3. – The stratigraphic units of area B (source: Auriemma, 2014)

Area B was divided during the archaeological excavation in two main zone identified as TSS 3 and TSS 4: all the fragments analyzed in this study come from the area TSS4 (Figure 2.), characterized by a stratified deposit of ship cargo remains, where five different stratigraphic units, consisting of several anthropogenic and natural layers, were individuated during the excavation campaigns carried out between 2007 and 2012. A conspicuous number of wine and oil amphorae, dated back to the Republican period were found in the stratigraphic unit US 2 (Figure 3.) which, despite being scrambled and heavily disrupted by powerful swells (Figure 4.), appeared to be in place at the time of its discovery (Auriemma, 2014).

Figure 4. – Picture of crushed and scrambled fragments on the seabed. (source: Auriemma, 2014)

## 3.2 GIANCOLA AND APANI

The archaeological sites of Giancola (GC) (40°40'47"N 17°52'19" E) and Apani (AP) are respectively about 13 and 16 kilometers (40°41'33"N 17°50'03" E) from Torre S. Sabina, (Figure 5.) and they are very close each other, being about 3 kilometers from each other.

Any production center should be established in a place with availability of raw materials for ceramic production and also needs potters capable of developing good production technology (Maritan, 2024). These factors certainly apply to Apani and Giancola, both were well-known production centers in the region, from where ceramics were exchanged or traded in consumption areas that were sometimes very distant (Manacorda, & Pallecchi, 2012).

The archaeological site of Giancola underwent excavation during the 1980s where kilns alongside a mound of production waste, were revealed creating a data-rich archive which allowed an in-depth examination considering various aspects such as stratigraphy, typology, epigraphy, and archaeometry (Manacorda & Pallecchi, 2012).

During the 2nd and 1st centuries B.C. the kilns in Apani and Giancola were utilized to manufacture both oil and wine amphorae on a large scale across the Mediterranean (Carre et al., 2014; Manacorda & Pallecchi, 2012). During the third quarter of the 2nd century BCE, trade towards the West started from these sites, (Benquet & Capelli, 2018) which played a crucial role

in the economic and social history of Brindisi's agricultural landscape during the late Republican age and the early years of the Empire (Manacorda, Pallecchi, 2012).


Figure 5. – Google Earth photo of Apulia region with the location of the archeological sites of Torre Santa Sabina, Apani e Giancola.

# 4 Geological framework

Understanding local and regional geology is crucial for petrographic studies aimed at determining the provenance of ceramics.

Geological maps are particularly valuable as they show the geographic distribution of various bedrock types and more recent sedimentary deposits like alluvium, talus, and glacial drift. The geological maps indicate specific lithologies available in the hydrographic basin or in general in the area of an archaeological site and its nearby. They typically show the extent of major stratigraphic or lithological units using distinct colors or shading and the map's legend usually offers detailed descriptions of the lithologies within these units (Quinn, 2022).

Raw materials, like clay and temper, are typically sourced from nearby production sites, reflecting the local geology (Figure 6.). These materials usually come from alluvial deposits or outcrops located within a range of 7 to 10 kilometers from the production center. To determine whether ceramic sherds found at archaeological sites were locally made or exchanged/imported, their petrographic composition should be compared with local geological materials. Additionally, the presence of temper from non-local rocks, possibly recycled from ancient objects, must be considered (Maritan, 2024; Maritan, 2021). These inclusions can mislead provenance studies unless they are correctly identified. It is also important to consider that recent geomorphological processes and changes in the land may have altered the availability of raw material sources that ancient potters once utilized. Therefore, careful analysis and comparison with the local geological context are essential to accurately determine the origins of archaeological ceramics (Maritan, 2024).

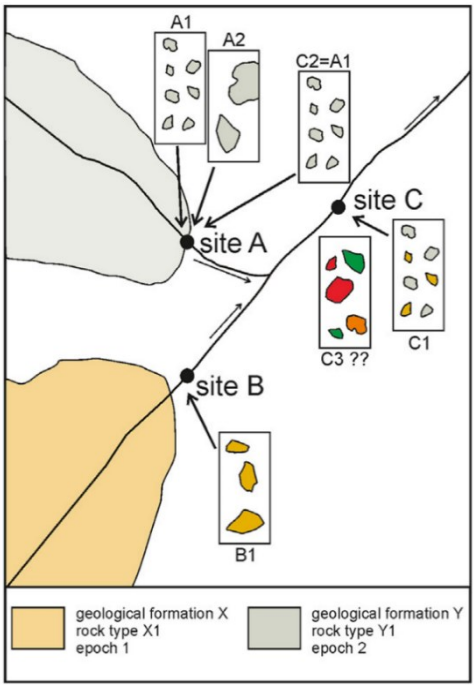


Figure 6. – Schematic representation of the principle of source localization of inclusions (source: Maritan, 2024)

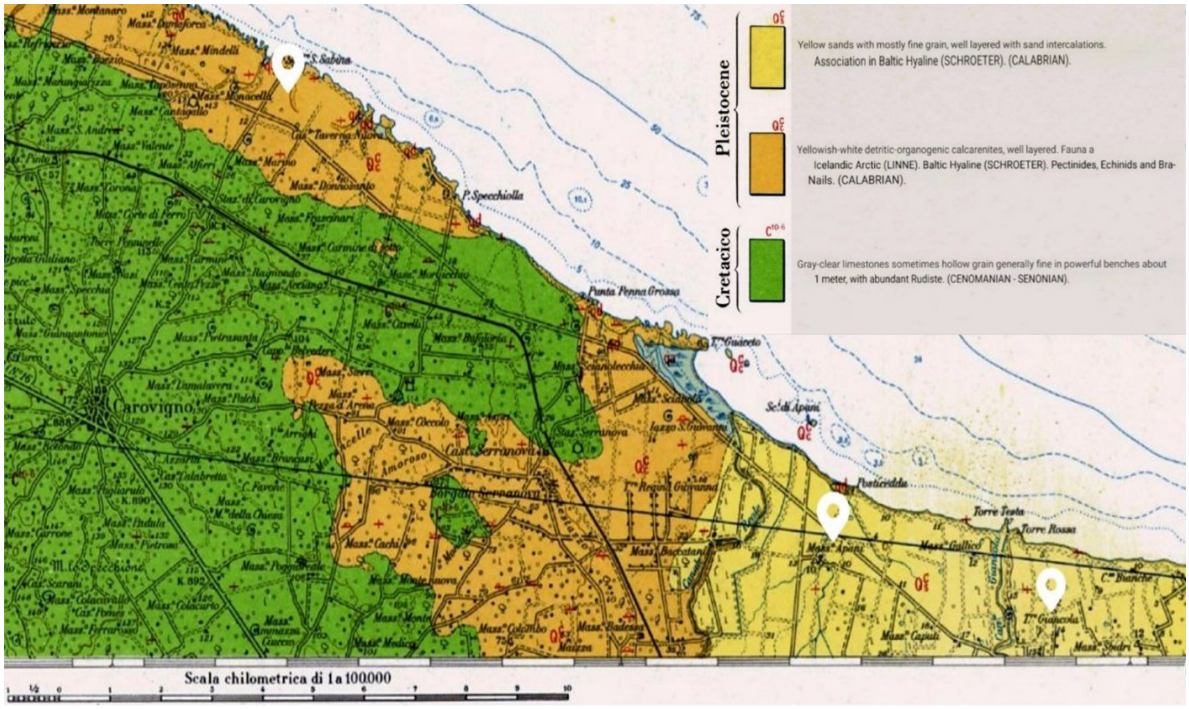


Figure 7. – Geological map of the understudy region taken from the Geological map 1.100.000 of Italy, sheet Ostuni (Source: https://sgi.isprambiente.it/geologia100k/mostra_foglio.aspx?numero_foglio=191).

As mentioned before Apani and Giancola are approximately 3 kilometers apart from each other, but they both insist on the same geological unit, so the raw materials used in their productions likely originated from a similar source. In this area, formations consist of sands and conglomerates dated to the Pleistocene and specifically to the Calabrian, with sand deposits as primary with respect to the conglomerates. At the base of this formation, yellow-grayish marly clays form a level, as described by Vezzani 1968. These argillaceous deposits contain various types of foraminifera and those of the area of Giancola are particularly rich in *Hyalinea islandica* (Vezzani 1968). The formation of the Torre Santa Sabina area consists of detrital and organogenic bench-type limestones from the Pleistocene (Calabrian) rich in fossils (Figure 7.).

In general, Knowledge of the geological context together with the study of the composition of ceramic samples help in the identification of the areas of supply of clayey raw materials and the economic connections between ceramic workshops and the surrounding georesources.

# 5 Materials and methods

## 5.1 MATERIALS

For this study, 30 ceramic samples sourced from the Apulia region in southeastern Italy were selected for analysis. While various types of ceramic containers were excavated from the archeological sites, this thesis focuses only on amphora.

Amphorae are a unique type of ceramic container with significant variation in terms of size, shape and decoration. They typically have a tall cylindrical body, two handles and a narrow neck with a stopper or lid. These vessels originated in antiquity and were extensively utilized for the storage and transport of foodstuff such as oil, wine, pitch and dried fish. The design of amphorae was highly functional: the pointed or rounded bottom facilitated stacking during maritime transport, while the handles and narrow neck enabled efficient handling and pouring. Over time, the morphology of amphorae evolved, becoming more elongated to enhance their storage and handling efficiency on ships. This evolution in form underscores the adaptability of ceramic design to meet the practical demands of ancient trade and transport (Johnston & Grace, 2015; Oleson, 2008). Although there were various techniques and styles among different production centers and periods, also in relations to the type of content they were produced for, the common method for crafting amphorae was wheel-throwing.

For this study, 19 samples were selected from the amphorae belonging to ship cargo TSS4, related to the Republican deposit and situated at the US2 level of the stratigraphic sequence in area B of the underwater site of Torre Santa Sabina. The materials in this area are extremely heterogeneous in terms of shape, manufacturing and chronology (Auriemma, 2014).

Moreover, in addition to the samples from the underwater site, 11 samples were selected from Apani and Giancola (7 and 4 respectively) considered potential production sites.

The samples considered in this work do not show any evidence of decorative elements, however, there are traces of stamps on 5 samples from Apani, 2 samples from Giancola and 2 samples from Torre Santa Sabina. Stamps on amphorae were usually impressed on their handles before firing and served as control marks according to their geographical class and particular size.

These stamps included the name of the potter or manufacturer, which can typically indicate the origin of the production center, and a dating authority that in some cases can provide valuable chronological data for archaeological studies (Palazzo, 1989; Johnston & Grace, 2015).

Identified stamps among samples here studied are: *ANINIAS, C.VEHILI, MENECRATES, VEHILI* and *ANINIANA* on the Apani's amphorae; *APELLAE* and *DIOCLES* on those from Giancola; *FALLI* and *VEHILI* on those recovered underwater from TSS.

The typological classification of underwater fragments includes: 14 samples of Ovoidal Adriatic (Brindisi) type, 9 samples of Apani I/Giancola II type, 5 samples of Lamboglia 2 type, one African type and one for Dressel 2-4 type. All the samples examined in this study are listed in Table 1, where the sample ID (consisting of the initials of the finding site and the inventory number), the photo of the original fragment, the type, the drawing of the shape and the stamp (when present) are reported.

| Label | Photographs of the sampled amphorae | Type | Drawing | Stamp |
|---|---|---|---|---|
| AP-1 | 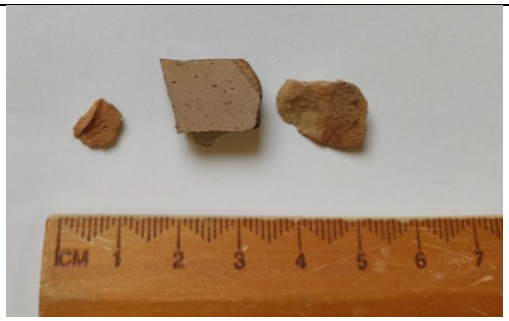 | Ovoidal Adriatic (Brindisi) |  | *ANINIAS* |
| AP-2 |  | Apani I/Giancola II | 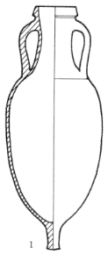 | *C.VEHILI* |

| | | | | |
|---|---|---|---|---|
| AP-3 |  | Apani I/Giancola II | 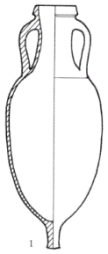 | - |
| AP-4 |  | Apani I/Giancola II | 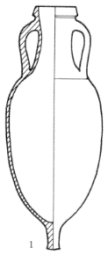 | - |
| AP-5 |  | Ovoidal Adriatic (Brindisi) | 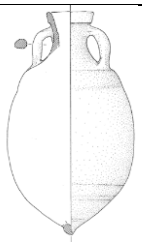 | *MENECRATES* |
| AP-6 |  | Ovoidal Adriatic (Brindisi) | 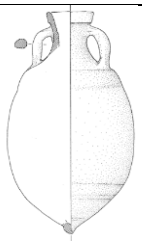 | *VEHILI* |

| | | | | |
|---|---|---|---|---|
| AP-7 |  | Ovoidal Adriatic (Brindisi) | 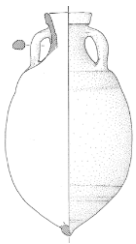 | *ANINIANA* |
| GC-7 | 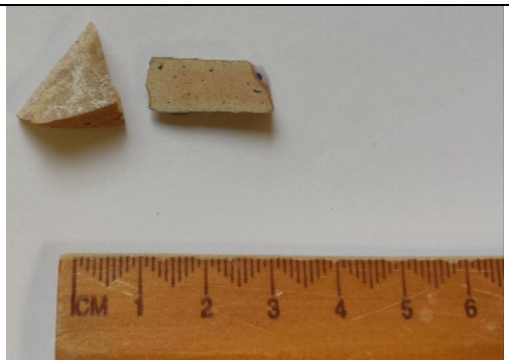 | Ovoidal Adriatic (Brindisi) |  | - |
| GC-8 | 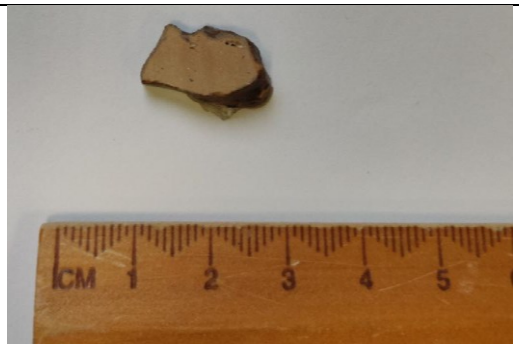 | Ovoidal Adriatic (Brindisi) | 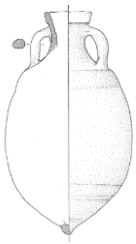 | - |
| GC-9 | 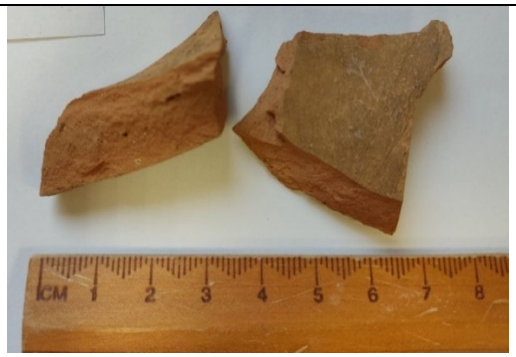 | Ovoidal Adriatic (Brindisi) | 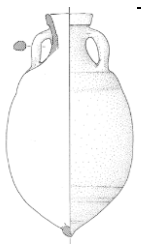 | *APELLAE* |

| | | | | |
|---|---|---|---|---|
| GC-10 | 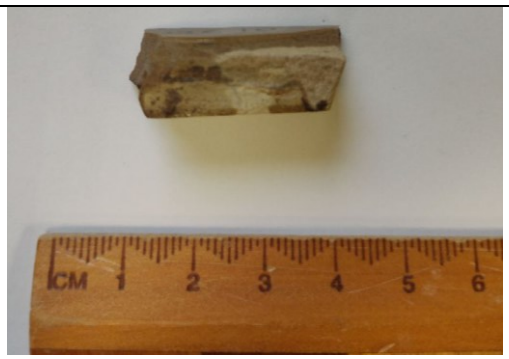 | Ovoidal Adriatic (Brindisi) | 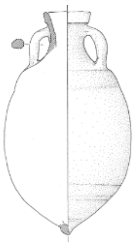 | *DIOCLES* |
| TSS-1 |  | Apani I/Giancola II | 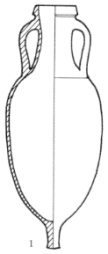 | - |
| TSS-3 |  | Apani I/Giancola II | 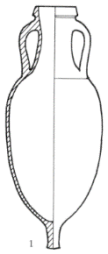 | - |
| TSS-4 |  | Apani I/Giancola II | 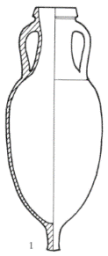 | - |

| | | | | |
|---|---|---|---|---|
| TSS-5 |  | Apani I/Giancola II | 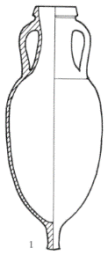 | - |
| TSS-6 |  | Apani I/Giancola II | 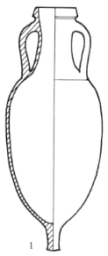 | - |
| TSS-8 |  | Apani I/Giancola II | 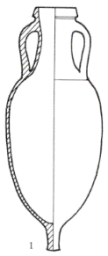 | - |
| TSS-11 |  | Lamboglia2 | 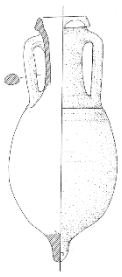 | - |

| | | | | |
|---|---|---|---|---|
| TSS-12 | 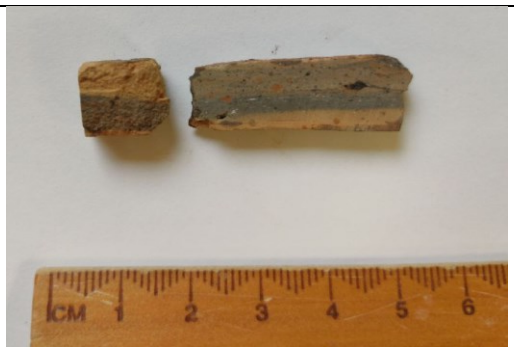 | Lamboglia2 | 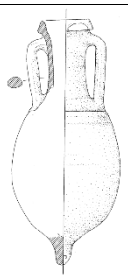 | - |
| TSS-13 |  | Lamboglia2 | 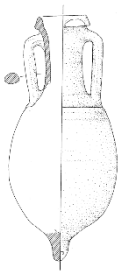 | - |
| TSS-14 |  | Lamboglia2 | 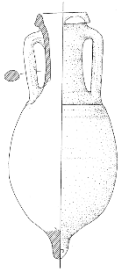 | *FALLI* |
| TSS-15 |  | Lamboglia2 | 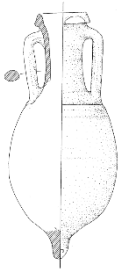 | - |

| | | | | |
|---|---|---|---|---|
| TSS-19 |  | Dressel2-4 | 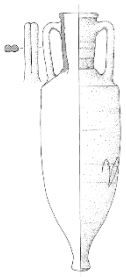 | - |
| TSS-23 |  | Ovoidal Adriatic (Brindisi) |  | *VEHILI* |
| TSS-24 |  | African |  | - |
| TSS-27 | 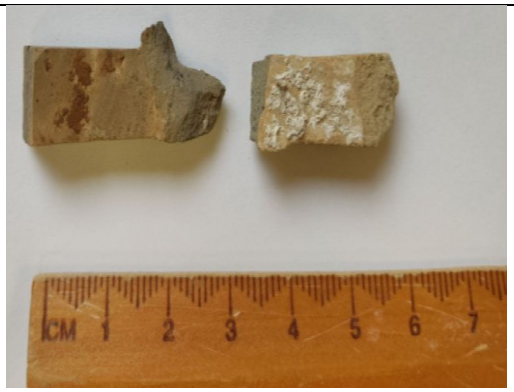 | Ovoidal Adriatic (Brindisi) | 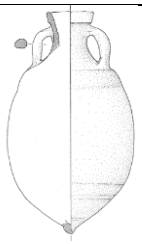 | - |

| | | | | |
|---|---|---|---|---|
| TSS-28 | 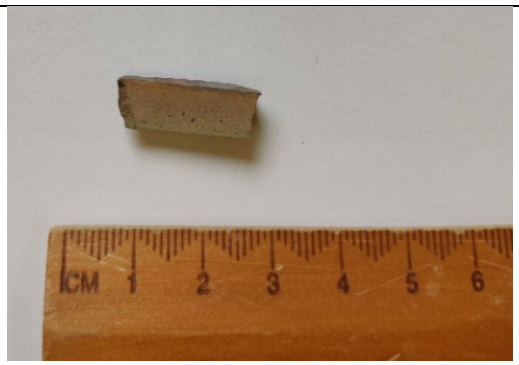 | Ovoidal Adriatic (Brindisi) | 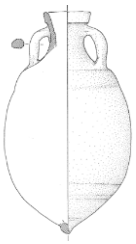 | - |
| TSS-29 |  | Ovoidal Adriatic (Brindisi) | 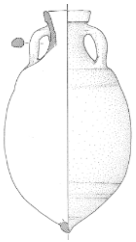 | - |
| TSS-30 | 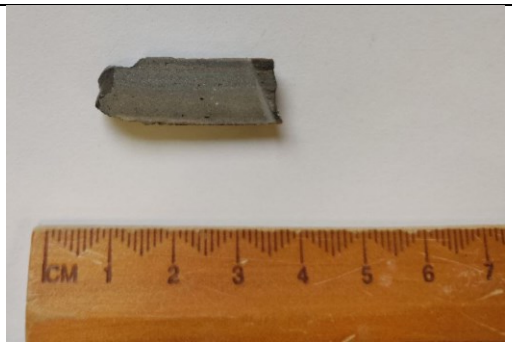 | Ovoidal Adriatic (Brindisi) | 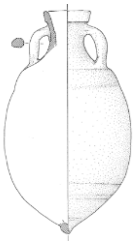 | - |
| TSS-31 |  | Ovoidal Adriatic (Brindisi) | 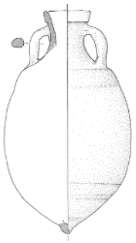 | - |

Table 1. - list of the analyzed samples with reported the relative photograph, type, drawing and stamp when present.

Lamboglia 2 amphorae were produced along the Adriatic coasts of Italy from the late 2nd century to the late 1st century BCE and primarily used for transporting wine and/or oil. Ovoidal Adriatic (Brindisi) amphora type originated from the southern Adriatic coasts of Italy, mainly for transporting oil from the late 2nd century to the mid-1st century BCE. African vessels were produced in Tunisian area for transporting oil and fish sauce and their circulation is attested from the 3rd to the early 5th century CE. Dressel 2-4 type were in use from the late 1st century BCE to the 1st century CE, produced in Tyrrhenian Italy, northern Italy, Istria and Apulia, primarily for transporting wine (Toniolo, 1995). Finaly type Apani I/Giancola II type, originating from the Adriatic coast of southern Italy, was produced between the second half of the 2nd century BCE and the mid-1st century BCE and primarily used for transporting wine (Palazzo, 1989).

All 30 samples were analyzed in the laboratories of the Department of Geosciences in Padova. A sample from each fragment was cut to prepare thin sections, with a portion powdered for XRPD and XRF analysis. At the same time, the residual fragment was set aside for macroscopic examination of the ceramic cross-section.

## 5.2 ANALYTICAL TECHNIQUES

The complete reading of a ceramic material consists of a series of different moments, each one consisting of specific analytical procedures aimed at revealing all the information that an artefact has accumulated throughout its history, from the extraction of the clay to the burial of the finished object. Since the late 19th century, numerous studies employed scientific methods, such as petrographic and chemical analyses, for the investigation of ancient ceramics as powerful tool for answering important questions about their provenance and production technologies. (Maritan, 2019, 2024).

In this study an archaeometric investigation was carried out with a multi-analytical approach using advanced optical and spectroscopic techniques available in the laboratories of the Department of Geosciences at the University of Padova, for mineralogical, petrographic, and geochemical analyses.

For the macroscopic characterization of the ceramic samples, a Zeiss Stereomicroscope was used on the fresh-cut fragments for the observation of color, thickness, grain size, texture and inclusions, when visible at low magnifications. The petrographic analyses of the ceramic bodies were carried out through thin section observation performed using the microscope equipped with a high-resolution camera and related software for image acquisition and management. This made it possible to obtain information on the nature and type of inclusions and the textural characteristics of ceramic pastes. X-ray powder diffraction (XRPD) was carried out using a Malvern PANalytical X'Pert PRO diffractometer in Bragg–Brentano geometry, equipped with a Co X-ray tube in order to investigate the mineralogical composition of the ceramic bodies. All the samples were also chemically analyzed in terms of their major, minor ($SiO_2$, $TiO_2$, $Al_2O_3$, $Fe_2O_3$, MnO, MgO, CaO, $Na_2O$, $K_2O$, $P_2O_5$), and trace elements (Sc, V, Cr, Co, Ni, Cu, Zn, Ga, Rb, Sr, Y, Zr, Nb, Ba, La, Ce, Nd, Pb, Th, U) by X-ray fluorescence (XRF), using a sequential WDS Panalytical Zetium spectrometer. For a more in-depth observation of the ceramic bodies, a microstructural analysis by Scanning Electron Microscope (SEM) was performed on polished carbon-coated sections of some selected samples using the FEG-FIB SEM TESCAN SOLARIS.

Chemical and mineralogical data were processed using statistical methods to simultaneously process and compare the numerous data obtained in order to identify patterns and variations useful for a more detailed characterization of ceramic samples. Different analytical techniques require specific sample preparations: some need to be cut into pieces, while some should be powdered, for instance, XRF requires some grams of the sample also to be representative of the ceramic body. Thus, understanding these parameters is essential to ensure that the correct type and quantity of the sample is collected, facilitating thorough and accurate mineral analysis (Quinn, 2022).

### 5.2.1 Macroscopic analysis

The first analytical method for ancient ceramics is usually macroscopic observation. In this way, before going through other methods more in detail, it is possible to check on the morphology, color and fabric as well as their coded shape type (Maritan, 2024).

Employing a stereomicroscope on freshly cut fragments is useful for closely examining ceramic surfaces for examination of fabric, voids, and inclusions, also giving us a first look into ancient pottery-making technology. This primary step helps to have an initial overview of all the samples, with the aim of identifying potential similarities, in order to group the ceramic bodies according to the fabrics.

### 5.2.2 PETROGRAPHIC ANALYSIS

Ceramics are mostly composed of mineral phases; therefore, it is possible to characterize them through examination with a polarized light microscope (Maritan, 2024). The observation of ceramic features at high magnification makes thin-section petrography a very useful analytical tool to detect various aspects that can be important markers of their provenance and production technology (Maritan, 2023). Yet, petrographic analysis is the most popular due to its simple technological investment requirements (Quinn 2022). With some knowledge of optical mineralogy, it becomes possible to analyze ceramic thin sections (30 μm thick slices) using both plain polarized light (PPL) and crossed polarized light (XPL). Plain-polarized light mode aids in detailing characteristics such as color, crystal habits, cleavage, relief, and potential pleochroism, while crossed polarized light mode shows interference colors and twinning of inclusions (mineral and rock fragments) as well the features of the micromass especially its optically activity and orientation (when occurring) by crossed-polarized light observation and the voids (Maritan, 2024).

The three primary components of the ceramic fabric that can be examinate through the microscopic analysis of thin sections are: micromass, inclusions, and voids (Quinn, 2022).

The inclusions, representing the coarser elements of ceramic bodies, which are microscopically described by their nature, shape, grain size, abundance, and spatial distribution. Inclusions are categorized into mineral, organic, and artificial types, ranging from angular to well-rounded shapes (Maritan, 2024). Inclusions consist of singular mineral phases or pieces of rock and are always present in ceramics, while organic and artificial inclusions can be added by potters on purpose to enhance ceramic quality (Quinn, 2022). Organic inclusions include materials like straw or vegetal fibers, while artificial inclusions can be formed by crushed ceramics known as grog. Additionally, finding fossil traces in ceramic thin sections, (such as foraminifera, ostracods)

is useful for revealing the geological characteristics of the raw materials. In general, identifying inclusions in ceramic bodies aids provenance suggesting potential areas of raw material supply. (Quinn, 2022).

The characterization of clay matrix (as addressed by some authors or better defined as micromass since the clay transformed during firing.) is another important step in the observation of thin sections at the polarized light microscope. Clay originates from the weathering of rocks containing alumina-rich silicate minerals (phyllosilicates). It's tough to spot the specific type of clay mineral in thin sections due to their small size, also during the firing process, they can undergo decomposition and reaction with other mineral phases, which makes it hard to distinguish them. Clay matrix/micromass represents the finest part (less than 10 μm) of the raw material and appears as a homogeneous mass, including tiny mineral inclusions, commonly quartz, mica, calcite, and opaque materials. It is also the dominant component of ancient ceramics, comprising more than 50% of a sherd. Micromass gives important insights into the nature and origins of ceramic raw materials and through examination of its color, composition and aspects possible to obtain information about the manufacturing techniques (Quinn, 2022). For example, studying the birefringence in the matrix helps determine the formation of pottery, such as coiling, slow wheel or fast wheel (Maritan, 2024). Various factors such as the abundance and oxidation state of iron and the presence of other fine particles such as calcite, influence the color of the clay matrix in thin sections which can also reflect the history of its post-depositional conditions as well (Quinn, 2022).

Voids within ceramics are empty spaces visible as black areas in crossed polarized light (XPL) and colorless in plain polarized light (PPL). They can be the result of the evaporation of free water during the drying, and the release of structural water and carbon dioxide due to the decomposition of phyllosilicates and carbonates, and the loss of volatile materials or the disruption of organic material during the firing processes. Their size, quantity and shape are influenced by the production technology, raw materials used and the firing temperature, as well as by the pottery use and his history after its abandonment. The presence of channels suggests lower firing temperatures, while rounded vesicles indicate higher temperatures. Additionally, the distribution of pores can provide insights into the forming technique employed; for instance, parallel pores are often associated with molding or slab-building methods. Voids play an important role in the circulation of liquids that can penetrate the ceramic body and lead to the deposition or leaching of

chemical elements (Maritan, 2024). Secondary mineral phases, such as carbonates and sulphates, can grow within the porous system partially or completely filling the voids (Maritan, 2020). These is an important factor to consider when analyzing the alteration processes in ceramics deposited underwater.

### 5.2.3 X-RAY POWDER DIFFRACTION

Since the 1980s, X-ray powder diffraction (XRPD) has become a popular analytical technique in pottery petrology due to its accessibility, time consumption, and cost-effectiveness. XRPD is an analytical technique used to identify mineral phases in a sample by examining how X-rays diffract through the minerals' crystalline structure. This method is particularly useful for detecting specific mineral types and phases that are not visible in thin sections and that form during the manufacturing, firing, usage or degradation of ceramics. Identifying the types of clay minerals present in ceramics helps to characterize the raw materials and determine their provenance. The mineralogical assemblage revealed by XRPD analysis is useful to gain information on the firing conditions of the ceramic materials, such as firing temperature and firing atmosphere, based on the presence or absence of mineral indicators and by knowing their stability at specific temperatures and environmental conditions (Maritan, 2019; Quinn 2023). Additionally, it is also possible to identify and characterize potential post-depositional alteration processes (Maritan et al., 2015).

Nowadays scientists have access to libraries of known diffraction angles for thousands of minerals, such as the International Center for Diffraction Data (ICDD) Database and the Crystallography Open Database (COD). Minerals can be distinguished by their unique diffraction peaks. Algorithms analyze the detected peaks in a sample by comparing them to databases, identifying potential matches based on the known diffraction angles of different minerals. Each potential match is given a confidence rating, or 'figure of merit,' aiding the user in determining which matches to approve or dismiss (Quinn, 2022).

This method allows to classification of homogeneous sample groups based on the types of clay materials used, production recipes, and/or firing conditions, enabling the identification and differentiation of their respective characteristics (Maritan, 2019). It is necessary to complement

XRD with other methods to achieve a comprehensive mineralogical analysis and it is not ideal for independent mineralogical characterization (Quinn, 2022).

In this study from each ceramic sample, a powder with a grain size of less than 100μm was obtained by grinding in an agate mortar. HighScore Plus® 3.0 software by Malvern PANalytical was used to interpret the diffraction patterns and qualitatively analyze the mineral associations by comparison with reference patterns of the PDF database from the International Centre for Diffraction Data (ICDD). Statistical treatment of the XRPD data was performed by cluster analysis on the Quadratic Euclidean Distance according to Maritan et al. (2015), in order to group samples on the basis of their mineralogical patterns. It produces dendrograms that visually represent the degree of similarity between samples, helping in their classification.

### 5.2.4 X-RAY FLUORESCENCE

Since the 1960s, the bulk chemical composition of ceramics has been widely used, especially to study fine wares (Maritan, 2019). X-ray fluorescence spectroscopy (XRF) is one of the most widely used techniques for elemental analysis of ceramic materials. The process involves high-energy X-rays, which expel core electrons from the atoms. When these unstable ionized atoms return to their stable or ground state, they emit secondary X-rays, called fluorescence photons, which represent characteristics of the specific elements and can be used for the identification and quantification of the chemical elements (Artioli, 2010).

By XRF spectroscopy in is possible to measure a wide range of elements that are categorized into major and minor elements, which are reported as percentages, and trace elements, which are usually expressed as parts per million (ppm). In most cases, the measurement of the chemical composition of a ceramic material requires the sample to be ground and represent the whole object under study. The minimum quantity needed for analysis depends on the technique. XRF typically requires at least 1 gram of powdered sample which is then prepared as beads by mixing calcinated powder. It is also important to consider that any coating, slip, or glaze on the surface of potsherds must be removed before performing the analysis of any ceramic body (Maritan, 2024).

The statistical treatment which simultaneously processes a high number of data, helping to define differences or analogies between the ceramic bodies' composition. The most commonly used methods are cluster analysis (CA) and principal component analysis (PCA), which were obtained in this study using Statgraphics Centurion 19 software. Cluster allows to group the samples according to compositional similarities and it is represented by dendrogram graphs (Maritan, 2024). Principal component analysis is a powerful tool for analyzing and understanding complex data (Smith, 2002) of the analyzed set of samples, so it is possible to explore differences among samples as it can explain the variation in the bulk chemical composition of ceramics detecting similarities and correlations between the samples.

The analysis of the chemical composition is one of the main methods performed in the study of the provenance of ceramic materials and the use of statistical tools enabled archaeometry scientists to efficiently process large amounts of chemical data (Maritan, 2019).

By processing chemical data, it is important to consider the presence of alterations that may occur in ceramic materials during burial. Detailed microscopic and mineralogical analyses are valuable for identifying any possible post-depositional secondary phases, and a range of statistical treatments can be employed to explore the structure of the data. Therefore, in the petrographic analysis of ceramic bodies, it is prominent to couple microscopic observations with chemical analysis of inclusions to achieve a more precise characterization (Maritan, 2024).

### 5.2.5 SCANNING ELECTRON MICROSCOPE

Microstructure and chemical composition characterizations result in the discovery of ancient manufacturing techniques, provenance and post-depositional alteration. Scanning Electron Microscopy (SEM) is a technique for studying the microstructure and composition of materials at very high magnifications. SEM analysis is based on the interaction between a focused beam of electrons with the sample.

When the electron beam hits the sample, it transfers energy to the electrons in the atom, causing some of these electrons to be ejected which are called secondary electrons and are influenced by the surface topography of the sample. By detecting these secondary electrons, the

SEM can generate images that reveal the fine details of a sample. As the beam moves across the sample, a detector positioned at an angle above the sample collects the signals generated from the interactions between the electron beam and the atoms on or near the sample's surface (Artioli, 2010). SEM can also be used to see the distribution on polished sample, by back scattered electron mode (BSE), of the average atomic number (composition) of the various part of a polycrystalline material, such the ceramic is, allowing to identify compounds (minerals) and their size and distribution, therefore their texture and structure. Modern SEMs are equipped with computers that control the microscope's operating conditions, move the sample, collect images, and perform various analytical tasks using different detectors (Quinn, 2022).

An important point regarding sample preparation in this method is coating. The coating is made of either a metal when the conductivity for imaging is required or graphite when chemical analysis is the aim (Artioli, 2010). Ceramic samples typically need to be coated with a very thin layer of gold, carbon, or platinum. This coating allows the sample to conduct electrons, which is essential for obtaining clear and accurate images during SEM analysis (Quinn, 2022).

While most inclusions and features in ceramics can be studied with a light microscope, the micromass contains minerals often too small (< 2 μm) to be observed. So, higher magnification and resolution of SEM are advantages for analyzing ancient ceramics. Some of the key benefits of SEM are that in theory, it requires less training, allowing even an inexperienced analyst to generate data quickly, and its ability to focus the electron beam onto a very small area of the sample, enabling detailed micro-geochemical analysis of individual inclusions and features. Despite its advantages, it is not ideal to use only SEM as the primary research tool for analyzing ceramics. In this method, the lowest magnification is often too high to provide an overall impression of ceramic fabric unlike petrography or macroscopic analysis which are better through low magnification. Moreover, SEM is significantly more expensive, not portable, and complex than petrographic microscopes, requiring technicians and dedicated laboratory settings (Quinn, 2022).

EDS (Energy Dispersive Spectrometry) spectrometers are often associated on SEM to provide complementary chemical analysis alongside imaging and diffraction. (Artioli, 2010). Geochemical provenance determination can be possible with SEM-EDS through analysis of the base clay of tempered ceramics and its comparison with the composition of possible clay sources sampled in the field. When an electron beam excites a sample, the EDS spectrum reveals its

elements, which can be compared to a library of known mineral spectra for identification of mineral inclusion. It also can detect mineralogical characterization, post-depositional alterations, and compositional differences within a sample such as temper, clay mixing, and secondary depositions. One of the issues here is that SEM-EDS only offers major and minor elements and does not help in detecting the trace elements that are crucial in geochemical studies of provenance (Quinn, 2022).

These capabilities make SEM one of the important and complementary tools for researchers studying materials at the microscopic level, providing insights into the composition and structure of samples that are not possible with optical microscopy.

# 6 Results

## 6.1 Macroscopical analysis (stereomicroscope on fresh-cut fragments)

From a macroscopic point of view, all eleven ceramic samples from Apani and Giancola production sites show a thickness ranging from approximately 5 mm to 14 mm with a variation of colors from beige to blush pink and have a fine and compact texture with low porosity. Porosity is characterized by voids, some of which are elongated and aligned parallel to the surfaces. In some samples is possible to distinguish reddish-coloured nodules and quartz inclusions (Figure 8.).

**A** **B**

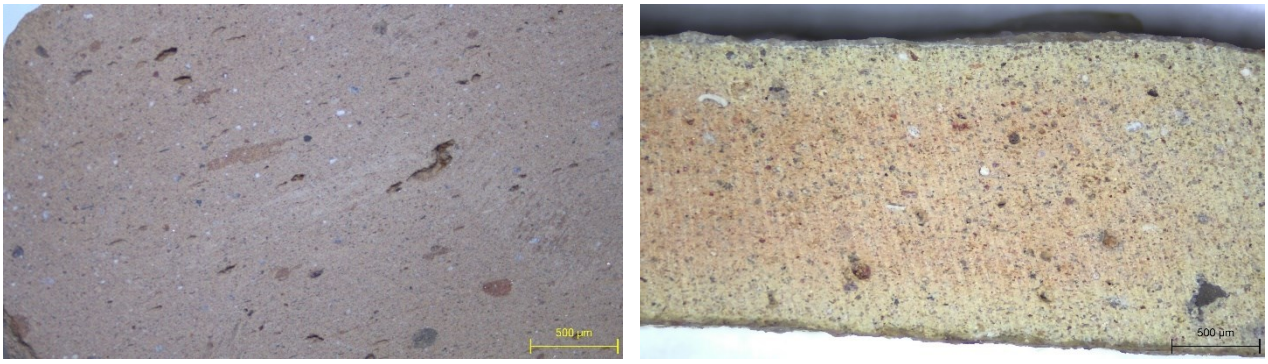


Figure 8. – Fresh-cut section of: (A) sample AP-2, showing clay pellets and parallel voids; (B) sample GC-7, with quartz inclusions and a texture with a blend of two colors.

As for the samples from the underwater site of TSS, the fresh cut analysis under the stereomicroscope, before preparing thin sections, proved to be a useful way to sort the samples at the beginning of the study. This preliminary step allowed for the grouping of samples, making the subsequent analysis under an optical microscope more efficient. Five main groups (defined as microfabrics) have been identified based on the combination of macroscopic characteristics, including the color of the bodies, the presence or absence of visible inclusions at low magnifications, porosity and sample thickness.

Macrofabric 1consists of samples TSS-11, TSS-23, TSS-27, TSS-28, TSS-29, TSS-30, and TSS-31. These samples are characterized by a thickness ranging from 6 mm to 9 mm, with the

exception of samples TSS-11 and TSS-23 which have a thickness of 12 mm and 17 mm respectively. The color of the bodies varies from beige to dark grey. They show a very fine texture with medium to low widespread porosity.

Macrofabric two includes samples TSS-5, TSS-8, TSS-12 and TSS-13, with a thickness ranging from 10 mm to 13 mm. The texture is fine and compact with low porosity and the color varies in shades of beige. A chromatic stratigraphy can be seen by featuring areas with a greyish color, probably related to post-depositional processes and the precipitation of secondary phases or to firing conditions. Rounded red nodules, which could be identified as clay pellets, are clearly visible and moderately abundant.

Macrofabric three includes samples TSS-3, TSS-14 and TSS-15, whose thickness varies from 8 mm to 19 mm. These samples are characterised by higher porosity and a lighter colour ranging from beige to yellow. The texture is more homogeneous but less compact compared to the other groups. In these samples, rounded red nodules are well visible and moderately abundant.

Macrofabric four consists of samples TSS-1, TSS-6 and TSS-4, with thickness from 10 mm to 15 mm. These fragments stand out from the other groups due to the appearance of their bodies, which display colours from light orange to grey with streaks that suggest the use of mixed clays.

Lastly, macrofabric five consists of two samples that do not fit into any of the previous groups and differ significantly from each other. Sample TSS-19 has a thickness of approximately 9 mm, with a homogeneous dark red matrix with a well-defined texture and clearly visible inclusions at low magnification. Sample TSS-24 has a thickness of around 5 mm and is characterized by a homogeneous orange-peach matrix and inclusions larger than a millimetre, some of which are visible to the naked eye.

In figure 9 macro photos of a representative sample of each macrofabric acquired under stereomicroscope are reported.

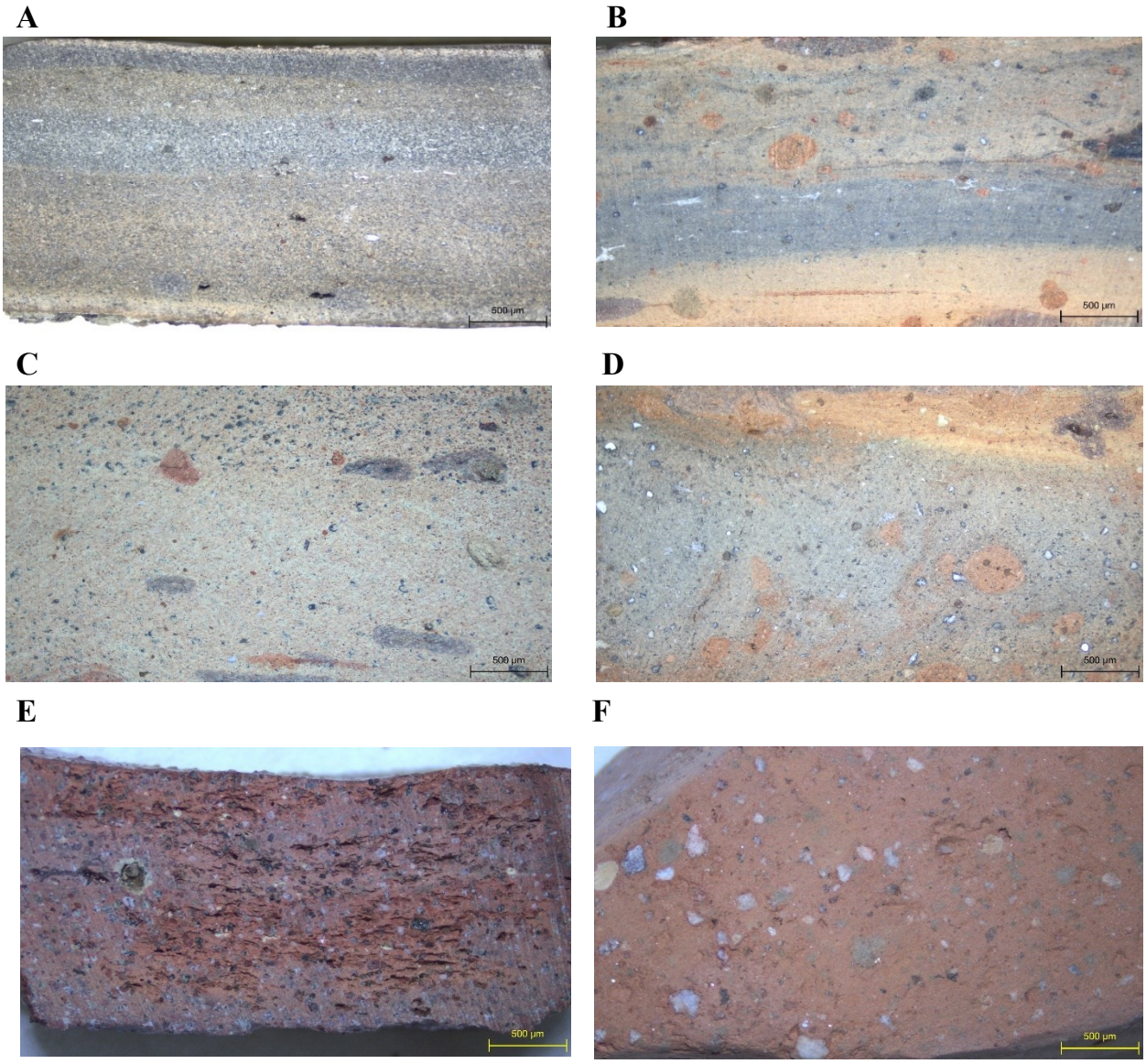


Figure 9. ─ Fresh-cut section of sample: (A) TSS-30; (B) TSS-12; (C) TSS-14; (D) TSS-1; (E) TSS-19; (F) TSS-24, representative of the microfabric.

## 6.2 PETROGRAPHIC ANALYSIS (OPTICAL MICROSCOPE ON THIN SECTIONS)

The observation of thin sections under the polarised light microscope lead to classify the terrestrial samples in two macro-groups: i) one characterised by matrix obtained by a carbonate-rich clay (AP-1, AP-4, GC-7, GC-8 and GC-10); ii) one with an iron-rich terrigenous matrix with clay pellets (samples: AP-2, AP-3, AP-5, AP-6, AP-7 and GC-9). Two samples representative of each group are shown in figure 10.

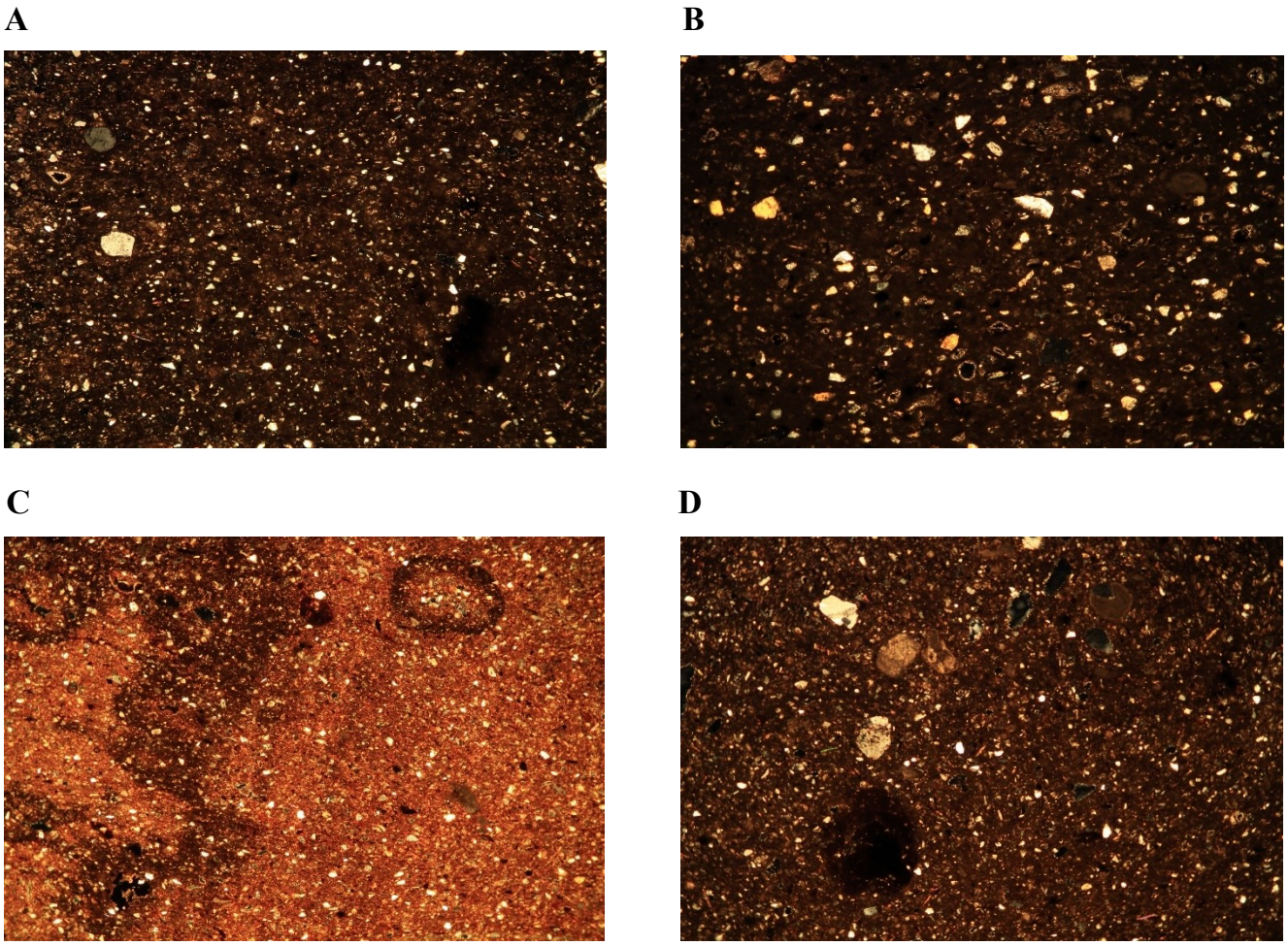


Figure 10. – Photomicrographs taken in crossed-polarized light of some of the terrestrial samples from Apani e Giancola: **(A)** sample AP-1; (B) sample GC-7; (C) sample AP-2; (D) sample GC-9. Image width: 3.6 mm

In terms of inclusions, quartz, micas and more rarely plagioclase, K-feldspars and pyroxenes are recognized. Traces of microfossils are visible in all samples and are abundant in some of them. The quantity of inclusions is around 5-10%.

Types of fossils include algae, foraminifera, gastropods, and bivalves suggesting that the raw materials were sourced from different depositional levels, including clays with a marine component. Additionally, carbonate mudstone fragments with a rounded brownish color were observed in all samples except AP-4, AP-5, GC-8 and GC-10. Secondary calcite is present inside and around voids in some of the samples. Angular fragments of chert were observed in sample GC-7. Some of these features can be seen in figure 11.

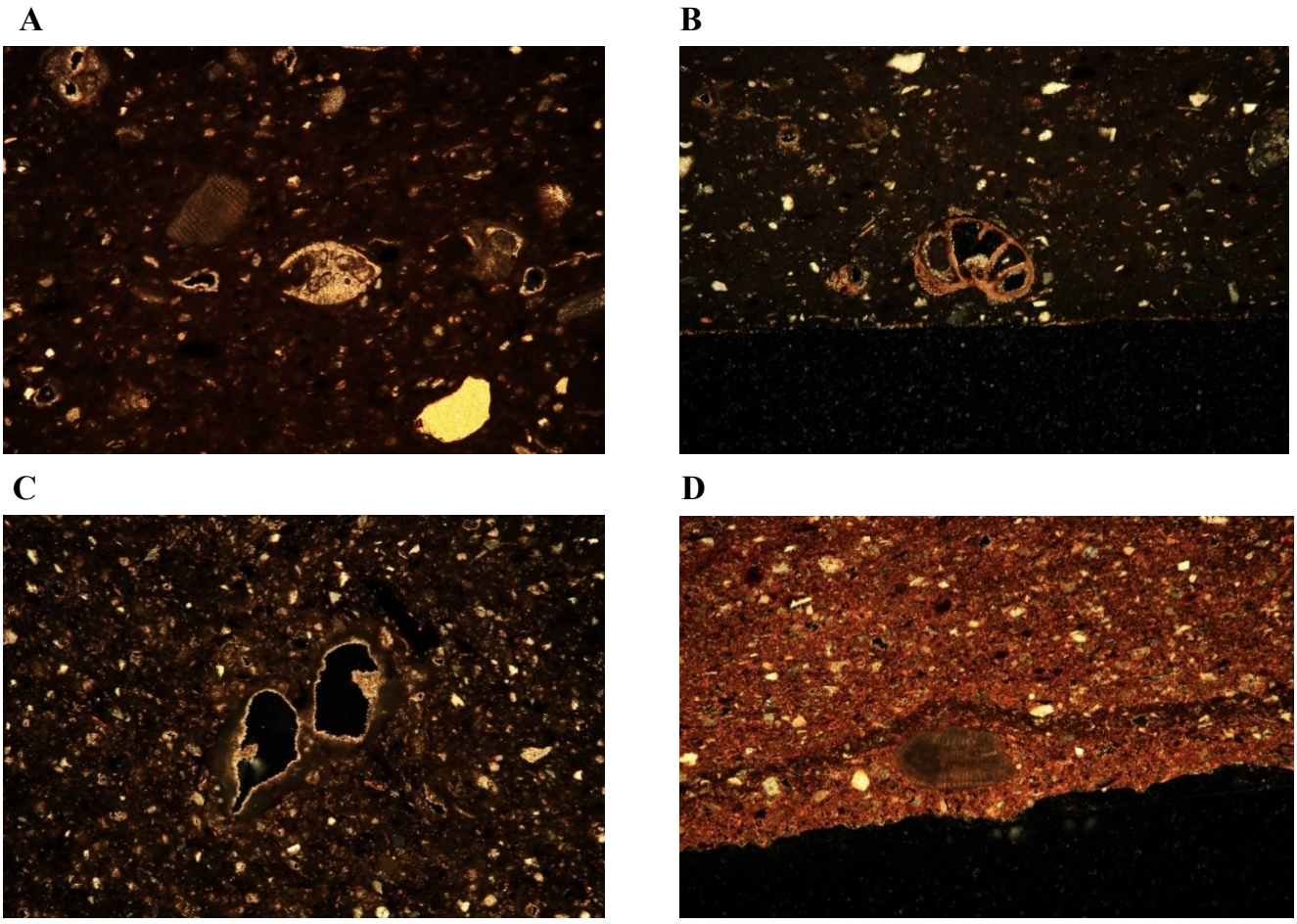


Figure 11.– (Photomicrographs taken in crossed-polarised light of some of: (A) fossil traces and carbonate mudstone in sample AP-6; (B) fossil trace in sample in GC-10; (C) secondary calcite around and inside voids in sample AP-5; (D) algae in sample AP-2. Image width: 1.85 mm

The petrographic analysis of the fragments forms the underwater context confirms the grouping recognized by macroscopic examination offering deeper insights into ceramic bodies petrographic features highlighting differences and similarities with terrestrial samples.

The underwater samples can also be divided in two macro groups, one rich in inclusions of carbonate origin and the other with an iron-rich micromass. Overall, all the ceramic bodies show fine textures composed of microcrystals of quartz and mica. Inclusions are characterized by quartz, micas (mainly white mica such as muscovite and illite, and subordinated biotite) and to a lesser extent by clinopyroxene, plagioclase and K-feldspar, and their quantity does not exceed 10%. The particle size is generally below 10 μm, except for samples TSS-1, TSS-8, TSS-13, TSS-23, TSS-31 and TSS-34, where there are sub-angular inclusions ranging in size from 20 to 50 μm. These inclusions are more densely packed, making up 15 to 20% of the total volume.

Although no clear evidence of fossils was found in samples TSS-5 and TSS-14, the remaining samples contain fragments of calcareous fossils, which are interestingly similar to those discovered in the samples from Apani and Giancola. The presence of rounded, brownish carbonate mudstones is detected in almost all samples. Oolites are an example of carbonates that were also observed in nearly all of the samples, which are common pseudofossils typically associated with shallow-water sediments (Fei et al., 2015).

Clay pellets are present in macrofabric 2, 3 and 4, with macrofabric 2 having the highest amount, as previously noted in the macroscopic analysis. Angular fragments of chert were observed in some samples of each macrofabric except in 5 including samples TSS-1, TSS-3, TSS-8, TSS-12, TSS-13, TSS-14 and TSS-31. Secondary calcite is present in almost all samples, around and within voids. In some samples, the calcite crystals are large and showing an idiomorphic habit, while in others, they are smaller and less distinct. Some of the features explained above can be seen in figure 12.

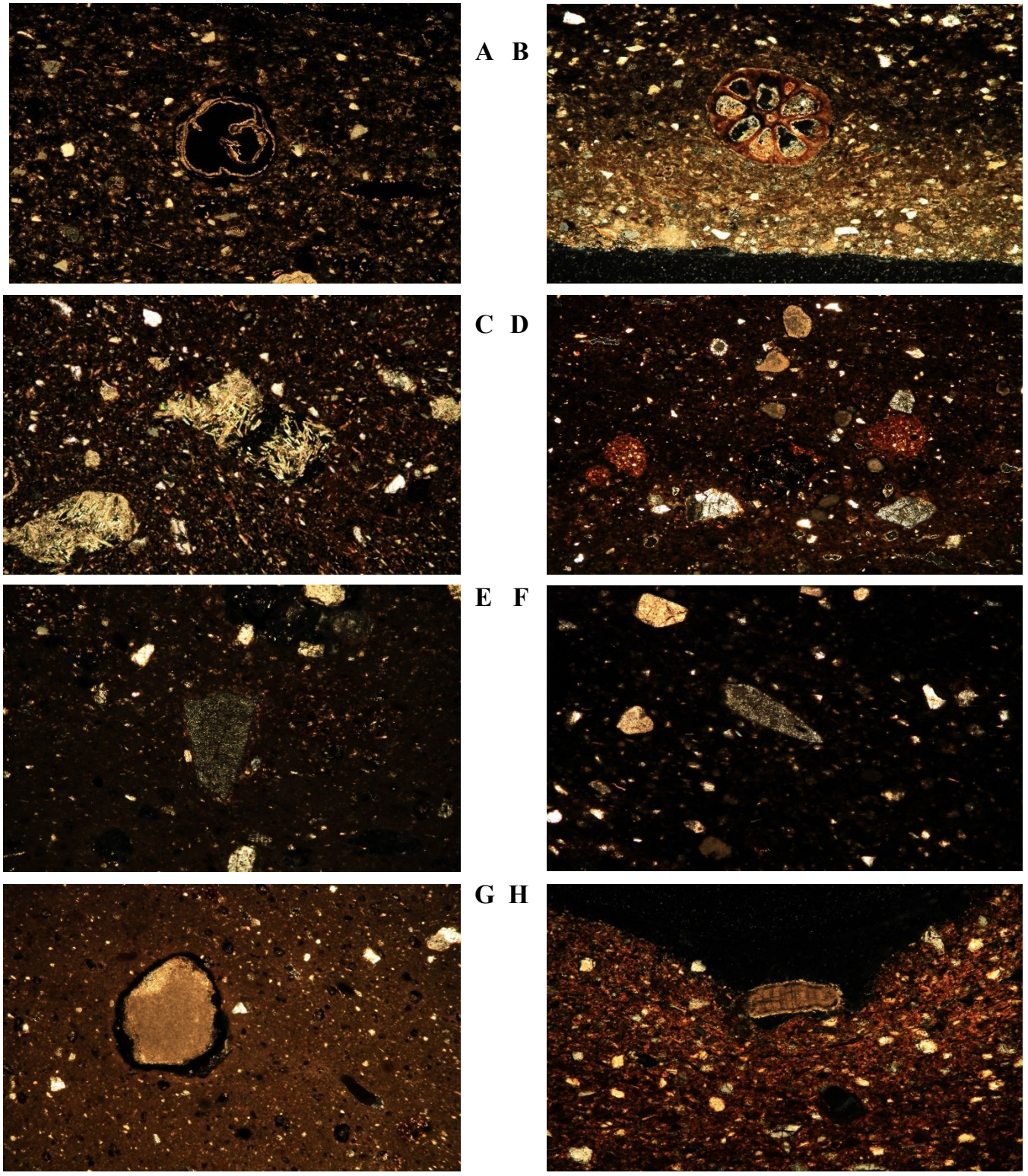


Figure 12. ─ Photomicrographs in crossed-polarized light of: (A) gastropod shells in samples TSS-27; (B) calcareous algae in sample TSS-30; (C) secondary calcite precipitations inside and around voids in sample TSS-1; (D) carbonate inclusions and clay pallets in sample TSS 8; (E) chert inclusion in sample TSS-3; and TSS13, respectively; (G) carbonate mudstone in sample TSS-15; (H) fossil trace replaced by carbonate in sample TSS-4. Image width: 3.7 mm (A-B-D-E-F-H), 1.85 mm in (C-G).

Exceptions are samples TSS-19 and TSS-20, which are different from all the others and from each other in terms of both matrix and type and grain size of the inclusions (Figure 13.). There are no evidence of fossil remains, carbonates, chert or secondary calcite in these two samples. Sample TSS-19 show a compact, and homogeneous black matrix., have relatively abundant inclusions (approximately 20%), sub-angular to angular in shapes, dimensions around 200 µm and with a predominant volcanic component given by abundant pyroxenes, and subordinated olivine plagioclase in addition to quartz and micas. Sample TSS-24, instead, is characterized by a brown matrix containing both carbonate and terrigenous components, in which inclusions account for approximately 20%, have grain size sometimes exceeding 600 µm and consist of fragments of metamorphic and volcanic rocks, along with K-feldspar  sillimanite, micas and quartz.

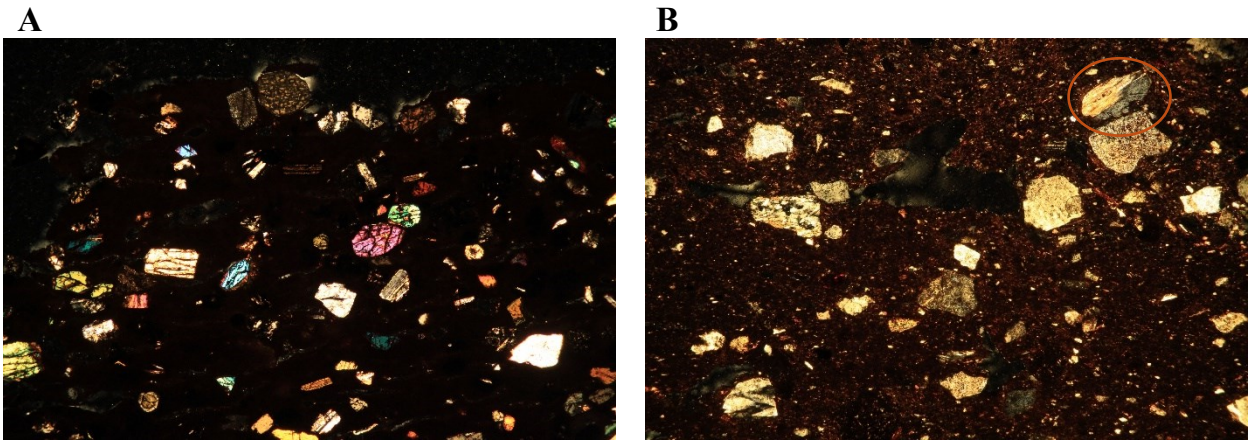


Figure 13. ─ Photomicrographs in crossed-polarized light of: (A) pyroxene inclusions in sample TSS-19; (B) sillimanite (circled in red) and quartz inclusions in sample TSS-24. Image width: 3.7 mm.

## 6.3 Mineralogical analysis (X-Ray Powder Diffraction)

X-ray diffraction analysis of the terrestrial samples reveals a largely homogeneous mineralogical composition without any clear difference between the production areas of Giancola and Apani. Quartz, K-feldspar (mostly microcline), plagioclase, illite/muscovite, and diopside-like pyroxene are the main mineral phases detected in all samples, except than in AP-2 and GC-8 where no pyroxenes were found. Hematite is ubiquitous and in samples AP-1, AP-4, GC-7 and GC-10 gehlenite phase is also present. Calcite is present in all samples, despite it represents a secondary

product of recrystallization (secondary calcite), as microscopically observed. A closer examination of the XRPD data reveals the diffraction patterns of haüyne-like phase, a felspathoid belonging to the sodalite group typical of the volcanic outcrop of Monte Vulture, in samples AP-4 and GC-8. In table 2 the mineralogical composition of the terrestrial samples and the relative estimation of firing temperature are reported.

| SAMPLE | Qz | Mus/Ill | Bt | Kfs | Pl | Hem | Px | Cal | Geh | Wo | Hyn | Temp °C |
|---|---|---|---|---|---|---|---|---|---|---|---|---|
| AP 1 | x | x | | x | x | x | x | x | x | x | | 900°-950° |
| AP 2 | x | x | | x | x | x | x | x | | | | ~ 800° |
| AP 3 | x | x | x | x | x | x | x | x | | | | 800-850° |
| AP 4 | x | x | | x | x | x | x | x | x | | x | 900°-950° |
| AP 5 | x | x | | x | x | x | x | x | | x | | 900°-950° |
| AP 6 | x | x | | x | x | x | x | x | | | | 850°-900° |
| AP 7 | x | x | | x | x | x | x | x | | | | 850°-900° |
| GC 7 | x | x | | x | x | x | x | x | x | | | 900°-950° |
| GC 8 | x | x | | x | x | | x | x | | | x | ~ 800° |
| GC 9 | x | x | | x | x | x | x | x | | | | 900°-950° |
| GC 10 | x | x | | x | x | x | x | x | x | | | 900°-950° |

Table 2. - mineralogical composition of the terrestrial samples analyzed by XRPD. Abbreviations of the mineral phases according to Warr (2021): Qz = quartz, Pl = plagioclases, Px = pyroxenes, hem = hematite, Kfs = K-feldspar, Mus/Ill = muscovite/Illite, Geh = gehlenite, Wo = wollastonite, Bt = biotite, Hyn = haüyne, Cal = calcite. Estimated firing temperature is also reported.

The mineralogical composition of the underwater samples includes both primary minerals as quartz, K-feldspar (microcline), illite/muscovite and new phases formed during the firing process as hematite, diopside-like pyroxene and plagioclase. Other secondary phases, such as gypsum, calcite, magnesian calcite, aragonite, pyrite and more rarely, zeolites and hydrotalcite-like phases, were identified in underwater samples as newly formed post-depositional phases. The mineralogical assemblage of the underwater samples and the relative estimation of firing temperature is given in (Table 3.).

| SAMPLE | Qz | Mus/Ill | Bt | Kfs | Pl | Hem | Px | Py | Gp | Mg-Cal | Cal | Arg | Geh | Zeo | Hyn | Sil | T°C |
|---|---|---|---|---|---|---|---|---|---|---|---|---|---|---|---|---|---|
| TSS 1 | x | x | | x | x | x | x | x | x | x | | x | | | | | 850°-900° |
| TSS 3 | x | x | | x | x | x | x | x | x | x | | | x | | | | 900°-950° |
| TSS 4 | x | x | x | x | x | x | | | x | | | | | | x | | ~ 800° |
| TSS 5 | x | x | | x | x | x | x | | x | x | | | | | x | | 850°-900° |
| TSS 6 | x | x | | x | x | x | x | x | x | x | x | | | | | | 850°-900° |
| TSS 8 | x | x | | x | x | x | x | x | x | x | | | | | | | 850°-900° |
| TSS 11 | x | x | | x | x | | x | x | x | x | x | | | | | | 850°-900° |
| TSS 12 | x | x | | x | x | | x | x | x | x | | | | | | | 850°-900° |
| TSS 13 | x | x | x | x | x | | x | x | | x | x | x | | | | | 850°- 900° |
| TSS 14 | x | x | | x | x | | x | | | x | | | | | | | 900°-950° |
| TSS 15 | x | x | | x | x | | x | | | x | x | | | | | | 900°-950° |
| TSS 19 | x | x | x | x | x | x | x | | | | | | | x | | | 950°-1000° |
| TSS 23 | x | x | | x | x | | x | x | | x | x | | | | | | 850°-900° |
| TSS 24 | x | x | x | x | x | x | x | | | | x | | x | | | x | 850°-900° |
| TSS 27 | x | x | | x | x | | x | x | | x | x | | | | | | 900°-950° |
| TSS 28 | x | x | | x | x | x | x | | x | x | x | | | | | | 900°-950° |
| TSS 29 | x | x | | x | x | | x | x | x | x | x | | | | | | 850°-900° |
| TSS 30 | x | x | | x | x | x | x | x | | x | x | | x | | | | 900°-950° |
| TSS 31 | x | x | | x | x | | x | x | x | x | x | | | | | | 850°-900° |

Table 3. - Mineralogical compositions of the underwater samples analyzed by XRPD. Abbreviations of the mineral phases according to Warr (2021): Qz = quartz, Pl = plagioclases, Px = pyroxenes, hem = hematite, Kfs = K-feldspar, Mus/Ill = muscovite/Illite, Geh = gehlenite, Bt = biotite, Py = pyrite, Arg = aragonite, Gp = gypsum, Hyn = haüyne, Cal = calcite, Mg-Cal = magnesium-calcite, Zeo = zeolite, Sil = sillimanite. Estimated firing temperature is also reported.

A cluster analysis of all raw XRPD data of underwater samples, using Euclidean distances and average linkage method, was performed to group the samples according to their diffraction patterns considering the position of the peaks (Maritan et al., 2015). The resulting dendrogram reported in figure 14. shows two main clusters which are the result of a number of factors such as the mineralogy and grain size of the base clay used, as well as the firing temperature, which all contribute to defining the groups (Maritan et al., 2015).

Cluster 1 is formed by samples TSS-3, TSS-14, TSS-15 and TSS-27 showing a mineralogical composition characterized by abundant pyroxene and anorthite-rich plagioclase and

scarce clay minerals suggesting a firing temperature between 900°C and 950°C. Mg-calcite is present as alteration secondary phases while pyrite is absent.

Cluster 2 contains the majority of the samples, which are mainly composed of quartz and muscovite while plagioclase and pyroxenes are less abundant with respect to the samples in cluster 1 suggesting a lower firing temperature around 850-900 °C. Mg-calcite is present almost in all samples as secondary phase as well as gypsum and pyrite.

Samples TSS-4, TSS-19 and TSS-24 do not group in any cluster and can be considered outliers as already evidenced by petrographic analysis, samples TSS-19 and TSS-24 deeply differ from all others also in terms mineralogical composition. Mineralogically, the sample TSS-19 is mainly composed of quartz, sanidine, anorthite-rich plagioclase, diopside-like pyroxenes, analcime and hematite suggesting a firing temperature exceeding 950°C. No post-depositional phases are present in sample TSS-19. Sample 24 consists mainly of quartz, micas (muscovite and biotite), K-feldspar (mainly microcline), diopside-like pyroxenes, anorthite-rich plagioclase and hematite, as well as sillimanite. Calcite and Mg-calcite are present as secondary phases. The firing temperature in sample TSS-24 is around 850-900 °C. Sample 4 is mainly composed by quartz and muscovite, followed by k-feldspar and albite-rich plagioclase. No pyroxenes are found while diffraction peaks of haüyne were detected, and gypsum is present as alteration phase. This mineralogical assemblage suggests a firing temperature around 800°C.

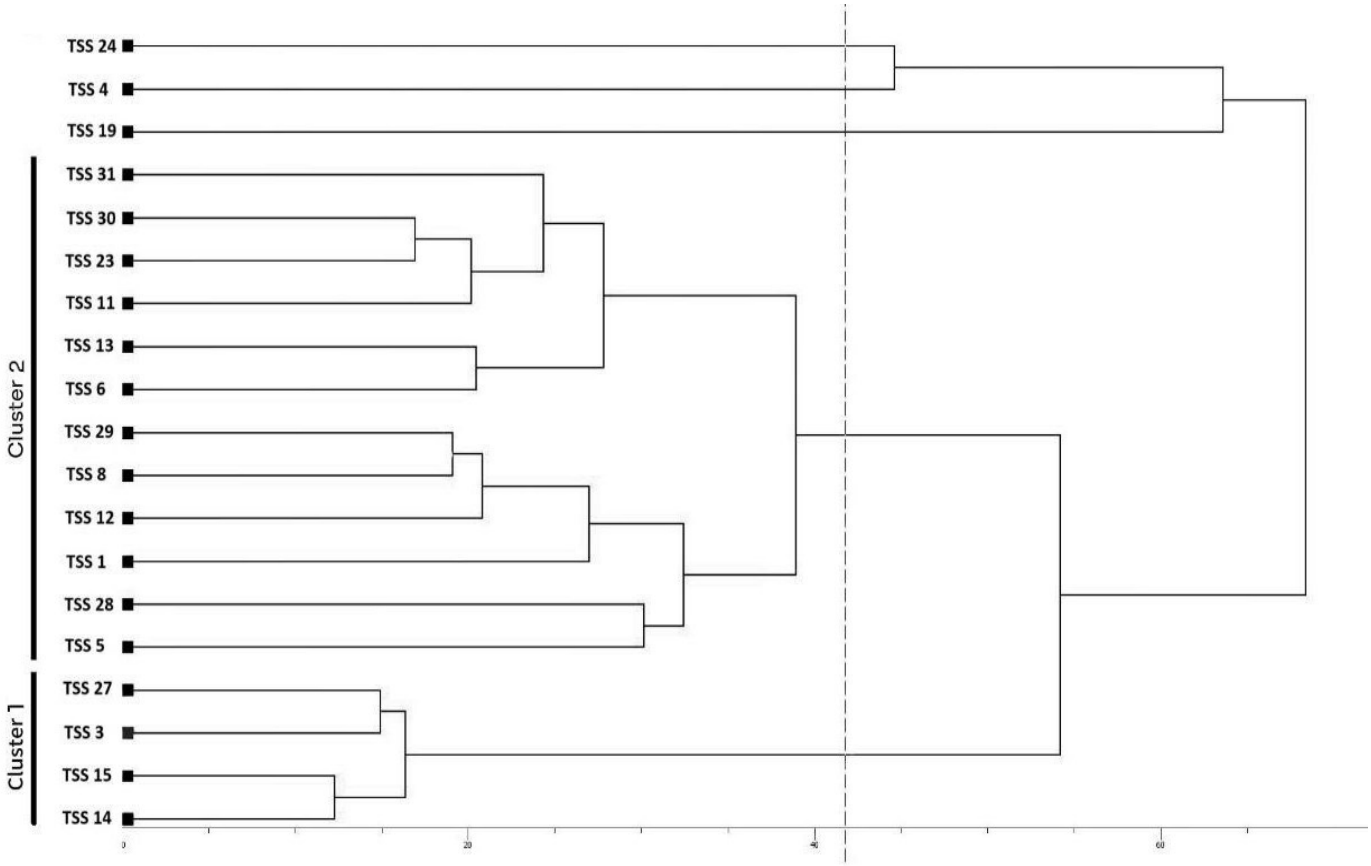


Figure 14. ─ from the cluster analysis of XRPD patterns of TSS samples, according to Euclidean distance and average linkage method. Dissimilarity cut-off is based on KGS test.

## 6.4 CHEMICAL ANALYSIS (X-RAY FLUORESCENCE)

In this study, each sample was a chemically analyzed by X-ray fluorescence (XRF) to determine the concentrations of both major and minor elements ($SiO_2$, $TiO_2$, $Al_2O_3$, $Fe_2O_3$, MnO, MgO, CaO, $Na_2O$, $K_2O$, $P_2O_5$) as well as trace elements (Sc, V, Cr, Co, Ni, Cu, Zn, Ga, Rb, Sr, Y, Zr, Nb, Ba, La, Ce, Nd, Pb, Th, U).

The chemical data were statistically treated using only the most stable elements, which were not affected by post-depositional processes and therefore remained unaltered, such as Al, Fe, Ti, Ce, Co, Cr, Cu, La, Nd, Sc, and Th facilitating a clearer understanding of the sample distribution

and allowing for more reliable comparisons with terrestrial samples, which show distinct post-depositional phases compared to those found in underwater environments.

From the chemical perspective, the data relative to the terrestrial samples reveals a high degree of homogeneity as it is indicated by the low standard deviation values for both major and trace elements, as detailed in Table 4. This uniformity suggests consistency in compositional characteristics across the samples. However, there is a notable variation in the calcium content, which ranges from 13.17% to 20.86%. Additionally, among the trace elements, sulfur exhibits the most significant variation, with the highest concentration recorded in sample GC-8 (1005 ppm) probably related to the presence of haüyne-like phase where sulfur can occur as additional anion.

(Table 5.) summarizes the concentrations of various elements indicating both major and trace elements present in the samples detected by X-ray Fluorescence (XRF) in the underwater samples. They have fairly homogenous chemical compositions, regardless of the amphora type they represent which is evident from the low levels of standard deviation for the majority of the elements. However, few major and minor elements (expressed in percentage of oxides) such as CaO demonstrate higher variation in their concentrations. In addition, some trace elements (in ppm) like sulfur (S) show greater variation due to their involvement in the precipitation of secondary phases, such as pyrite ($FeS_2$) and gypsum ($CaSO_4 \cdot H_2O$), during post-depositional processes.

The chemical analysis of samples TSS-19 and TSS-24 aligns with the results of macroscopic, petrographic, and mineralogical analysis, confirming their distinct characteristics compared to the other samples. Regarding sample TSS-19, there are no significant chemical differences compared to the other samples except for its higher aluminum content ($Al_2O_3$ = 18.76%), and lower silicon content ($SiO_2$ = 52.44%). Additionally, the sulfur content (S = 188 ppm) is too low that it can be linked to the absence of pyrite as alteration phase. Sample TSS-24, on the other hand, contains the highest amount of aluminum ($Al_2O_3$ = 19.21%) and exhibits low values of magnesium and calcium, this latter notably the lowest amount among all the samples, being of 5.26%.

| Samples | $SiO_2$ | $TiO_2$ | $Al_2O_3$ | $Fe_2O_3$ | MnO | MgO | CaO | $Na_2O$ | $K_2O$ | $P_2O_5$ | Tot | L.O.I. | S | Sc | V | Cr | Co | Ni | Cu | Zn | Ga | Rb | Sr | Y | Zr | Nb | Ba | La | Ce | Nd | Pb | Th | U |
|---|---|---|---|---|---|---|---|---|---|---|---|---|---|---|---|---|---|---|---|---|---|---|---|---|---|---|---|---|---|---|---|---|
| AP1 | 57.70 | 0.75 | 14.88 | 5.61 | 0.10 | 1.98 | 16.68 | 1.18 | 2.58 | 0.16 | 101.62 | 6.27 | 208 | 36 | 136 | 122 | 16 | 66 | 24 | 90 | 2 | 124 | 411 | 25 | 172 | 12 | 328 | 30 | 69 | 35 | 11 | 16 | 4 |
| AP2 | 54.99 | 0.70 | 14.03 | 5.87 | 0.09 | 1.87 | 18.44 | 1.08 | 2.57 | 0.16 | 99.80 | 14.65 | 230 | 38 | 148 | 115 | 18 | 70 | 35 | 92 | 6 | 122 | 412 | 26 | 159 | 4 | 295 | 33 | 66 | 29 | 18 | 10 | 3 |
| AP3 | 51.87 | 0.72 | 14.71 | 5.71 | 0.15 | 3.60 | 18.49 | 1.33 | 3.05 | 0.24 | 99.87 | 13.81 | 847 | 31 | 118 | 120 | 17 | 67 | 61 | 119 | 4 | 135 | 492 | 27 | 164 | 15 | 395 | 31 | 71 | 35 | 18 | 14 | 5 |
| AP4 | 58.16 | 0.74 | 14.99 | 5.51 | 0.10 | 1.84 | 15.78 | 1.21 | 2.48 | 0.16 | 100.97 | 5.84 | 766 | 29 | 131 | 119 | 14 | 65 | 21 | 93 | 6 | 120 | 406 | 25 | 169 | 17 | 333 | 29 | 65 | 32 | 17 | 14 | 3 |
| AP5 | 58.20 | 0.75 | 15.11 | 5.83 | 0.10 | 1.83 | 15.57 | 1.19 | 2.86 | 0.16 | 101.60 | 8.38 | 220 | 33 | 129 | 128 | 14 | 69 | 24 | 96 | 4 | 124 | 390 | 28 | 171 | 9 | 420 | 30 | 66 | 32 | 16 | 13 | 2 |
| AP6 | 54.97 | 0.70 | 14.17 | 5.70 | 0.09 | 1.92 | 18.97 | 0.90 | 2.24 | 0.12 | 99.78 | 16.14 | 312 | 38 | 114 | 111 | 15 | 69 | 20 | 85 | 2 | 101 | 420 | 23 | 161 | 6 | 477 | 26 | 63 | 34 | 12 | 13 | 3 |
| AP7 | 59.61 | 0.78 | 15.52 | 5.93 | 0.09 | 1.97 | 13.17 | 1.13 | 2.77 | 0.17 | 101.14 | 9.02 | 229 | 31 | 132 | 140 | 17 | 74 | 26 | 87 | 2 | 128 | 397 | 26 | 175 | 8 | 343 | 32 | 71 | 33 | 15 | 17 | 3 |
| GC7 | 53.36 | 0.66 | 13.59 | 5.58 | 0.09 | 2.30 | 20.86 | 0.96 | 2.37 | 0.12 | 99.89 | 10.74 | 871 | 39 | 85 | 116 | 16 | 95 | 23 | 86 | 7 | 111 | 573 | 24 | 176 | 18 | 287 | 38 | 81 | 33 | 16 | 14 | 3 |
| GC8 | 53.15 | 0.71 | 14.11 | 5.49 | 0.09 | 2.48 | 19.70 | 0.99 | 2.68 | 0.16 | 99.56 | 15.74 | 1005 | 36 | 138 | 135 | 16 | 85 | 24 | 92 | 10 | 125 | 439 | 24 | 147 | 17 | 371 | 25 | 58 | 30 | 15 | 15 | 3 |
| GC9 | 57.56 | 0.71 | 14.23 | 5.35 | 0.09 | 2.14 | 17.05 | 1.18 | 2.57 | 0.17 | 101.05 | 11.22 | 520 | 28 | 125 | 110 | 14 | 64 | 18 | 85 | 4 | 126 | 369 | 26 | 161 | 19 | 278 | 27 | 66 | 32 | 18 | 11 | 2 |
| GC10 | 56.20 | 0.77 | 15.51 | 6.18 | 0.10 | 2.45 | 15.60 | 0.92 | 2.55 | 0.20 | 100.48 | 8.51 | 184 | 29 | 132 | 142 | 17 | 87 | 22 | 86 | 5 | 124 | 406 | 27 | 162 | 19 | 425 | 32 | 70 | 34 | 12 | 12 | 2 |
| SD | 2.49 | 0.04 | 0.64 | 0.24 | 0.02 | 0.52 | 2.23 | 0.14 | 0.22 | 0.03 | - | - | 320.68 | 4.08 | 16.50 | 11.26 | 1.40 | 10.44 | 12.06 | 9.72 | 2.45 | 8.99 | 57.18 | 1.51 | 8.51 | 5.52 | 64.17 | 3.64 | 5.81 | 1.91 | 2.57 | 2.07 | 0.89 |

Table 4. - Chemical composition of major, minor (expressed as oxide wt.%), and trace elements (expressed as ppm) of the terrestrial samples.

| Samples | $SiO_2$ | $TiO_2$ | $Al_2O_3$ | $Fe_2O_3$ | MnO | MgO | CaO | $Na_2O$ | $K_2O$ | $P_2O_5$ | Tot | L.O.I. | S | Sc | V | Cr | Co | Ni | Cu | Zn | Ga | Rb | Sr | Y | Zr | Nb | Ba | La | Ce | Nd | Pb | Th | U |
|---|---|---|---|---|---|---|---|---|---|---|---|---|---|---|---|---|---|---|---|---|---|---|---|---|---|---|---|---|---|---|---|---|
| TSS1 | 56.35 | 0.89 | 16.34 | 7.28 | 0.11 | 3.39 | 9.64 | 1.53 | 2.82 | 0.15 | 98.50 | 9.62 | 5705 | 25 | 149 | 140 | 22 | 97 | 80 | 119 | 12 | 127 | 699 | 31 | 196 | 15 | 359 | 38 | 82 | 31 | 29 | 16 | 10 |
| TSS3 | 54.56 | 0.78 | 15.72 | 6.43 | 0.09 | 3.66 | 13.66 | 1.86 | 2.62 | 0.21 | 99.59 | 6.28 | 2006 | 30 | 135 | 148 | 21 | 95 | 48 | 111 | 11 | 124 | 454 | 24 | 159 | 10 | 340 | 35 | 78 | 29 | 11 | 13 | 7 |
| TSS4 | 62.59 | 0.93 | 17.46 | 7.17 | 0.10 | 2.50 | 3.32 | 2.20 | 2.99 | 0.15 | 99.41 | 12.93 | 4296 | 13 | 142 | 142 | 24 | 84 | 44 | 111 | 14 | 136 | 165 | 31 | 264 | 13 | 376 | 40 | 87 | 41 | 35 | 22 | 18 |
| TSS5 | 58.61 | 0.83 | 16.14 | 6.54 | 0.10 | 3.10 | 8.82 | 1.93 | 3.02 | 0.17 | 99.26 | 8.14 | 1337 | 20 | 133 | 122 | 18 | 71 | 56 | 106 | 12 | 144 | 312 | 29 | 206 | 18 | 374 | 33 | 76 | 31 | 26 | 20 | 7 |
| TSS6 | 55.69 | 0.90 | 16.91 | 7.28 | 0.11 | 3.89 | 9.31 | 2.02 | 2.86 | 0.18 | 99.15 | 15.67 | 6610 | 25 | 162 | 141 | 18 | 107 | 66 | 116 | 12 | 121 | 297 | 30 | 213 | 4 | 331 | 30 | 73 | 34 | 20 | 19 | 30 |
| TSS8 | 54.24 | 0.94 | 16.14 | 8.00 | 0.13 | 4.22 | 10.83 | 1.27 | 2.75 | 0.23 | 98.75 | 14.69 | 7738 | 26 | 144 | 164 | 32 | 138 | 65 | 139 | 12 | 116 | 411 | 30 | 198 | 7 | 313 | 29 | 66 | 37 | 34 | 22 | 27 |
| TSS11 | 47.45 | 0.75 | 14.18 | 6.34 | 0.15 | 5.60 | 19.80 | 1.47 | 2.18 | 0.22 | 98.14 | 19.68 | 16850 | 41 | 143 | 133 | 20 | 101 | 51 | 108 | 6 | 84 | 560 | 25 | 155 | 6 | 220 | 29 | 72 | 37 | 8 | 14 | 18 |
| TSS12 | 52.30 | 0.92 | 17.86 | 7.47 | 0.09 | 5.48 | 10.56 | 1.68 | 2.67 | 0.23 | 99.26 | 19.72 | 5484 | 26 | 188 | 149 | 24 | 107 | 51 | 128 | 14 | 110 | 386 | 30 | 190 | 3 | 330 | 38 | 82 | 38 | 38 | 22 | 47 |
| TSS13 | 55.36 | 0.75 | 14.34 | 5.98 | 0.07 | 3.71 | 13.87 | 1.76 | 2.58 | 0.15 | 98.57 | 13.45 | 12305 | 30 | 127 | 129 | 16 | 72 | 52 | 100 | 7 | 108 | 536 | 25 | 164 | 7 | 310 | 33 | 69 | 33 | 18 | 16 | 18 |
| TSS14 | 53.87 | 0.78 | 15.42 | 6.57 | 0.11 | 4.99 | 13.87 | 1.27 | 2.44 | 0.19 | 99.51 | 6.93 | 702 | 29 | 140 | 152 | 22 | 101 | 59 | 116 | 12 | 87 | 477 | 25 | 149 | 14 | 314 | 28 | 64 | 27 | 23 | 16 | 6 |
| TSS15 | 53.19 | 0.89 | 16.89 | 7.56 | 0.17 | 3.99 | 13.22 | 1.14 | 2.40 | 0.22 | 99.67 | 11.58 | 811 | 31 | 153 | 174 | 27 | 134 | 51 | 129 | 10 | 94 | 567 | 30 | 182 | 14 | 382 | 32 | 74 | 34 | 22 | 18 | 11 |
| TSS19 | 52.44 | 0.99 | 18.76 | 8.31 | 0.14 | 4.21 | 10.78 | 2.11 | 2.81 | 0.36 | 100.91 | 2.48 | 188 | 29 | 195 | 142 | 28 | 64 | 45 | 110 | 18 | 108 | 492 | 29 | 206 | 31 | 777 | 53 | 111 | 47 | 30 | 20 | 3 |
| TSS23 | 55.30 | 0.82 | 15.55 | 6.25 | 0.10 | 5.53 | 12.95 | 1.10 | 2.01 | 0.20 | 99.81 | 13.74 | 4610 | 28 | 148 | 132 | 20 | 89 | 23 | 107 | 3 | 83 | 314 | 26 | 180 | 2 | 254 | 32 | 69 | 36 | 25 | 18 | 27 |
| TSS24 | 58.74 | 0.97 | 19.21 | 7.81 | 0.14 | 2.28 | 5.26 | 2.46 | 2.93 | 0.16 | 99.96 | 3.46 | 353 | 17 | 138 | 104 | 23 | 51 | 31 | 118 | 13 | 127 | 259 | 28 | 166 | 15 | 533 | 41 | 86 | 41 | 22 | 15 | 4 |
| TSS27 | 53.78 | 0.79 | 15.49 | 6.34 | 0.10 | 3.06 | 16.60 | 1.67 | 2.46 | 0.20 | 100.49 | 7.38 | 3275 | 32 | 140 | 145 | 16 | 86 | 35 | 102 | 6 | 110 | 516 | 27 | 172 | 11 | 299 | 37 | 76 | 37 | 12 | 11 | 11 |
| TSS28 | 53.27 | 0.80 | 15.53 | 6.14 | 0.09 | 3.33 | 15.34 | 1.55 | 2.82 | 0.22 | 99.09 | 10.25 | 7325 | 28 | 137 | 139 | 16 | 90 | 26 | 119 | 7 | 122 | 512 | 25 | 167 | 6 | 298 | 29 | 66 | 36 | 11 | 11 | 15 |
| TSS29 | 58.98 | 0.81 | 13.56 | 6.87 | 0.08 | 4.48 | 10.05 | 1.90 | 2.49 | 0.16 | 99.38 | 7.84 | 5598 | 25 | 124 | 394 | 24 | 258 | 37 | 93 | 2 | 107 | 300 | 23 | 169 | 4 | 267 | 25 | 53 | 32 | 11 | 11 | 7 |
| TSS30 | 53.42 | 0.72 | 14.15 | 5.46 | 0.09 | 3.76 | 16.44 | 2.06 | 2.33 | 0.19 | 98.62 | 12.48 | 12104 | 28 | 127 | 128 | 19 | 76 | 26 | 90 | 4 | 97 | 390 | 25 | 162 | 9 | 285 | 32 | 67 | 34 | 7 | 12 | 9 |
| TSS31 | 57.88 | 0.72 | 14.68 | 5.95 | 0.07 | 5.22 | 9.97 | 2.03 | 1.94 | 0.12 | 98.58 | 14.71 | 12682 | 21 | 143 | 101 | 17 | 64 | 22 | 76 | 2 | 86 | 278 | 39 | 210 | 2 | 336 | 61 | 116 | 52 | 24 | 23 | 58 |
| SD | 3.28 | 0.09 | 1.56 | 0.78 | 0.03 | 1.00 | 3.95 | 0.38 | 0.32 | 0.05 | - | - | 4800.55 | 6.04 | 18.61 | 61.27 | 4.41 | 44.44 | 16.05 | 14.65 | 4.60 | 18.04 | 134.43 | 3.71 | 27.72 | 7.06 | 121.54 | 8.80 | 15.23 | 6.01 | 9.45 | 4.08 | 14.76 |

Table 5. - Chemical composition of major, minor (expressed as oxide wt.%), and trace elements (expressed as ppm) of the terrestrial samples.

The results of the statistical treatment of chemical by principal component analysis are reported in figure 15. and figure 16. as the score plot and plot of component weights. In the score plot, PC2 in most of the samples are almost similar or close to another and there is not a big difference between underwater and terrestrial samples however samples differ along the Principal Component 1 (PC1), which accounts for 51% of the total variance. All terrestrial samples are concentrated in the negative part of PC1, with enrichment in scandium (Sc). Among the chemical elements, $Al_2O_3$, $Fe_2O_3$ and $TiO_2$ are the variables with the highest weight for positive values. The underwater samples that are characterized by negative values on PC1, including samples TSS-11, TSS-13, TSS-14, TSS-27, TSS-28, and TSS-30 show much greater chemical similarity to the terrestrial samples from Apani and Giancola. On contrary, samples located towards the positive values of PC1 tend to diverge from the terrestrial samples.

Despite there is not a definite overlap between the terrestrial samples and those received underwater at Torre Santa Sabina, the fact that the underwater samples show a continuity and do not isolate forming a defined separate cloud in the score plot (Figure 15), indicate that the samples share a common raw material for their production and that the small differences are related possibly to post-depositional alteration which affect the other elements not considered in this statistical treatment. To solve this issue, statistical treatment should be performed on ratio between the chemical elements and that probably representing the most stable one, defined using a variation matrix (not purpose of this thesis).

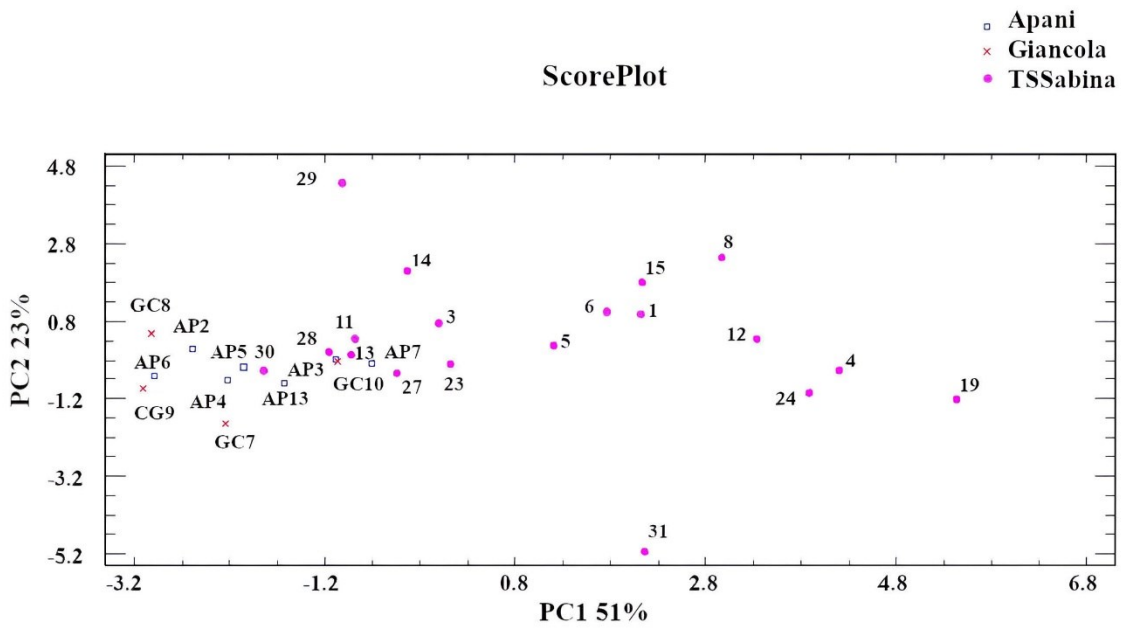


Figure 15. ─ Scoreplot of PC1 and PC2 for the studied samples, performed on a subset of chemical data. PC1 and PC2 explaining 51% and 23% of the total variance, respectively.

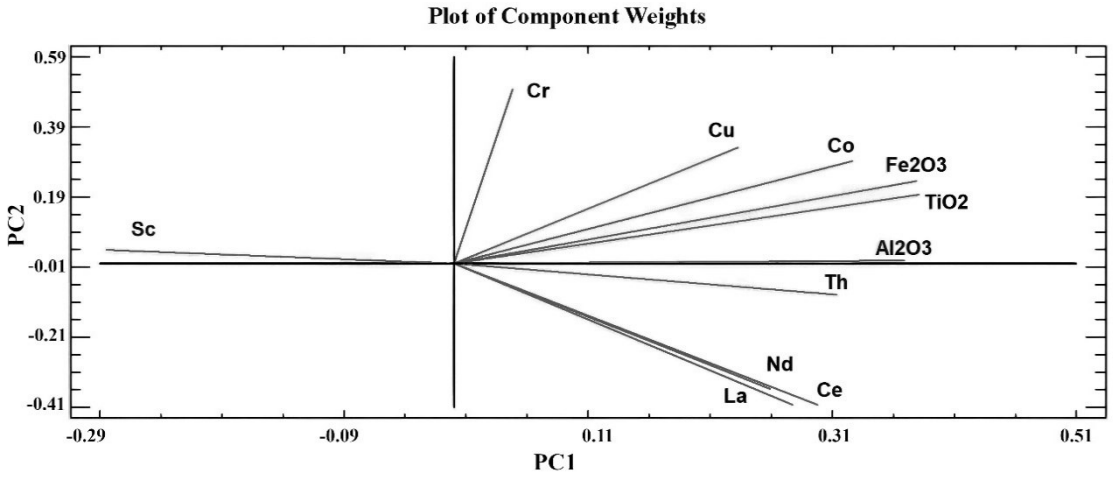


Figure 16. ─ Plot of component weights for studied samples, using only stable elements. PC1 and PC2 explaining 51% and 23% of the total variance, respectively.

## 6.5 SCANNING ELECTRON MICROSCOPE

SEM provides more in depth- observation of the microstructural features in ceramics, offering useful insights into the processes of alteration, especially in underwater samples. In marine environments, ceramics undergo chemical reactions that alter their composition, structure, and appearance. In general, seawater contains various salts of sodium, magnesium, calcium, potassium, and strontium as cations along with chloride, sulfate, bromide, and bicarbonate as anions. These salts penetrate ceramic pores leading to salt crystallization, a major cause of decay in such environments. In addition to precipitation in pores, certain elements may leach out or become concentrated within the ceramic (López-Arce et al., 2013; Maritan, 2020). In the samples from Torre Santa Sabina, SEM analysis revealed significant secondary mineral deposition including the formation of secondary calcite and pyrite crystals.

One of the most important alterations observed by SEM imaging in the samples is the deposition of secondary calcite. The abundance of calcium in seawater enables calcite to crystallize within the pores and fractures of the ceramic matrix. Figure 17 (A) show a fossil trace partially filled by secondary calcite, revealing the distribution and extent of calcium carbonate crystallization within the ceramic structure.

In addition to calcite, the formation of pyrite ($FeS_2$) microcrystals was observed in several samples. Sulfur availability in the sea encourages the growth of pyrite crystals within the ceramic material. SEM microphotographs in figure 17 (B) show pyrite crystals filling the pores present in the ceramic body.

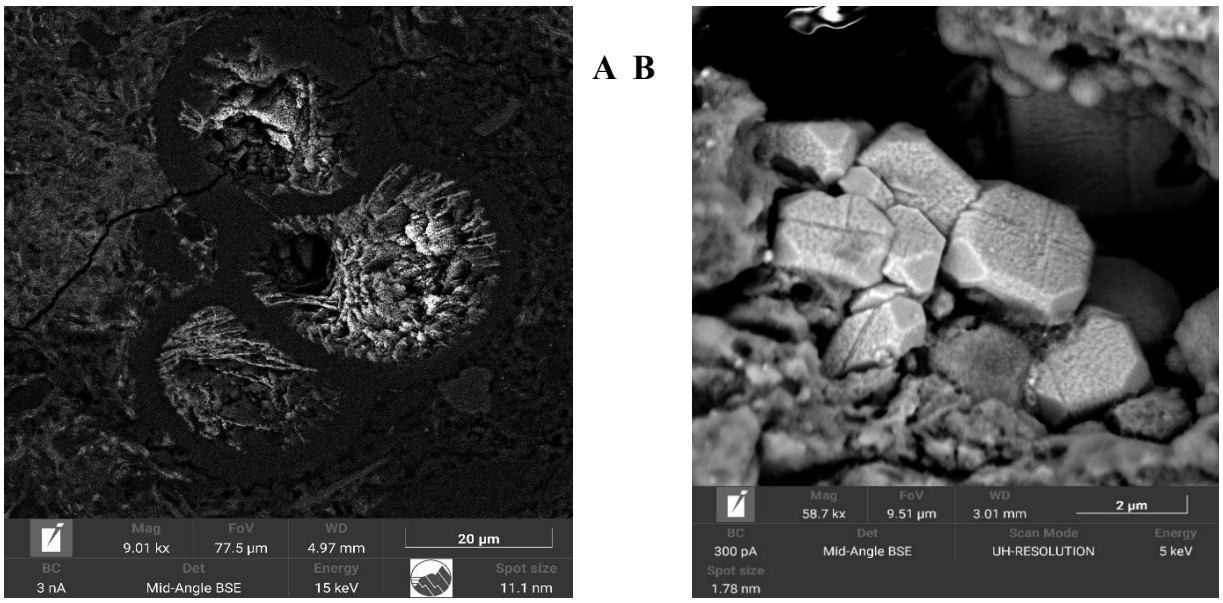


Figure 17. ─ SEM-BSE image of: (A)a cavity of a fossil (probably a foraminifer) filled by secondary calcite (sample AP3); (B) euhedral pyrite crystals precipitated into a pore (sample TSS-1)

# 7 Discussion

This study compares amphorae from the underwater archaeological site of Torre Santa Sabina with those discovered in two nearby ancient production centers, Apani and Giancola. The analysis involved a range of techniques, including macroscopic, petrographic, mineralogical, and chemical methods. However, the chemical and mineralogical transformations that occur in submerged ceramics due to post-depositional processes make it more difficult to identify and interpret the original characteristics of the clay. These differences were carefully considered during the comparison process.

By integrating chemical and mineralogical results with macroscopic observations, thin section studies under polarized light and historical-archaeological data, valuable insights have been gained into the composition and potential provenance of the underwater amphorae.

Samples from Apani and Giancola, despite showing some heterogeneity in the texture of the ceramic bodies, are compositionally very similar and attributable to the same supply basins for production. These findings are consistent with previous studies (Olcese, 1994; Benquet & Capelli 2018) which highlight a clear correlation between the compositional and petrographic characteristics of the ceramic fragments and the geo-lithological context of the region. More in detail, they presence of microfossil clearly indicates that the raw material can come from the base of the formations of sands and conglomerates outcropping in the area of Giancola and Apani, dated to the Pleistocene. This base level consists in yellow-grayish marly clays Vezzani (1968), containing various types of fossils, among which abundant foraminifera.

The cargo discovered in the TSS4 area, from which the underwater samples were taken, shows heterogeneous characteristics. However, by combining the analytical results, compositional similarities emerge between fragments from Torre Santa Sabina and those from Apani and Giancola, suggesting these sites as potential production centers for some of the amphorae found in the underwater context.

The macroscopic examination allowed a preliminary grouping of samples preliminary grouping based on color, texture, thickness and porosity which was consistent with the classification made through petrographic analysis.

Petrographic analysis revealed compositional differences, particularly in the clay matrix: some samples are rich in carbonate, while others are of more terrigenous nature. The presence of the same fossil microfauna traces in both terrestrial and underwater samples suggests that the raw materials were sourced from marine-component clay.

The XRPD analysis was essential to distinguish between the primary mineralogical phases originally present in the clay raw material and those formed during the firing process, allowing the firing temperature to be estimated. Other post-depositional secondary phases formed during the burial of the pottery on the seabed have also been identified.

Firing temperatures can often be inferred from the presence of specific mineral assemblages. For example, in this case, the identification of pyroxenes, which are not primary minerals but are formed during firing starting at around 850°C, and muscovite, persisting up to 950°C before completely decomposing, can be considered as the main indicators for the estimation of the firing temperature. The mineralogical associations in the terrestrial samples suggest that the clay was fired at temperatures between 800°C and 950°C. Samples AP-2 and GC-8 are characterized by the absence of pyroxenes and hematite and mainly composed of muscovite and quartz, suggesting a lower firing temperature around 800°C. For underwater samples a firing temperature range between 850° C and 950° C was estimated except for sample 19 for which, being composed mainly of anorthite-rich plagioclase and pyroxenes, a temperature exceeding 950°C was supposed. On the other hand, sample 4 shows a composition that suggests a lower firing temperature, around 800°C.

Secondary phases such as magnesium-calcite, gypsum and pyrite present in the majority of underwater samples, and absent in terrestrial samples, can be considered as post-depositional phases formed due to the interaction between the underwater environment and the ceramic material.

The chemical analysis shows that, despite some differences related to the precipitation of secondary phases in the underwater samples (especially pyrite and magnesium calcite), show similarity with those form Apani and Giancola, indicating that at least part of them can come for this production area.

As mentioned previously, all samples are from cargo TSS4 in area B, but the results suggest the possibility that not all amphorae may originate from the same shipment. The underwater

samples of the Adriatic ovoid type show the closest resemblance to Apani production, particularly aligning with samples AP-5 and AP-7. These samples exhibit variability in textural characteristics, grain size distribution, and carbonate content, along with the presence of fossils. Similarly, fragments of the Lamboglia 2 type are in general comparable to both Apani and Giancola samples in terms of chemical composition and mineralogy, with some variability primarily in grain size distribution. Sample TSS-19, of the Dressel 2-4 type, exhibits characteristics suggesting a different provenance, likely from the Tyrrhenian region, while sample TSS-24 of the African type, aligns with its typological classification, displaying features that confirm a distinct origin, likely from North African production.

These findings could result from various scenarios: a foreign ship depositing near a sunken local cargo, the dislocation of amphorae from their original cargo due to underwater dynamics or a local ship returning home with a mix of local and foreign containers. Archaeological data support the hypothesis of the diverse origins of amphorae. However, further analysis and comparison with specimens from certified production centers across the Mediterranean are necessary to validate these hypotheses.

# 8 Conclusion

Most of the amphorae analyzed in this study are attributed to local production, highlighting the need to further explore the activity of the Apani and Giancola kilns to better understand their production methods. The discovery of two amphorae from two different Mediterranean regions, probably Campania and North Africa, adds complexity to the provenance studies and opens up interesting possibilities for future research.

These results help us to deeply understand the history of the underwater site of Torre Santa Sabina and expand our knowledge about the trade routes linked to this important Mediterranean port.

Further research will be essential to confirm these initial observations offering a clearer view of the archaeological context and the historical importance of Torre Santa Sabina.

# 9 References


ANTONAZZO A., 2014, *Torre S. Sabina. I Materiali Da Recupero Subacqueo (1972-1983): Distribuzione Spaziale ed Ipotesi Interpretative*, "Atti Del III Convegno di Archeologia Subacquea (Manfredonia 4-6 October 2007)"; pp.181-197.

ARTIOLI G. 2010, *Scientific Methods and Cultural Heritage: An Introduction to the Application of Materials Science to Archaeometry and Conservation Science*, Oxford University Press.

AURIEMMA R., 2014, *Torre S. Sabina. (Carovigno, BR). L'Approdo Ritrovato*, "Atti Del III Convegno di Archeologia Subacquea (Manfredonia 4-6 October 2007)"; pp.151-177.

Benquet, L. & Capelli, C. (2018). *The italic ovoid amphorae in the Toulouse area at the end of the Iron Age (Midi-Pyrénées, France)*, Actes de la table-ronde tenue à Séville (10-11 déc. 2015), Dec 2015, Séville, Spain. pp.274-297.

CARRE M-B., MONSIEUR P., PESAVENTO MATTIOLI S. 2014, *Transport Amphorae Lamboglia 2 and Dressel 6A: Italy and/or Dalmatia? Some Clarifications.* "Journal of Roman Archaeology", 27, 417-428; doi:10.1017/S1047759414001329.

JOHNSTON A., GRACE V., 2015, *Amphorae and Amphora Stamps, Greek*, "Oxford Classical Dictionary", https://doi.org/10.1093/acrefore/9780199381135.013.380.

LI. F., YAN J., CHEN Z., OGG J., TIAN L., KORNGREEN D., LIU K., MA Z., WOODS A. 2015, *Global Oolite Deposits Across the Permian–Triassic Boundary: A Synthesis and Implications for Palaeoceanography Immediately after the End-Permian Biocrisis* "Earth Science Review", 149, 163-180, https://doi.org/10.1016/j.earscirev.2014.12.006.

LOPEZ-ARCE P., ZORNOZA-INDART A., GOMEZ-VILLALBA L., PÉREZ-MONSERRAT E., ALVAREZ DE BUERGO M., VIVAR G., FORT R. 2013, *Archaeological Ceramic Amphorae from Underwater Marine Environments: Influence of Firing Temperature on Salt Crystallization Decay*, "Journal of the European Ceramic Society", 33, 10, 2031-2042; https://doi.org/10.1016/j.jeurceramsoc.2013.03.009.

MARITAN L. 2020, *Ceramic abandonment. How to recognise post-depositional transformations*, "Archaeological and Anthropological Science", 12, 199; https://doi.org/10.1007/s12520-020-01141-y.

MARITAN L. 2020, *Ceramics Investigation: Research Questions and Sampling Criteria*, "Archaeological and Anthropological Science", 12, 202; https://doi.org/10.1007/s12520-020-01128-9.

MARITAN L., Ganzarolli G., Antonelli F., Rigo M., Kapatza A., Bajnok K., Coletti C., Mazzoli C., Lazzarini L., P. Vedovetto, Chavarria Arnau A., 2021. *What kind of calcite? Disclosing*

*the origin of sparry calcite temper in ancient ceramics*. "Journal of Archaeological Science", 129, 105358; https://doi.org/10.1016/j.jas.2021.105358.

MARITAN L., HOLAKOOEI P., MAZZOLI C. 2015, *Cluster Analysis of XRPD Data in Ancient Ceramics: What for?,* "Applied Clay Science", 114, 540-549; https://doi.org/10.1016/j.clay.2015.07.016.

MARITAN L. 2024, *Ceramics: Chemical and Petrographic Analysis*, NIKITA E., REHREN T. (eds.), Encyclopedia of Archaeology (Second Edition), v. 2B, pp. 386-397, https://doi.org/10.1016/B978-0-323-90799-6.00020-3.

MARTAN L. 2019, *Archaeo-Ceramics 2.0: Investigating Ancient Ceramics Using Modern Technological Approaches*, "Archaeological and Anthropological Science", 11, 5085-5093, https://doi.org/10.1007/s12520-019-00927-z.

OLESON J.P., 2012, *The Oxford Handbook of Engineering and Technology in the Classical World*. Oxford University Press.

Olcese G., Le anfore di Giancola (Br): archeologia, archeometria, storia, in: Ceramica romana e archeometria. Lo stato degli studi, in: Atti del Convegno, a cura di G. Olcese, Castello di Montegufoni (Firenze) 26-27 aprile 1993, Quaderni del Dipartimento di Archeologia e Storia dell'Arte dell'Università di Siena, All'Insegna del Giglio, Firenze 1994, pp. 277-285 (con D. Manacorda e H. Patterson), ISBN: 88-7814-010-4.

OPDEBEECK J. 2005, *Shipwrecks and Amphorae: Their Relationship with Trading Routes and the Roman Economy in the Mediterranean*, PhD dissertation, University of Southampton.

PALAZZO P., 1989, *Le Anfore di Apani (Brindisi),* Amphores Romaines et Histoire Économique". Dix ans de recherche. Actes du colloque de Sienne (22-24 mai 1986): Publications de l' École Française de Rome, 114, 548-553.

PALLECCHI S., MANACORDA D., 2012, *Le Fornici Romane di Giancola (Brindisi),* Ed-puglia srl.

QUINN P. S. 2013, *Ceramic Petrography: The Interpretation of Archaeological Pottery & Related Artefacts in Thin Section,* Archaeopress.

QUINN P. S. 2022, *Thin Section Petrography Geochemistry and Scanning Electron Microscopy of Archaeological Ceramics*, Archaeopress.

RUPPÉ C.V., BARSTAD J. F. 2002, *International Handbook of Underwater Archaeology*, Kluwer Academic / Plenum Publishers.

SMITH L. 2002, *A tutorial on Principal Components Analysis*.

TONIOLO A. 1995, *Anfore in Area Padana Come Riconoscerle*, Linea AGS.

Vezzani L. 1968, *Note illustrative alla carta geologica d'Italia alla scala* 1:100.000. Foglio 191 Ostuni. Poligrafica e Cartevalori Ercolano (Napoli), pp.1-27.

Warr LN 2021, *IMA–CNMNC approved mineral symbols*. “Mineralogical Magazine ”, 2021;85(3):291-320; doi:10.1180/mgm.2021.43.

# 10 Appendix

Petrographic analysis based on groups:

| Underwater samples | Ca matrix | Fe matrix | Clay pellet | Secondary calcite | Fossils | Carbonate | Flint |
|---|---|---|---|---|---|---|---|
| Group 1[1] | X | | Not available | Present | Present | Present | Present |
| Group 2[2] | X | X | Present | Present | Present | Present | Present |
| Group 3[3] | X | X | Present | Present | Present | Present | Present |
| Group 4[4] | | X | Present | Present | Present | Present | Present |
| Group 5[5] | | X | Not available | Not available | Not available | Not available | Not available |

| Terrestrial samples | Ca matrix | Fe matrix | Clay pellet | Secondary calcite | Fossils | carbonate | Flint |
|---|---|---|---|---|---|---|---|
| Group 1[6] | X | | Not available | Present | Present | Present | Present |
| Group 2[7] | | X | Present | Present | Present | Present | Not available |

[1] TSS-11, TSS-23, TSS-27, TSS-28, TSS-29, TSS-30, TSS-31
[2] TSS-5, TSS-8, TSS-12, TSS-13
[3] TSS-3, TSS-14, TSS-15
[4] TSS-1, TSS-4, TSS-6
[5] TSS-19, TSS-24
[6] AP-1, AP-4, GC-7, GC-8, GC-10
[7] AP-2, AP-3, AP-5, AP-6, AP-7, GC-9

Sample: **AP- 1** Site: Apani

| Fragment | Type | Fresh-cut surface |
|---|---|---|

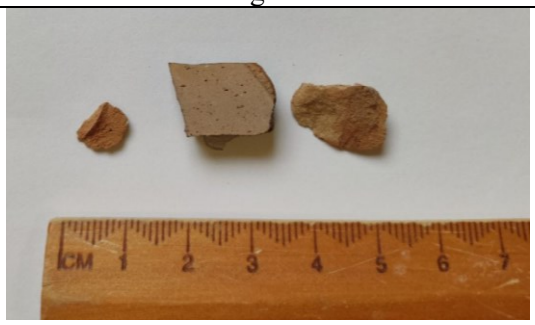


Ovoidal Adriatic type, 10mm thickness, beige color, presence of small inclusions, small porosities all over in fine texture.

| Thin section (x5, XPL) | Microscopic characteristics |
|---|---|

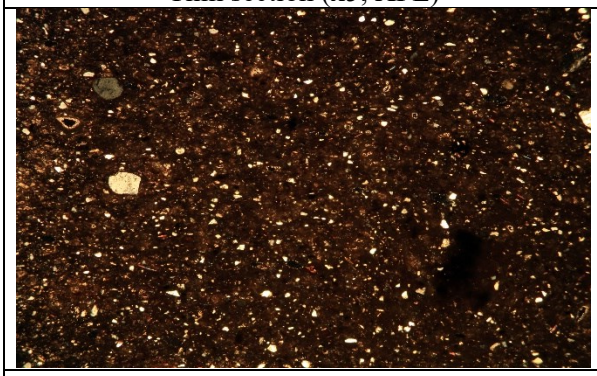

| | | | |
|---|---|---|---|
| Color | Brownish | Clay pellets | N/A |
| Inclusion abundance | 5 -7 % | Carbonate mudstone | Present |
| Matrix | Ca | Flints | N/A |
| Inclusion size | Small | Other minerals | Quartz – Muscovite – Biotite - Plagioclase – K-feldspar – Secondary calcite |
| Fossils trace | Present | | |

XRPD

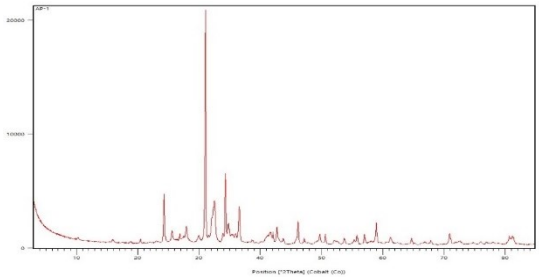

| Qz | Mus/Ill | Bt | Kfs | Pl | Hem | Px | Cal | Geh | Wo | Hyn | Temp °C |
|---|---|---|---|---|---|---|---|---|---|---|---|
| x | x | | x | x | x | x | x | x | x | | 900°-950° |

XRF

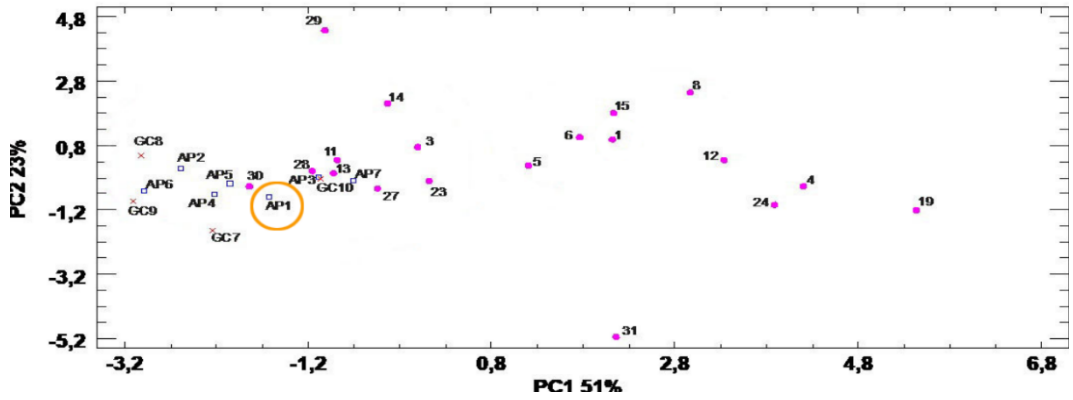

Sample: **AP- 2** Site: Apani

| Fragment | Type | Fresh-cut surface |
|---|---|---|

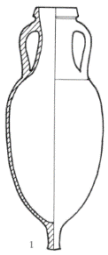


Apani I/Giancola II type, 9mm thickness, beige color, presence of inclusions such as quartz and red nodules. Fine texture with voids.

| Thin section (x5, XPL) | Microscopic characteristics |
|---|---|

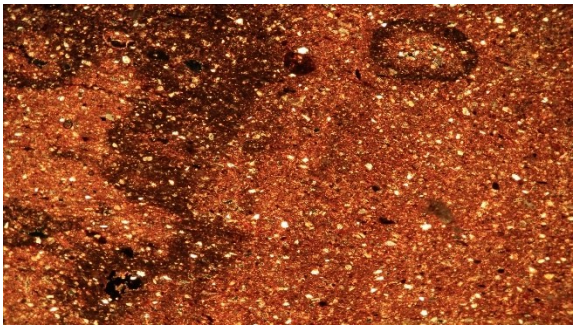

| | | | |
|---|---|---|---|
| Color | Reddish | Clay pellets | Present |
| Inclusion abundance | 5% | Carbonate mudstone | Present |
| Matrix | Fe | Flints | N/A |
| Inclusion size | Small | Other minerals | Quartz – Muscovite – Biotite – Plagioclase – Pyroxene |
| Fossils trace | Present | | |

XRPD

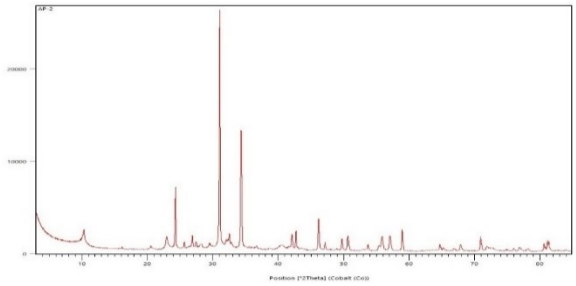

| Qz | Mus/Ill | Bt | Kfs | Pl | Hem | Px | Cal | Geh | Wo | Hyn | Temp °C |
|---|---|---|---|---|---|---|---|---|---|---|---|
| x | x | | x | x | x | x | x | | | | ~ 800° |

XRF

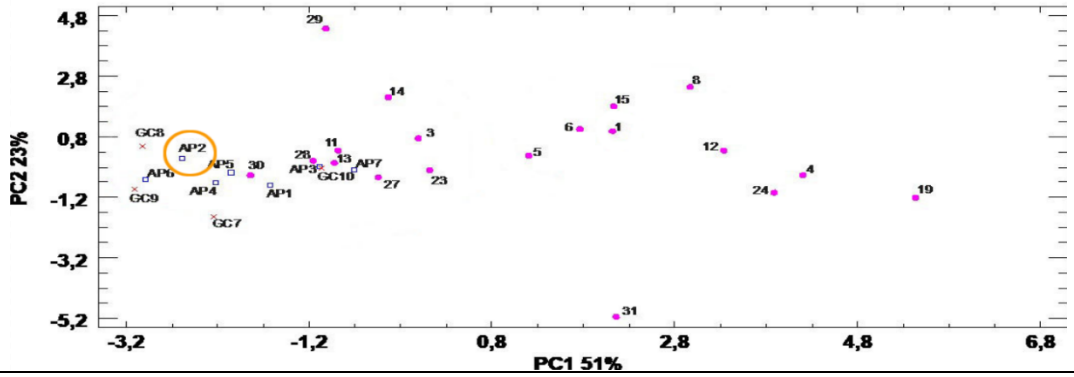

Sample: **AP- 3** Site: Apani

| Fragment | Type | Fresh-cut surface |
|---|---|---|

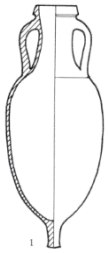


Apani I/Giancola II type, 5mm thickness, grayish beige color, presence of inclusions like red nodules, fine texture with porosity.

| Thin section (x5, XPL) | Microscopic characteristics |
|---|---|

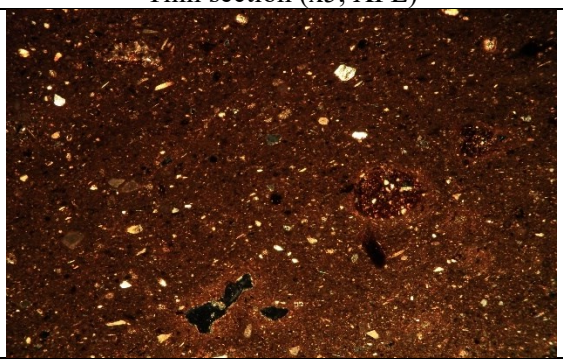

| | | | |
|---|---|---|---|
| Color | Reddish | Clay pellets | Present |
| Inclusion abundance | 5 – 7 % | Carbonate mudstone | Present |
| Matrix | Fe | Flints | N/A |
| Inclusion size | Small | Other minerals | Quartz – Muscovite – Biotite – Plagioclase – Secondary calcite |
| Fossils trace | Present | | |

XRPD

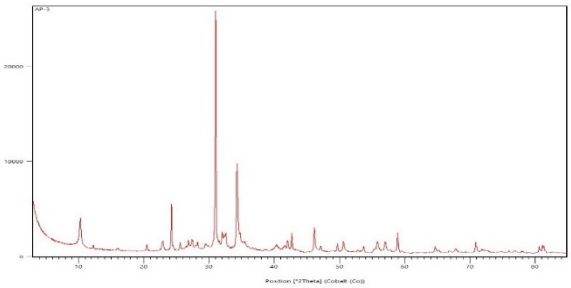

| Qz | Mus/Ill | Bt | Kfs | Pl | Hem | Px | Cal | Geh | Wo | Hyn | Temp °C |
|---|---|---|---|---|---|---|---|---|---|---|---|
| x | x | x | x | x | x | x | x | | | | 800-850° |

XRF

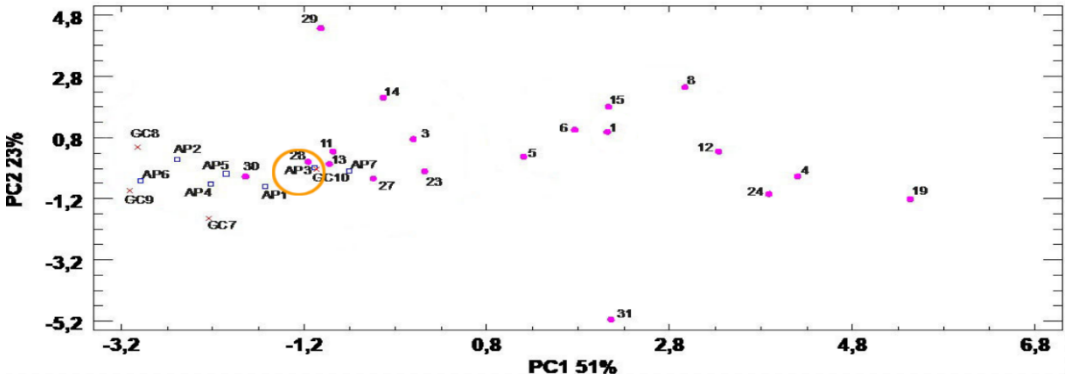

Sample: **AP- 4** Site: Apani

| Fragment | Type | Fresh-cut surface |
|---|---|---|

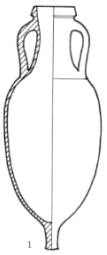

Apani I/Giancola II type, 7mm thickness, grayish beige color, fine compact texture, lower presence of inclusions.

| Thin section (x5, XPL) | Microscopic characteristics |
|---|---|

| | | | |
|---|---|---|---|
| Color | Brownish red | Clay pellets | N/A |
| Inclusion abundance | <5% | Carbonate mudstone | N/A |
| Matrix | Ca | Flints | N/A |
| Inclusion size | Small | Other minerals | Quartz – Muscovite – Biotite – Pyroxene – Secondary calcite |
| Fossils trace | Present | | |

XRPD

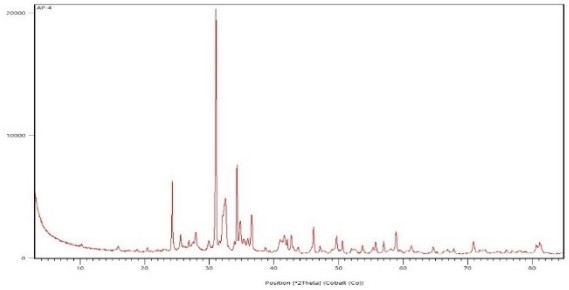

| Qz | Mus/Ill | Bt | Kfs | Pl | Hem | Px | Cal | Geh | Wo | Hyn | Temp °C |
|---|---|---|---|---|---|---|---|---|---|---|---|
| x | x | | x | x | x | x | x | x | | x | 900°-950° |

XRF

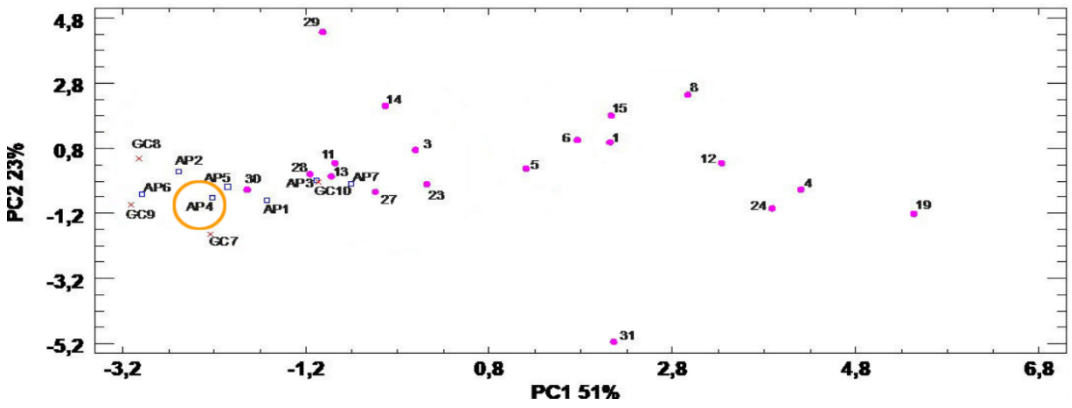

Sample: **AP- 5** Site: Apani

| Fragment | Type | Fresh-cut surface |
|---|---|---|

Ovoidal Adriatic type, 11mm thickness, grayish color, fine texture with porosity, inclusions are small on the surface.

| Thin section (x5, XPL) | Microscopic characteristics |
|---|---|

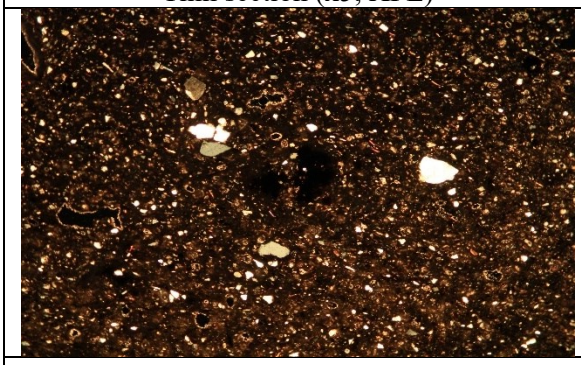

| | | | |
|---|---|---|---|
| Color | Reddish brownish | Clay pellets | Present |
| Inclusion abundance | 5% | Carbonate mudstone | N/A |
| Matrix | Fe | Flints | N/A |
| Inclusion size | Small | Other minerals | Quartz – Muscovite – Biotite – Plagioclase – Secondary calcite |
| Fossils trace | Hardly visible | | |

XRPD

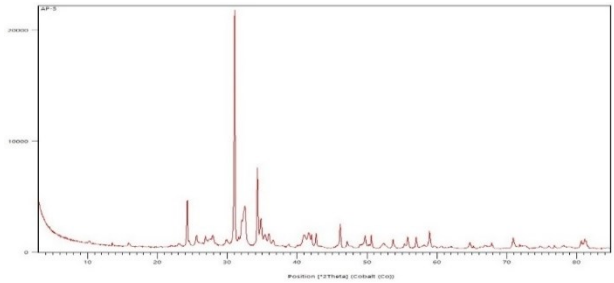

| Qz | Mus/Ill | Bt | Kfs | Pl | Hem | Px | Cal | Geh | Wo | Hyn | Temp °C |
|---|---|---|---|---|---|---|---|---|---|---|---|
| x | x | | x | x | x | x | x | | x | | 900°-950° |

XRF

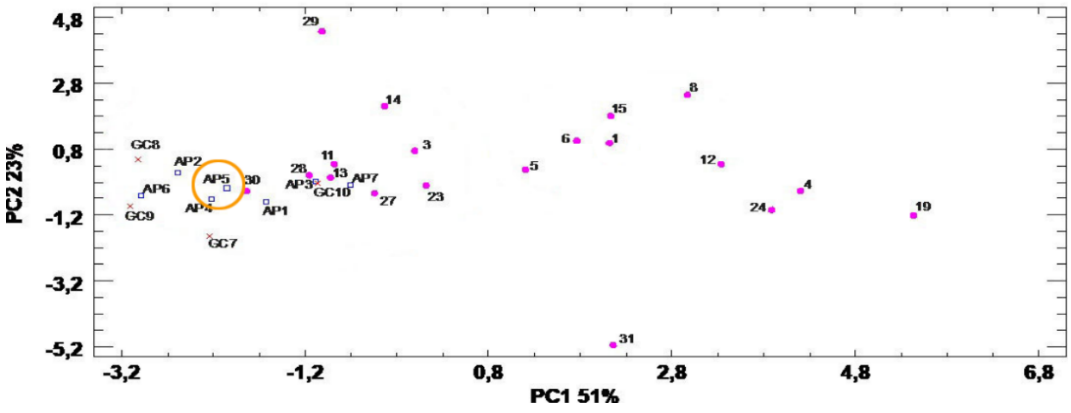

Sample: **AP- 6** Site: Apani

| Fragment | Type | Fresh-cut surface |
|---|---|---|

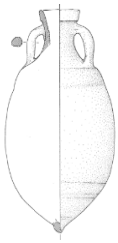

N/A

Ovoidal Adriatic type, beige color. 10mm thickness

| Thin section (x5, XPL) | Microscopic characteristics |
|---|---|

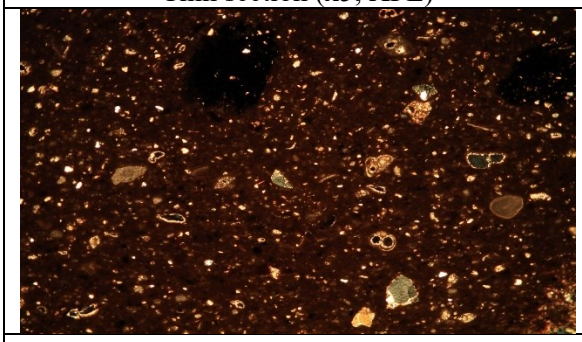

| | | | |
|---|---|---|---|
| Color | Reddish Brown | Clay pellets | Present |
| Inclusion abundance | 5% | Carbonate mudstone | Present |
| Matrix | Fe | Flints | N/A |
| Inclusion size | Small | Other minerals | Quartz – Muscovite – Biotite – Pyroxene – Plagioclase – Secondary calcite |
| Fossils | Present | | |

XRPD

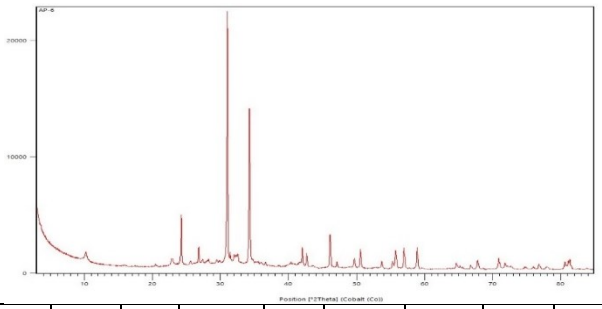

| Qz | Mus/Ill | Bt | Kfs | Pl | Hem | Px | Cal | Geh | Wo | Hyn | Temp °C |
|---|---|---|---|---|---|---|---|---|---|---|---|
| x | x | | x | x | x | x | x | | | | 850°-900° |

XRF

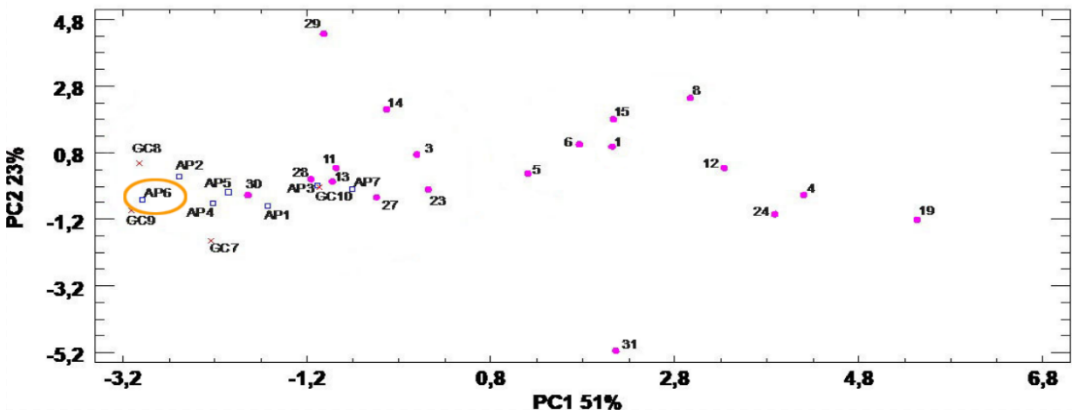

Sample: **AP- 7** Site: Apani

| Fragment | Type | Fresh-cut surface |
|---|---|---|


Ovoidal Adriatic type, 8mm thickness, yellowish color, fine compact texture with rare inclusions on the surface and least porosity.

Thin section (x5, XPL)

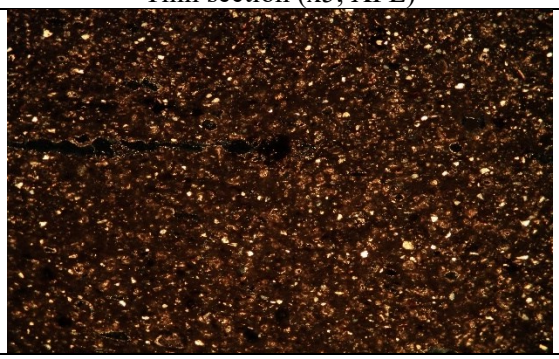

Microscopic characteristics

| | | | |
|---|---|---|---|
| Color | Reddish Brown | Clay pellets | Present |
| Inclusion abundance | 5% | Carbonate mudstone | Present |
| Matrix | Fe | Flints | N/A |
| Inclusion size | Small | Other minerals | Quartz – Muscovite – Biotite – Pyroxene – Secondary calcite |
| Fossils trace | Present | | |

XRPD

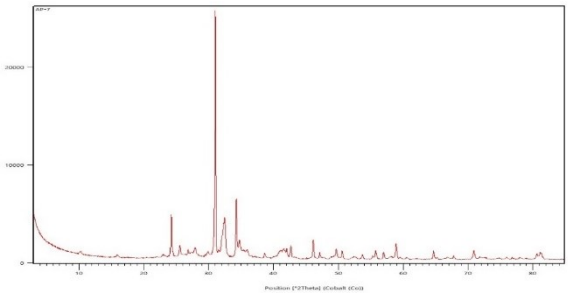

| Qz | Mus/Ill | Bt | Kfs | Pl | Hem | Px | Cal | Geh | Wo | Hyn | Temp °C |
|---|---|---|---|---|---|---|---|---|---|---|---|
| x | x | | x | x | x | x | x | | | | 850°-900° |

XRF

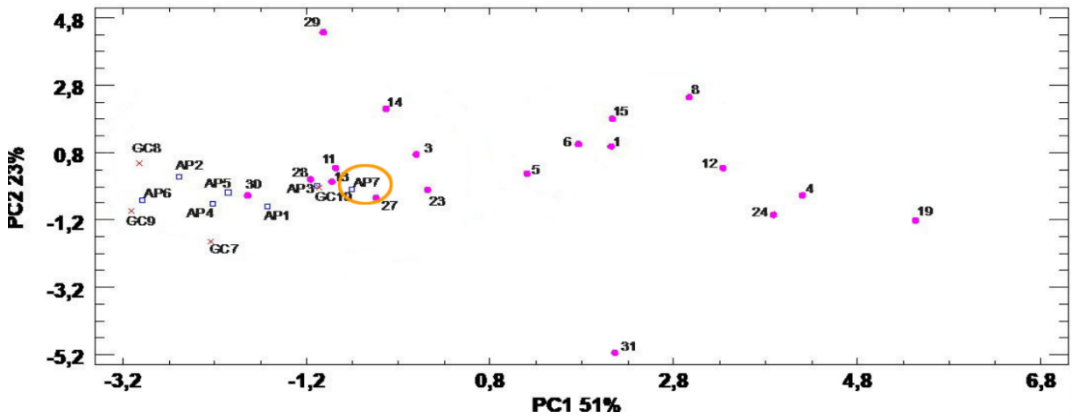

Sample: **GC- 7** Site: Giancola

| Fragment | Type | Fresh-cut surface |
|---|---|---|

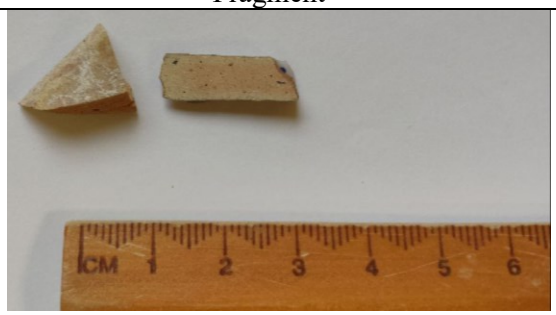

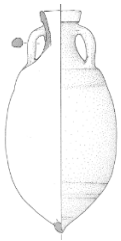

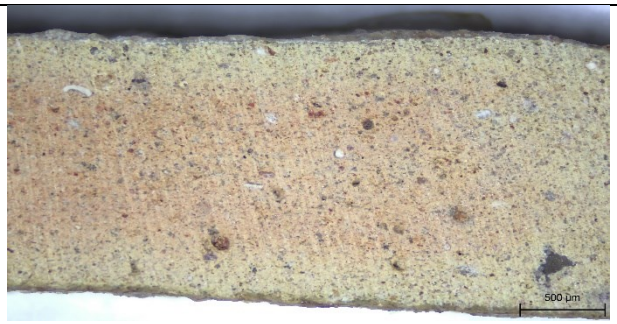


Ovoidal Adriatic type, 7mm thickness, beige color, presence of inclusions like quartz and nodules, fine texture with small porosity

| Thin section (x5, XPL) | Microscopic characteristics |
|---|---|

| | | | |
|---|---|---|---|
| Color | Brownish | Clay pellets | N/A |
| Inclusion abundance | 10% | Carbonate mudstone | Present |
| Matrix | Ca | Flints | Present |
| Inclusion size | Small | Other minerals | Quartz – Muscovite – Biotite – Pyroxene – Plagioclase – Secondary calcite |
| Fossils trace | Present | | |

XRPD

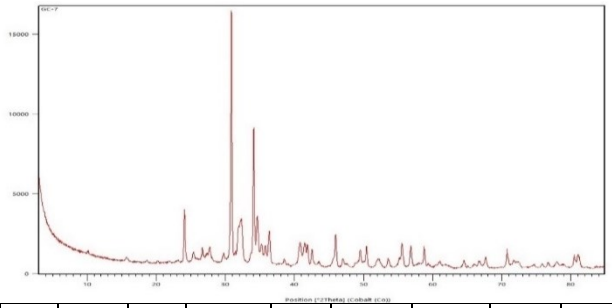

| Qz | Mus/Ill | Bt | Kfs | Pl | Hem | Px | Cal | Geh | Wo | Hyn | Temp °C |
|---|---|---|---|---|---|---|---|---|---|---|---|
| x | x | | x | x | x | x | x | x | | | 900°-950° |

XRF

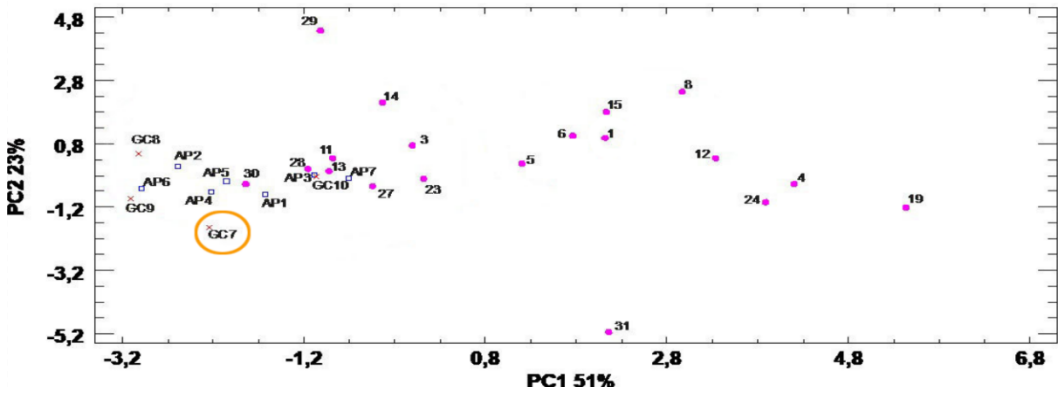

Sample: **GC- 8** Site: Giancola

| Fragment | Type | Fresh-cut surface |
|---|---|---|

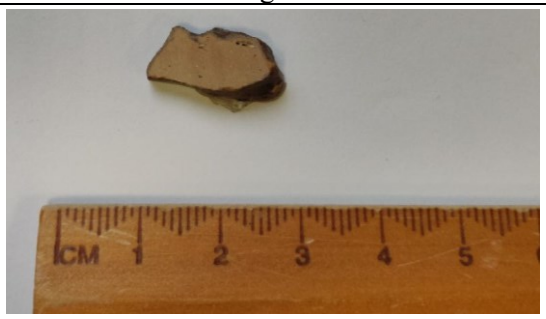

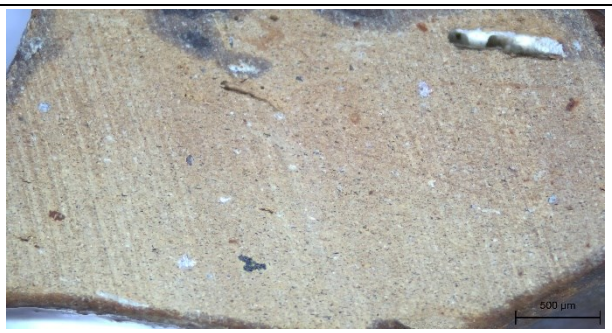

Ovoidal Adriatic type, 7mm thickness, beige color, fine texture with parallel voids, presence of inclusions such as quartz and red nodules.

| Thin section (x5, XPL) | Microscopic characteristics |
|---|---|

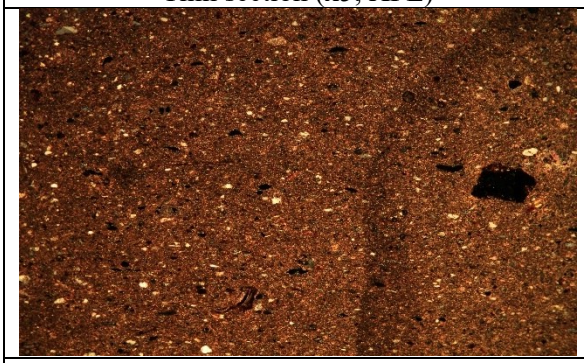

| | | | |
|---|---|---|---|
| Color | Brownish red | Clay pellets | N/A |
| Inclusion abundance | <5% | Carbonate mudstone | N/A |
| Matrix | Ca | Flints | N/A |
| Inclusion size | Small | Other minerals | Quartz – Muscovite – Biotite – Secondary calcite |
| Fossils trace | Present | | |

XRPD

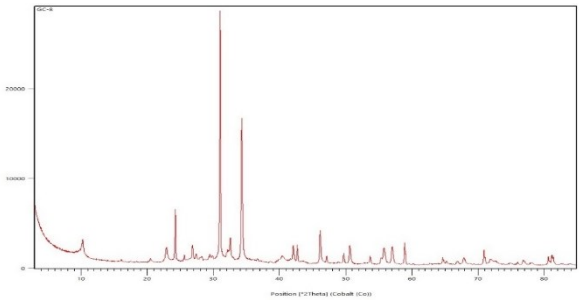

| Qz | Mus/Ill | Bt | Kfs | Pl | Hem | Px | Cal | Geh | Wo | Hyn | Temp °C |
|---|---|---|---|---|---|---|---|---|---|---|---|
| x | x | | x | x | | x | x | | | x | ~ 800° |

XRF

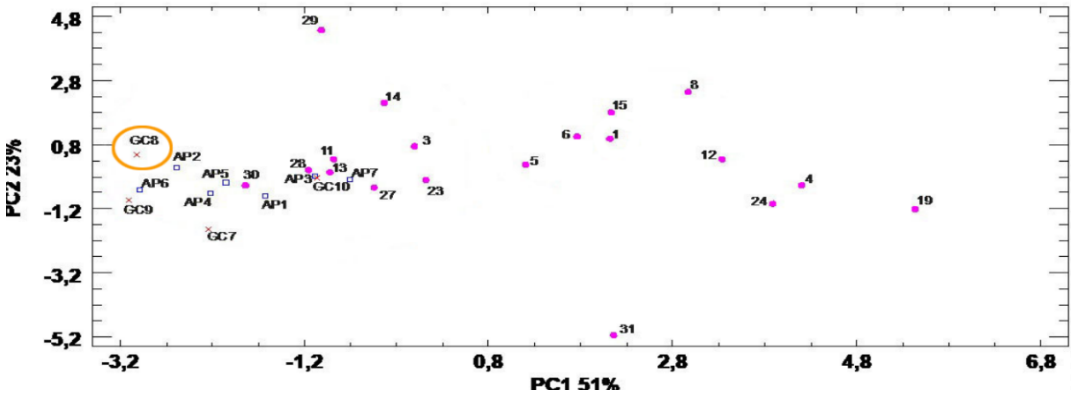

Sample: **GC -9** Site: Giancola

| Fragment | Type | Fresh-cut surface |
|---|---|---|

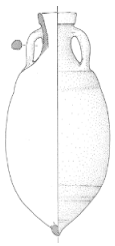

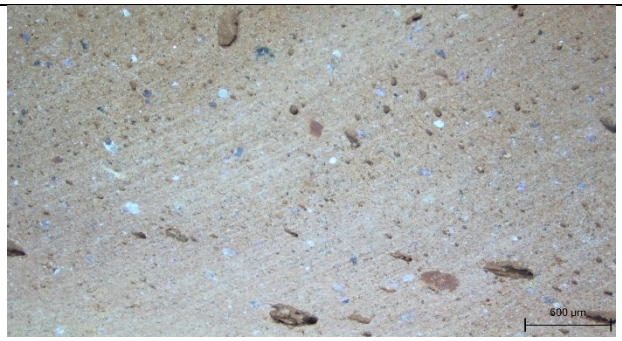


Ovoidal Adriatic type, 14mm thickness, beige color, fine texture with porosity, quartz and red nodules can be observed.

Thin section (x5, XPL)

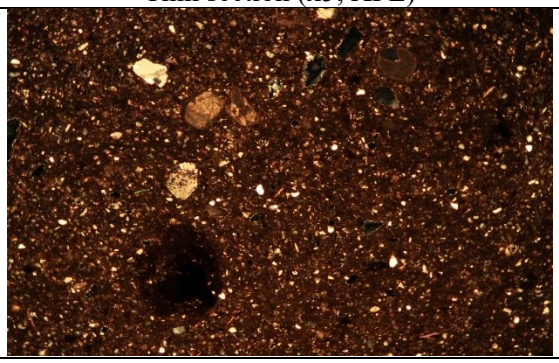

Microscopic characteristics

| | | | |
|---|---|---|---|
| Color | Reddish brown | Clay pellets | Precent |
| Inclusion abundance | 5 – 7 % | Carbonate mudstone | Present |
| Matrix | Fe | Flints | Present |
| Inclusion size | Small | Other minerals | Quartz – Muscovite – Biotite – Pyroxene – Secondary calcite |
| Fossils traces | Present | | |

XRPD

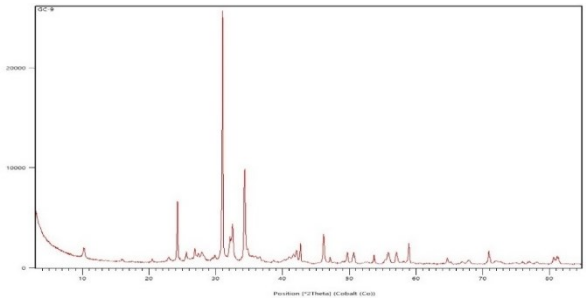

| Qz | Mus/Ill | Bt | Kfs | Pl | Hem | Px | Cal | Geh | Wo | Hyn | Temp °C |
|---|---|---|---|---|---|---|---|---|---|---|---|
| x | x | | x | x | x | x | x | | | | 900°-950° |

XRF

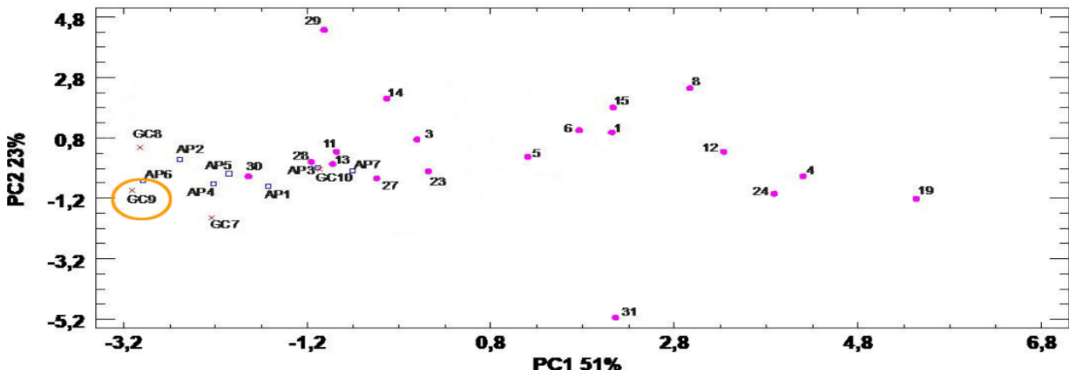

Sample: **GC- 10** Site: Giancola

| Fragment | Type | Fresh-cut surface |
|---|---|---|

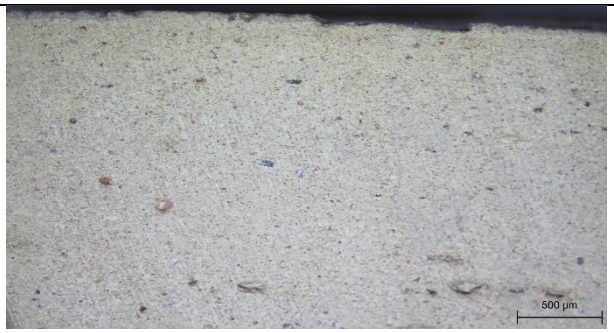


Ovoidal Adriatic type, 11mm thickness, grayish beige color, fine compact texture with small porosity and small inclusions.

Thin section (x5, XPL)

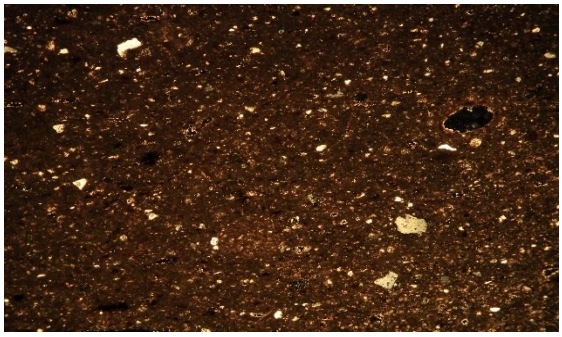

Microscopic characteristics

| | | | |
|---|---|---|---|
| Color | Brownish | Clay pellets | N/A |
| Inclusion abundance | <5% | Carbonate mudstone | N/A |
| Matrix | Ca | Flints | N/A |
| Inclusion size | Small | Other minerals | Quartz – Muscovite – Biotite – Pyroxene – Plagioclase – Secondary calcite |
| Fossils traces | Present | | |

XRPD

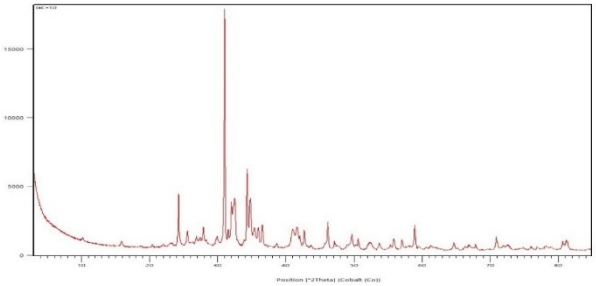

| Qz | Mus/Ill | Bt | Kfs | Pl | Hem | Px | Cal | Geh | Wo | Hyn | Temp °C |
|---|---|---|---|---|---|---|---|---|---|---|---|
| x | x | | x | x | x | x | x | x | | | 900°-950° |

XRF

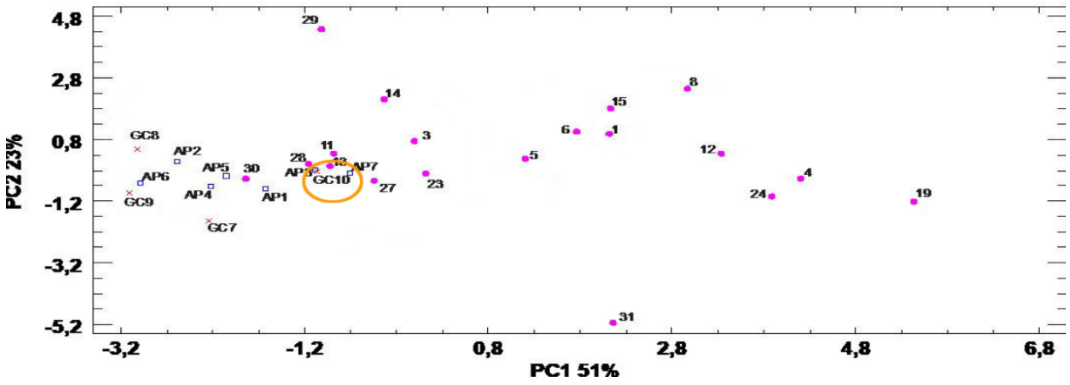

Sample: **TSS- 1** Site: Underwater, area B, US2 layer, TSS4

| Fragment | Type | Fresh-cut surface |
|---|---|---|

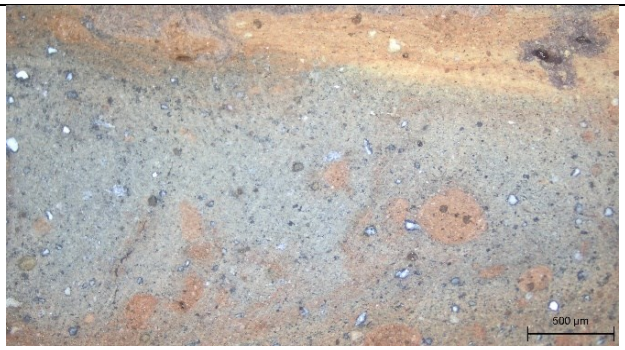


Apani I/Giancola II type, thickness is 15 mm with orange to gray color, fine mixed clay texture. Presence of red nodule and quartz.

| Thin section (x5, XPL) | Microscopic characteristics |
|---|---|

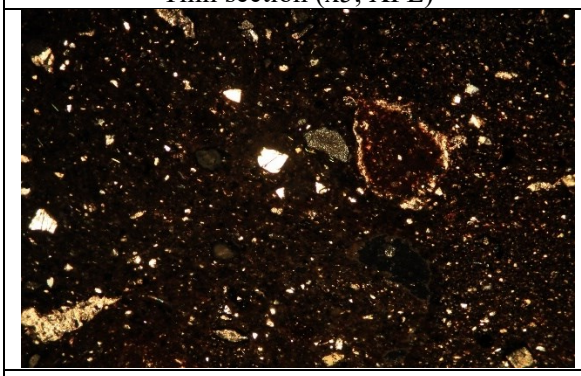

| | | | |
|---|---|---|---|
| Color | Reddish Brown | Clay pellets | Present |
| Inclusion abundance | 5 - 7% | Carbonate mudstone | Present |
| Matrix | Fe | Flints | Present |
| Inclusion size | Small | Other minerals | Quartz – Biotite – Muscovite - Secondary calcite |
| Fossils trace | Present | | |

XRPD

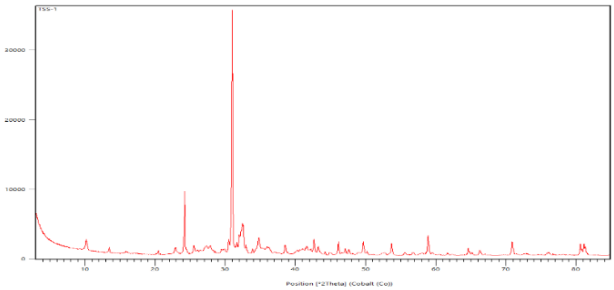

| Qz | Mus/Ill | Bt | Kfs | Pl | Hem | Px | Py | Gp | Mg-Cal | Cal | Arg | Geh | Zeo | Hyn | Sil | T°C |
|---|---|---|---|---|---|---|---|---|---|---|---|---|---|---|---|---|
| x | x | | x | x | x | x | x | x | x | | x | | | | | 850°-900° |

XRF

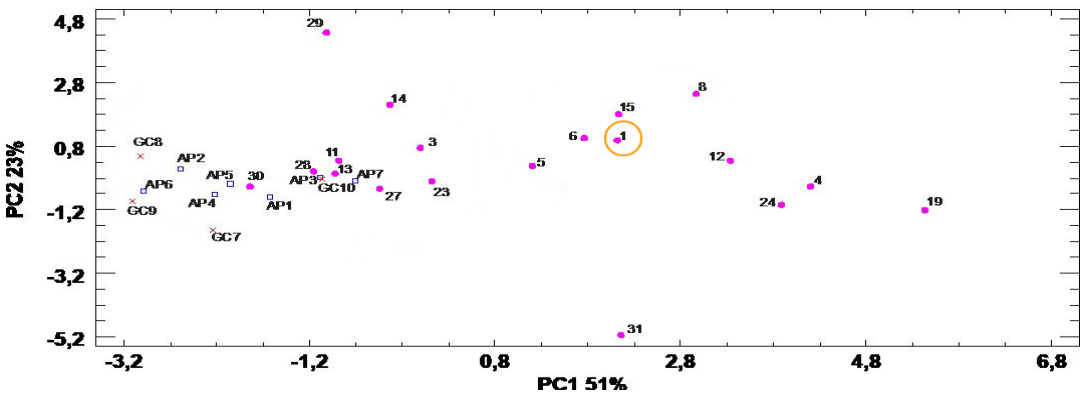

Sample: **TSS- 3** Site: Underwater, area B, US2 layer, TSS4

| Fragment | Type | Fresh-cut surface |
|---|---|---|

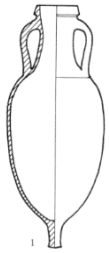

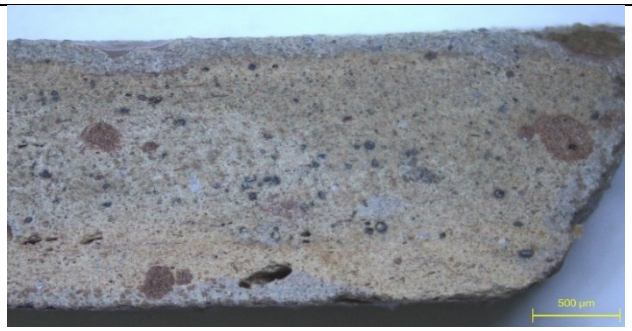

Apani I/Giancola II type, 8mm thickness, beige color, less compact fine texture with porosity. presence of red nodule and quartz.

Thin section (x5, XPL)

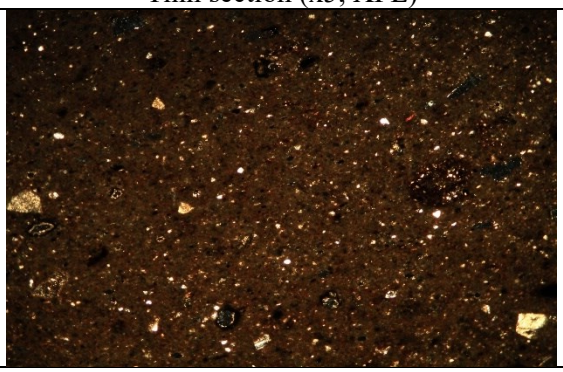

Microscopic characteristics

| | | | |
|---|---|---|---|
| Color | Brownish | Clay pellets | Present |
| Inclusion abundance | <5% | Carbonate mudstone | N/A |
| Matrix | Ca | Flints | Present |
| Inclusion size | Small | Other minerals | Quartz – Muscovite – Biotite – Secondary calcite |
| Fossils trace | Present | | |

XRPD

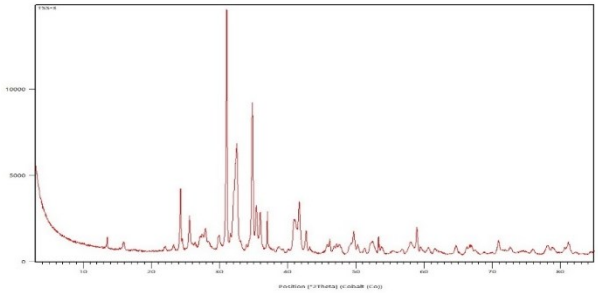

| Qz | Mus/Ill | Bt | Kfs | Pl | Hem | Px | Py | Gp | Mg-Cal | Cal | Arg | Geh | Zeo | Hyn | Sil | T°C |
|---|---|---|---|---|---|---|---|---|---|---|---|---|---|---|---|---|
| x | x | | x | x | x | x | x | x | x | | | x | | | | 900°-950° |

XRF

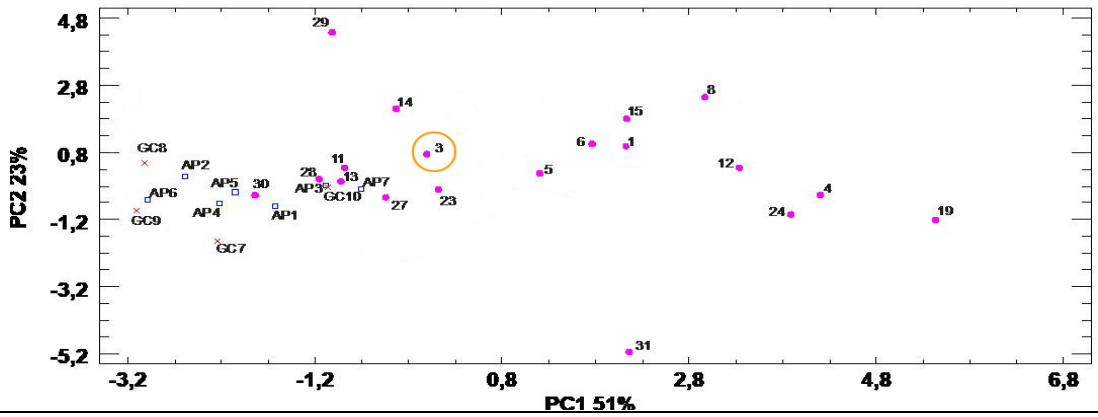

Sample: **TSS- 4** Site: Underwater, area B, US2 layer, TSS4

| Fragment | Type | Fresh-cut surface |
|---|---|---|

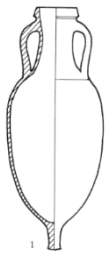

Apani I/Giancola II type, 10mm thickness, orange gray color, fine multicolor texture, presence of inclusions like quartz.

Thin section (x5, XPL)

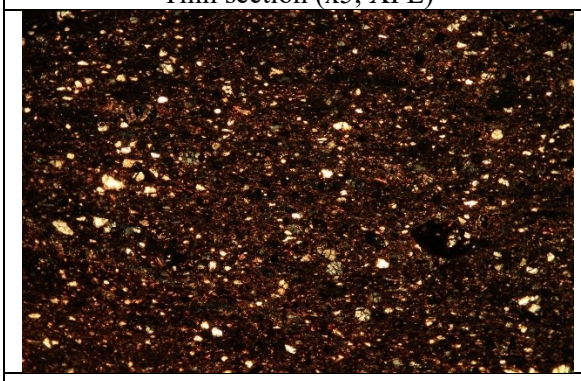

Microscopic characteristics

| | | | |
|---|---|---|---|
| Color | Reddish Brown | Clay pellets | Present |
| Inclusion abundance | 7 - 10% | Carbonate mudstone | Present |
| Matrix | Fe | Flints | N/A |
| Inclusion size | Small | Other minerals | Quartz – Muscovite – Biotite – Pyroxene |
| Fossils trace | Present | | |

XRPD

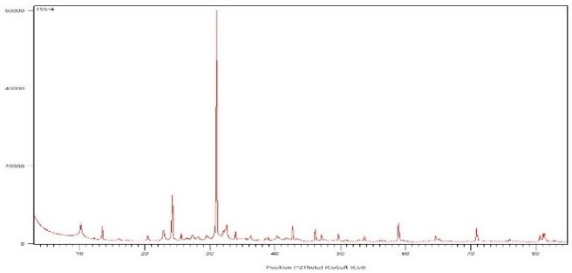

| Qz | Mus/Ill | Bt | Kfs | Pl | Hem | Px | Py | Gp | Mg-Cal | Cal | Arg | Geh | Zeo | Hyn | Sil | T°C |
|---|---|---|---|---|---|---|---|---|---|---|---|---|---|---|---|---|
| x | x | x | x | x | x | | | x | | | | | | x | | ~ 800° |

XRF

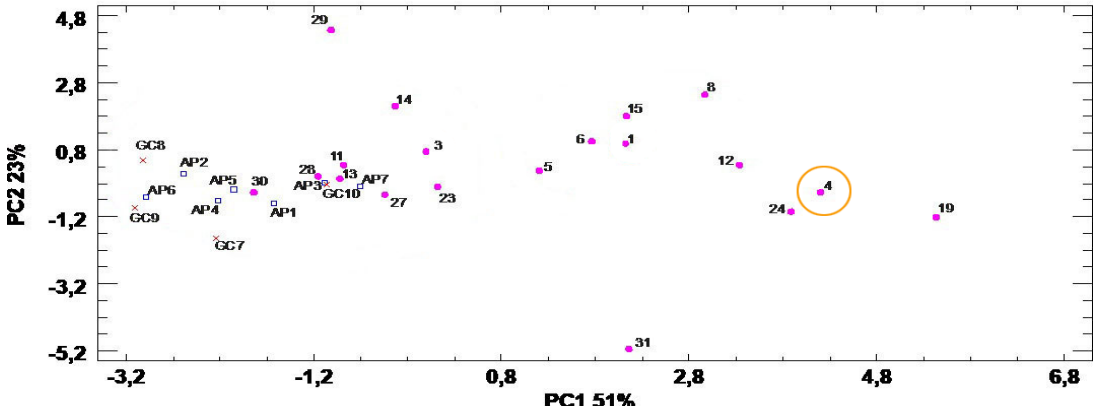

Sample: **TSS- 5** Site: Underwater, area B, US2 layer, TSS4

| Fragment | Type | Fresh-cut surface |
|---|---|---|

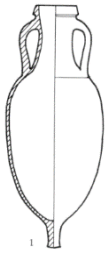

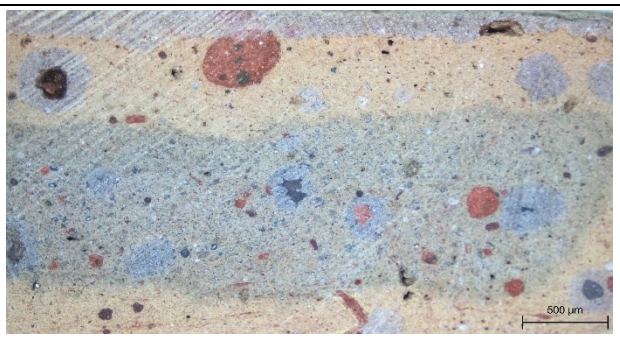


Apani I/Giancola II type, 11mm thickness, gray and beige color, fine compact mixed texture with porosity, clear evidence of red nodules.

| Thin section (x5, XPL) | Microscopic characteristics |
|---|---|

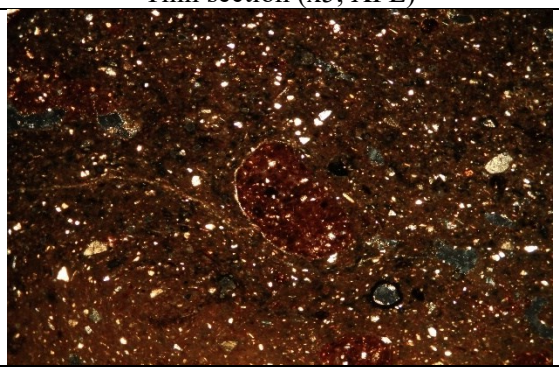

| | | | |
|---|---|---|---|
| Color | Reddish Brown | Clay pellets | Present |
| Inclusion abundance | 5 – 7% | Carbonate mudstone | Present |
| Matrix | Fe | Flints | N/A |
| Inclusion size | Small | Other minerals | Quartz – Muscovite – Biotite – Plagioclase |
| Fossils trace | N/A | | |

XRPD

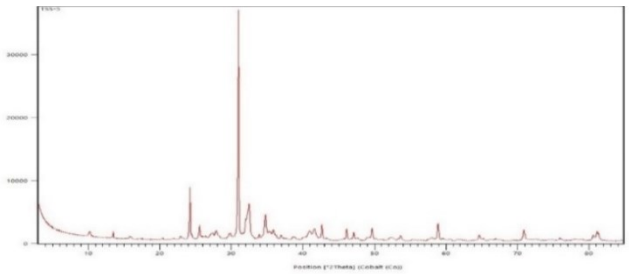

| Qz | Mus/Ill | Bt | Kfs | Pl | Hem | Px | Py | Gp | Mg-Cal | Cal | Arg | Geh | Zeo | Hyn | Sil | T°C |
|---|---|---|---|---|---|---|---|---|---|---|---|---|---|---|---|---|
| x | x | | x | x | x | x | | x | x | | | | | x | | 850°-900° |

XRF

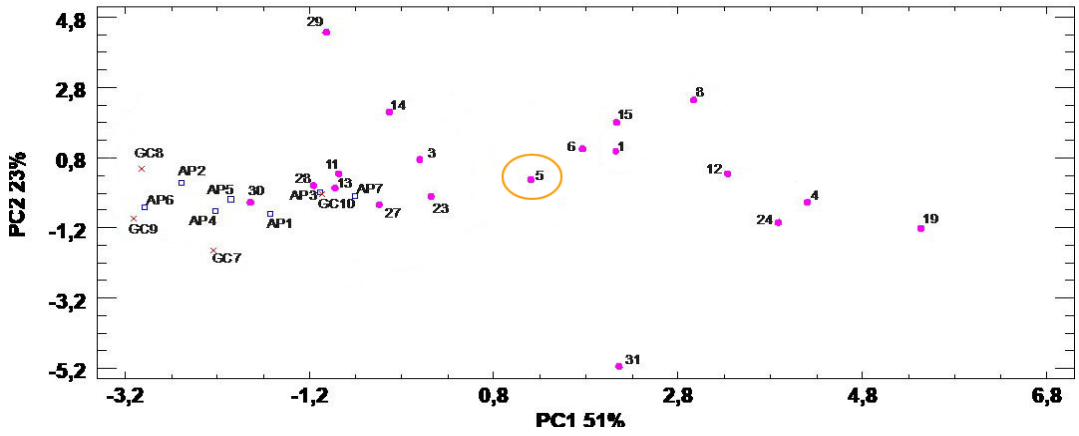

Sample: **TSS- 6** Site: Underwater, area B, US2 layer, TSS4

| Fragment | Type | Fresh-cut surface |
|---|---|---|

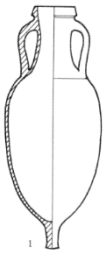

Apani I/Giancola II type, 11mm thickness, gray orange color, fine multicolor texture, small porosity, quartz and red nodules are present

Thin section (x5, XPL)

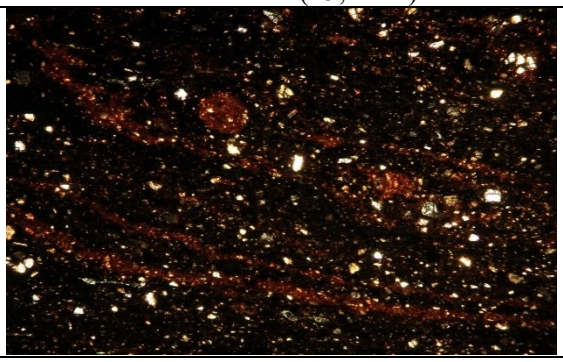

Microscopic characteristics

| | | | |
|---|---|---|---|
| Color | Reddish | Clay pellets | Present |
| Inclusion abundance | 5 – 7% | Carbonate mudstone | Present |
| Matrix | Fe | Flints | N/A |
| Inclusion size | Small | Other minerals | Quartz – Muscovite – Biotite |
| Fossils trace | Present | | |

XRPD

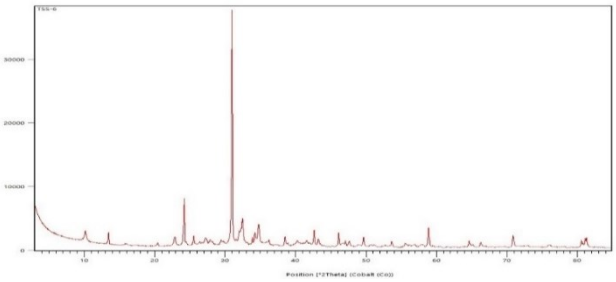

| Qz | Mus/Ill | Bt | Kfs | Pl | Hem | Px | Py | Gp | Mg-Cal | Cal | Arg | Geh | Zeo | Hyn | Sil | T°C |
|---|---|---|---|---|---|---|---|---|---|---|---|---|---|---|---|---|
| x | x | | x | x | x | x | x | x | x | x | | | | | | 850°-900° |

XRF

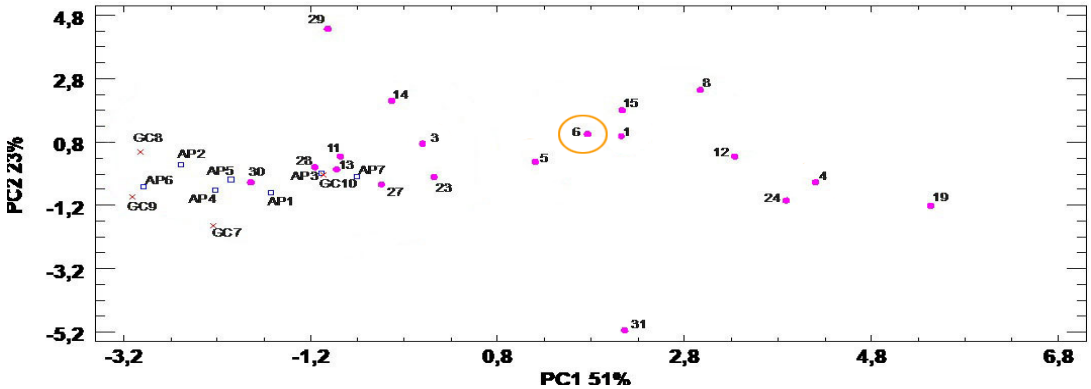

Sample: **TSS- 8** Site: Underwater, area B, US2 layer, TSS4

| Fragment | Type | Fresh-cut surface |
|---|---|---|

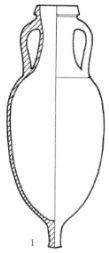


Apani I/Giancola II type, 10mm thickness, fine compact mixed texture, presence of quartz and red nodules.

Thin section (x5, XPL)

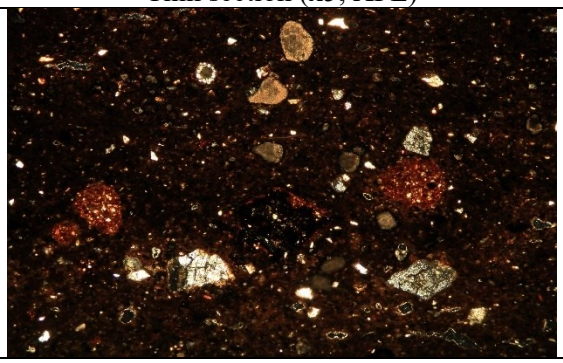

Microscopic characteristics

| | | | |
|---|---|---|---|
| Color | Reddish Brown | Clay pellets | Present |
| Inclusion abundance | 7 – 10 % | Carbonate mudstone | Present |
| Matrix | Fe | Flints | Present |
| Inclusion size | Small to Medium | Other minerals | Quartz – Muscovite – Biotite – Secondary calcite |
| Fossils trace | Present | | |

XRPD

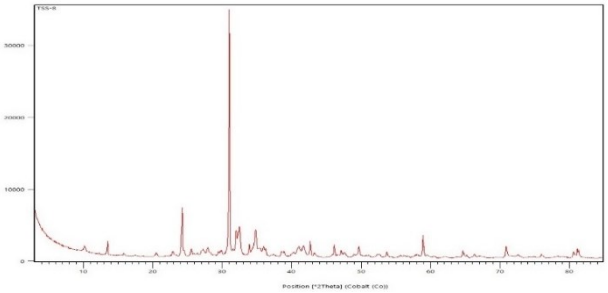

| Qz | Mus/Ill | Bt | Kfs | Pl | Hem | Px | Py | Gp | Mg-Cal | Cal | Arg | Geh | Zeo | Hyn | Sil | T°C |
|---|---|---|---|---|---|---|---|---|---|---|---|---|---|---|---|---|
| x | x | | x | x | x | x | x | x | x | | | | | | | 850°-900° |

XRF

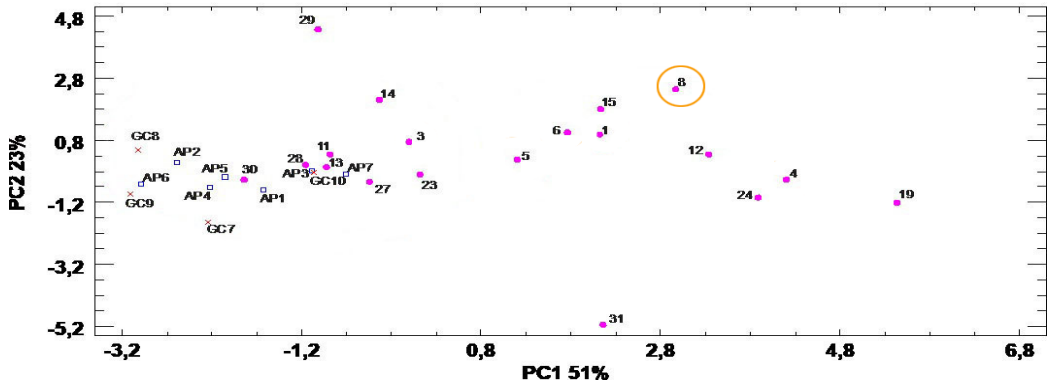

Sample: **TSS- 11** Site: Underwater, area B, US2 layer, TSS4

| Fragment | Type | Fresh-cut surface |
|---|---|---|

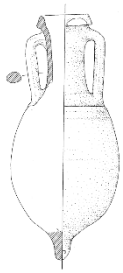

Lamboglia2 type, 17mm thickness, gray color, fine texture with low porosity, less evident of inclusions on surface.

Thin section (x5, XPL)

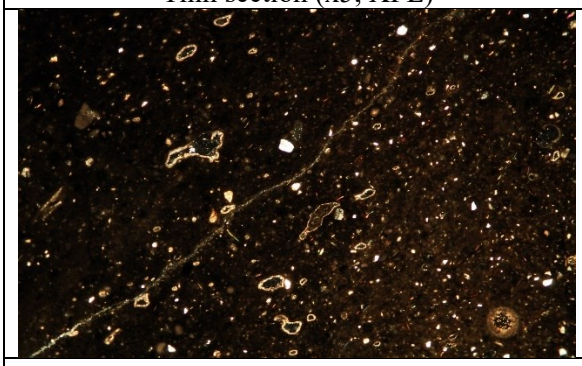

Microscopic characteristics

| | | | |
|---|---|---|---|
| Color | Reddish Brown | Clay pellets | Present |
| Inclusion abundance | <5% | Carbonate mudstone | Present |
| Matrix | Fe | Flints | N/A |
| Inclusion size | Small | Other minerals | Quartz – Muscovite – Biotite – Secondary calcite – Pyroxene - Plagioclase |
| Fossils trace | Present | | |

XRPD

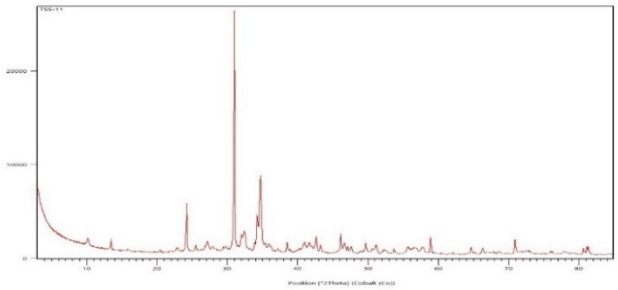

| Qz | Mus/Ill | Bt | Kfs | Pl | Hem | Px | Py | Gp | Mg-Cal | Cal | Arg | Geh | Zeo | Hyn | Sil | T°C |
|---|---|---|---|---|---|---|---|---|---|---|---|---|---|---|---|---|
| x | x | | x | x | | x | x | x | x | x | | | | | | 850°-900° |

XRF

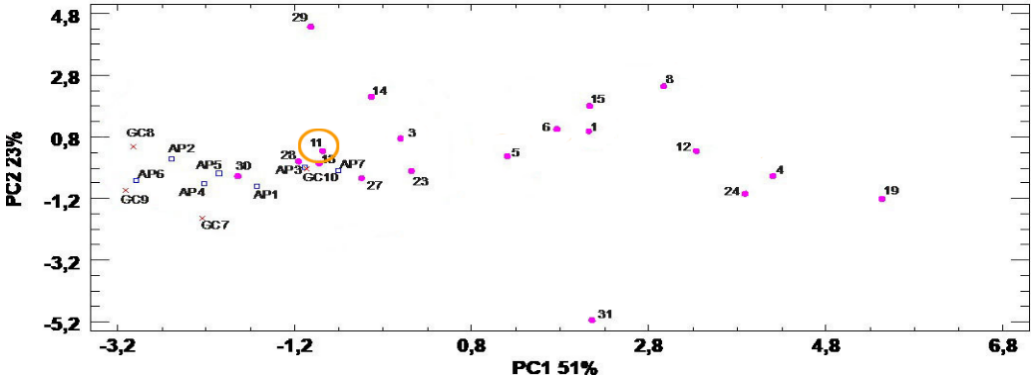

Sample: **TSS- 12** Site: Underwater, area B, US2 layer, TSS4

| Fragment | Type | Fresh-cut surface |
|---|---|---|

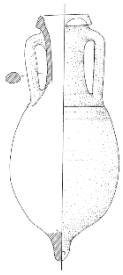


Lamboglia2 type, 10mm thickness, beige and gray color, fine mixed compact texture, presence of red nodules and quartz.

Thin section (x5, XPL)

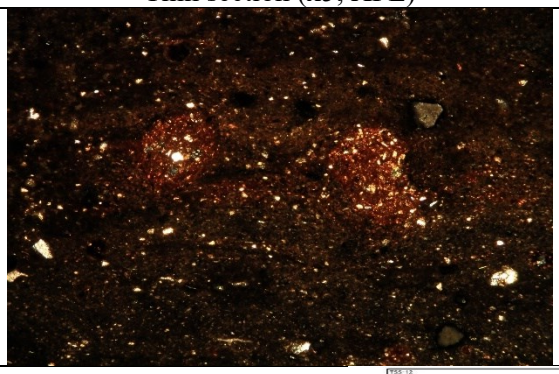

Microscopic characteristics

| | | | |
|---|---|---|---|
| Color | Reddish | Clay pellets | Present |
| Inclusion abundance | <5% | Carbonate mudstone | Present |
| Matrix | Fe | Flints | Present |
| Inclusion size | Small | Other minerals | Quartz – Muscovite – Biotite - Pyroxene – Secondary calcite |
| Fossils trace | Present | | |

XRPD

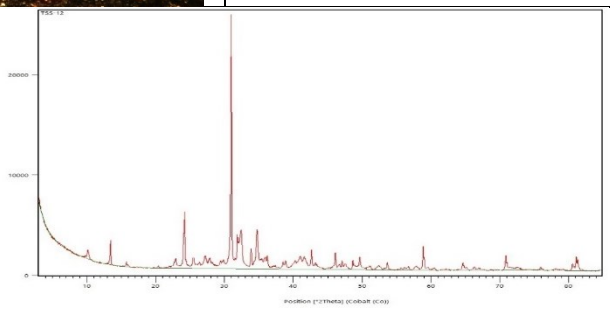

| Qz | Mus/Ill | Bt | Kfs | Pl | Hem | Px | Py | Gp | Mg-Cal | Cal | Arg | Geh | Zeo | Hyn | Sil | T°C |
|---|---|---|---|---|---|---|---|---|---|---|---|---|---|---|---|---|
| x | x | | x | x | | x | x | x | x | | | | | | | 850°-900° |

XRF

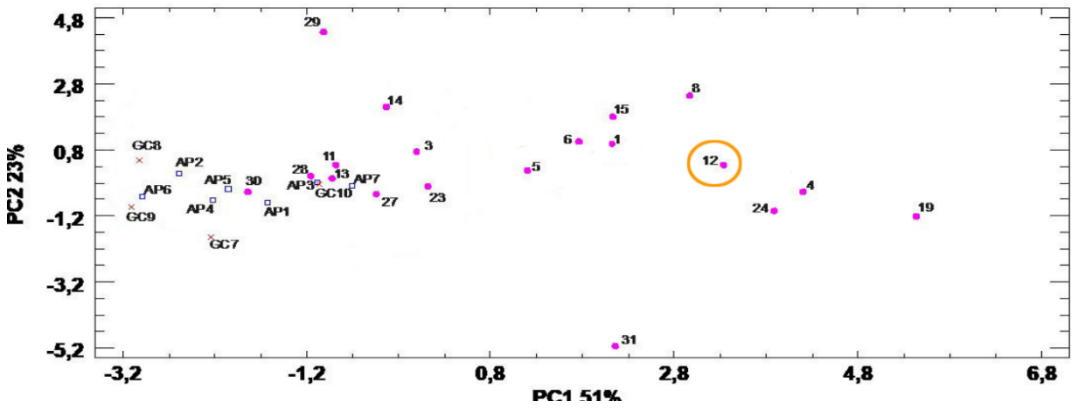

Sample: **TSS- 13** Site: Underwater, area B, US2 layer, TSS4

| Fragment | Type | Fresh-cut surface |
|---|---|---|

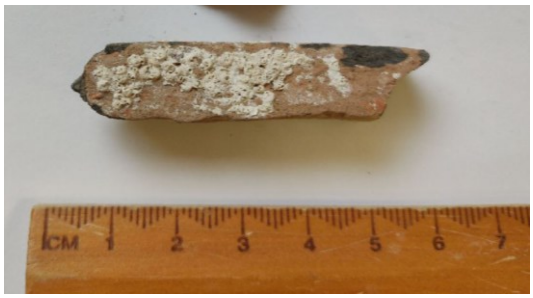

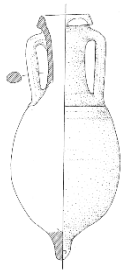


Lamboglia2 type, 13mm thickness, beige and gray color, fine mixed compact texture, presence of red nodules and quartz.

Thin section (x5, XPL)

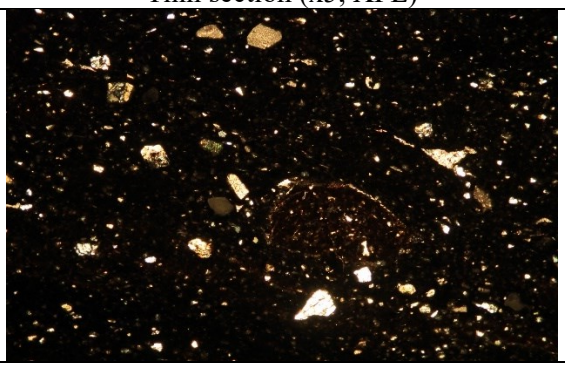

Microscopic characteristics

| | | | |
|---|---|---|---|
| Color | Brownish | Clay pellets | Present |
| Inclusion abundance | 7 - 10% | Carbonate mudstone | Present |
| Matrix | Ca | Flints | Present |
| Inclusion size | Small | Other minerals | Quartz – Muscovite – Biotite – Plagioclase – Pyroxene – Secondary calcite |
| Fossils trace | Present | | |

XRPD

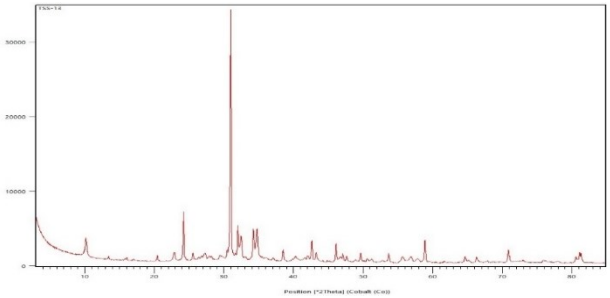

| Qz | Mus/Ill | Bt | Kfs | Pl | Hem | Px | Py | Gp | Mg-Cal | Cal | Arg | Geh | Zeo | Hyn | Sil | T°C |
|---|---|---|---|---|---|---|---|---|---|---|---|---|---|---|---|---|
| x | x | x | x | x | | x | x | | x | x | x | | | | | 850°- 900° |

XRF

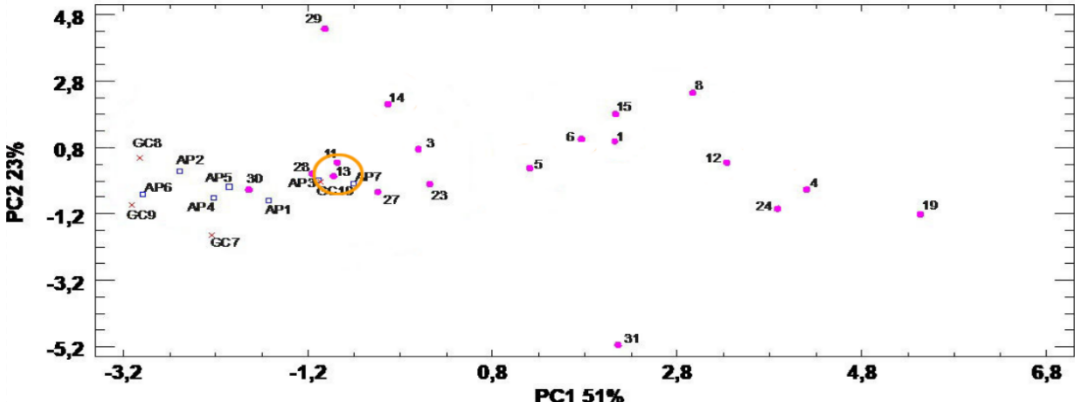

Sample: **TSS- 14** Site: Underwater, area B, US2 layer, TSS4

| Fragment | Type | Fresh-cut surface |
|---|---|---|

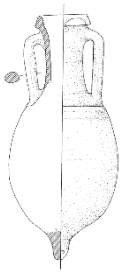

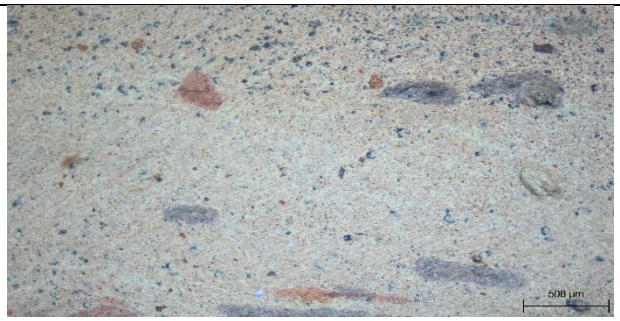

Lamboglia2 type, 19mm thickness, beige color, fine less compact texture, presence of red nodules on surface.

Thin section (x5, XPL)

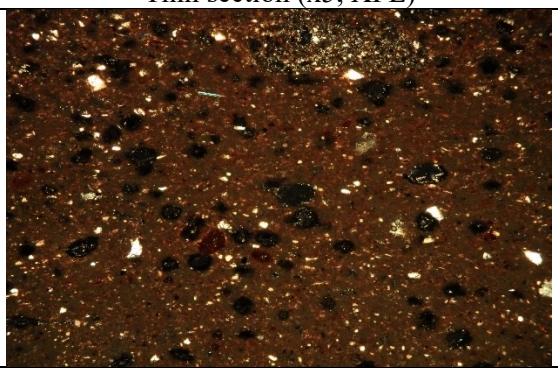

Microscopic characteristics

| | | | |
|---|---|---|---|
| Color | Reddish Brown | Clay pellets | Present |
| Inclusion abundance | 5 % | Carbonate mudstone | N/A |
| Matrix | Fe | Flints | Present |
| Inclusion size | Small | Other minerals | Quartz – Muscovite – Biotite – Plagioclase – Secondary calcite |
| Fossils trace | N/A | | |

XRPD

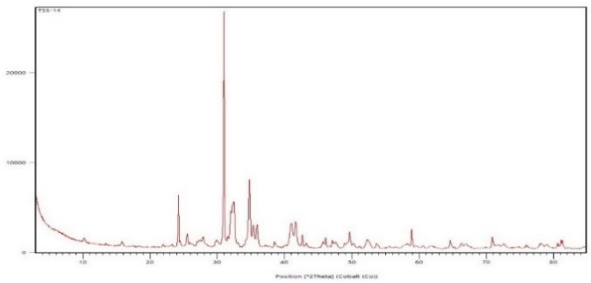

| Qz | Mus/Ill | Bt | Kfs | Pl | Hem | Px | Py | Gp | Mg-Cal | Cal | Arg | Geh | Zeo | Hyn | Sil | T°C |
|---|---|---|---|---|---|---|---|---|---|---|---|---|---|---|---|---|
| x | x | | x | x | | x | | | x | | | | | | | 900°-950° |

XRF

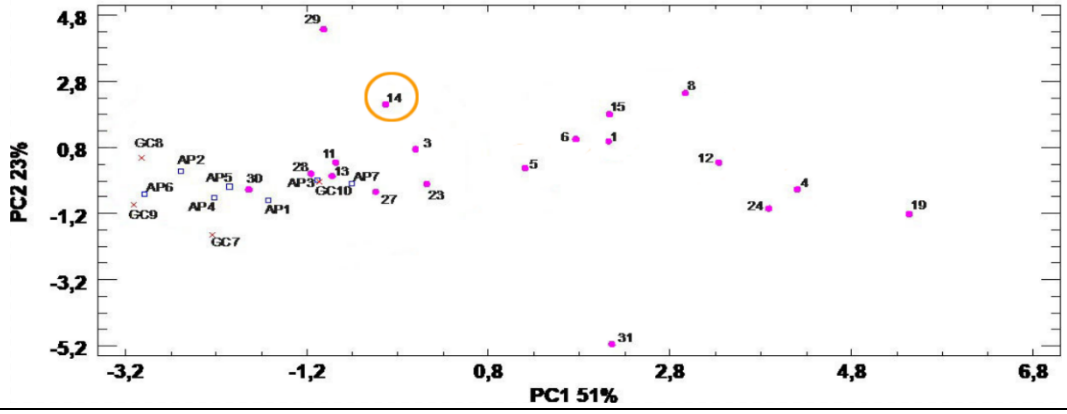

Sample: **TSS- 15** Site: Underwater, area B, US2 layer, TSS4

| Fragment | Type | Fresh-cut surface |
|---|---|---|

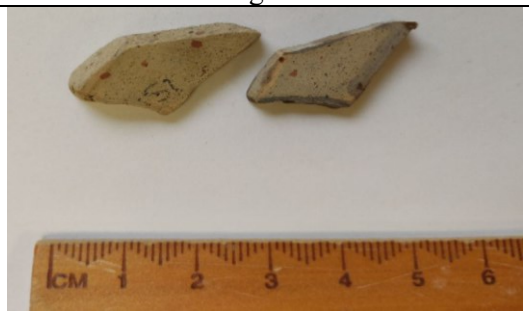

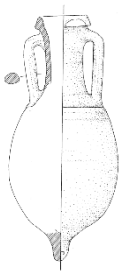


Lamboglia2 type, beige to yellow color, fine high porosity texture, presence of red nodules on the surface.

Thin section (x5, XPL)

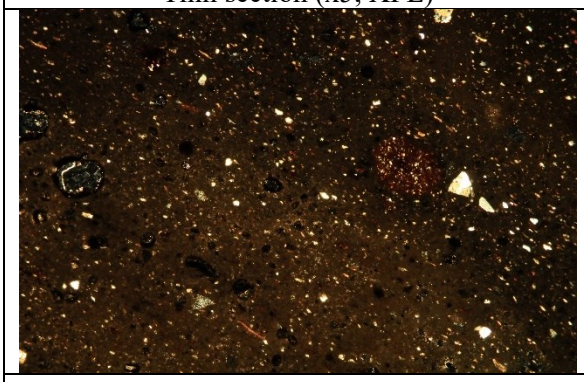

Microscopic characteristics

| | | | |
|---|---|---|---|
| Color | Brownish Red | Clay pellets | Present |
| Inclusion abundance | 5% | Carbonate mudstone | Present |
| Matrix | Ca | Flints | N/A |
| Inclusion size | Small | Other minerals | Quartz – Muscovite – Biotite - Pyroxene |
| Fossils trace | Present | | |

XRPD

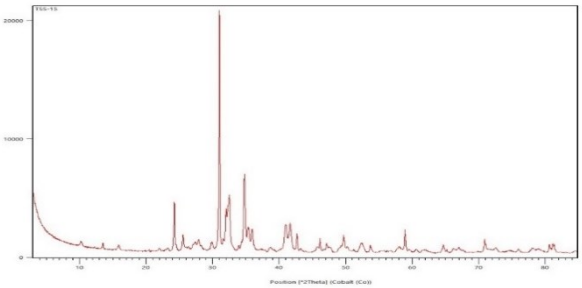

| Qz | Mus/Ill | Bt | Kfs | Pl | Hem | Px | Py | Gp | Mg-Cal | Cal | Arg | Geh | Zeo | Hyn | Sil | T°C |
|---|---|---|---|---|---|---|---|---|---|---|---|---|---|---|---|---|
| x | x | | x | x | | x | | | x | x | | | | | | 900°-950° |

XRF

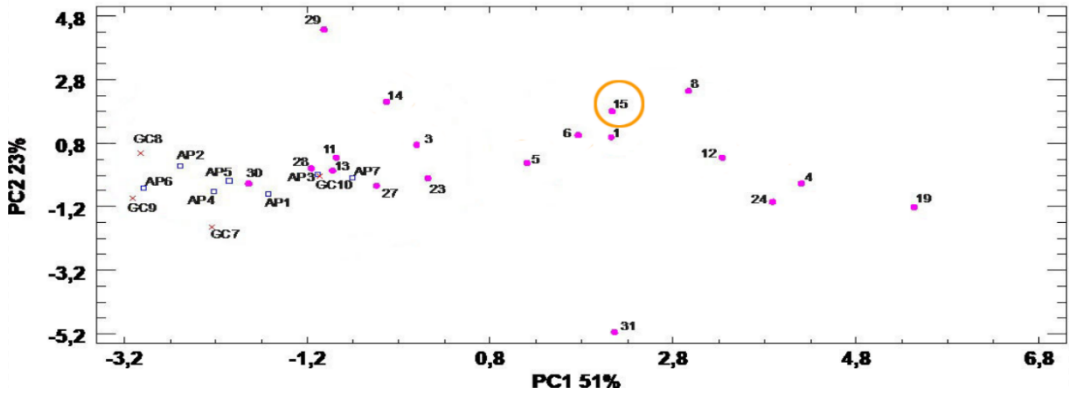

Sample: **TSS- 19** Site: Underwater, area B, US2 layer, TSS4

| Fragment | Type | Fresh-cut surface |
|---|---|---|

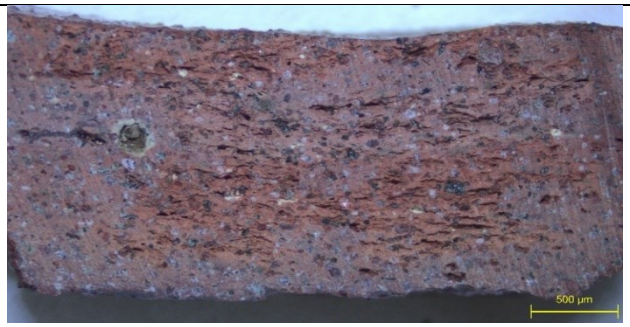

Dressel2-4 type, 9mm thickness, reddish color, less compact high porosity texture. More and different variety of inclusions on surface.

Thin section (x5, XPL)

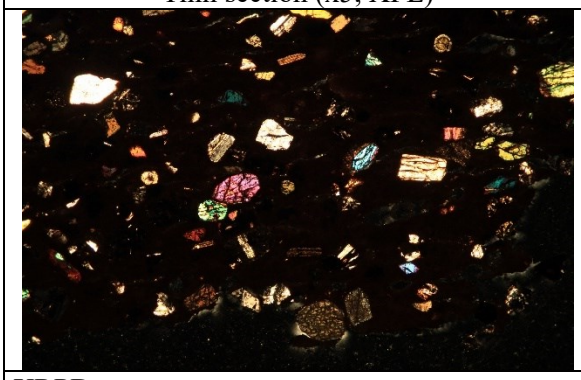

Microscopic characteristics

| | | | |
|---|---|---|---|
| Color | Dark Red | Clay pellets | Present |
| Inclusion abundance | 15 - 20% | Carbonate mudstone | N/A |
| Matrix | Fe | Flints | N/A |
| Inclusion size | Medium | Other minerals | Quartz – Muscovite – Biotite – Olivine – Pyroxene - Plagioclase |
| Fossils trace | N/A | | |

XRPD

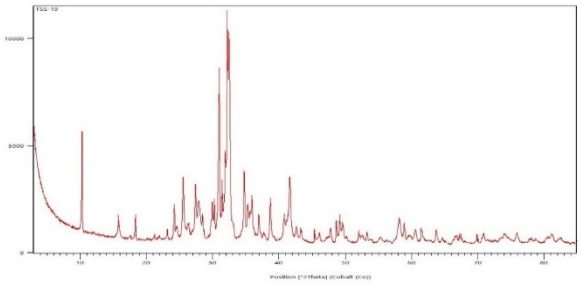

| Qz | Mus/Ill | Bt | Kfs | Pl | Hem | Px | Py | Gp | Mg-Cal | Cal | Arg | Geh | Zeo | Hyn | Sil | T°C |
|---|---|---|---|---|---|---|---|---|---|---|---|---|---|---|---|---|
| x | x | x | x | x | x | x | | | | | | | x | | | 950°-1000° |

XRF

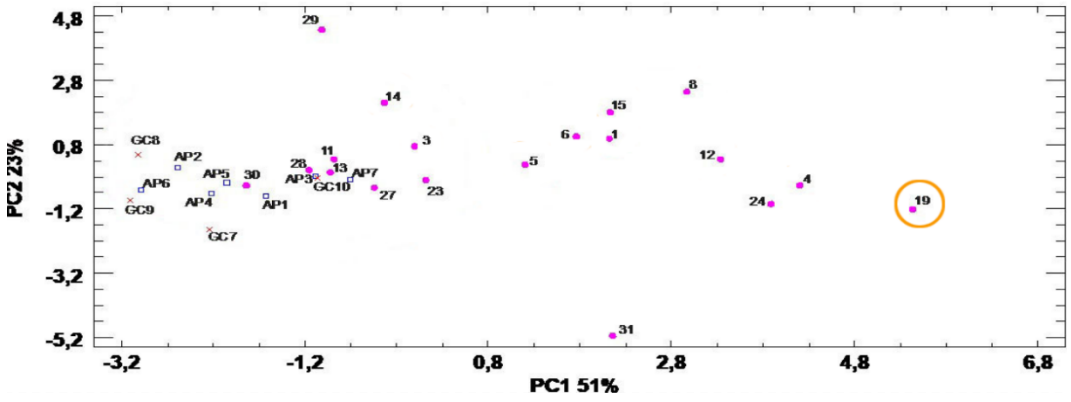

Sample: **TSS- 23** Site: Underwater, area B, US2 layer, TSS4

| Fragment | Type | Fresh-cut surface |
|---|---|---|

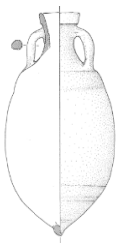

Ovoidal Adriatic type, 12mm thickness, grayish beige color, fine low porosity texture, presence of quartz as inclusion on surface.

Thin section (x5, XPL)

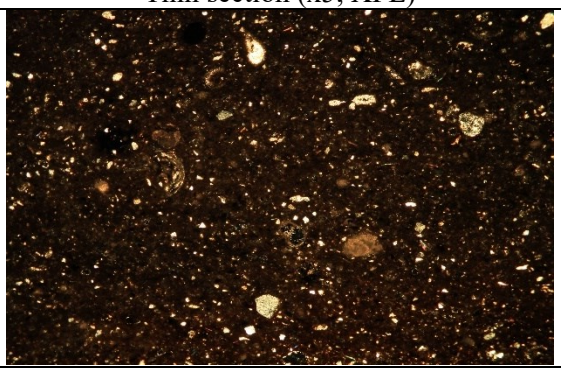

Microscopic characteristics

| | | | |
|---|---|---|---|
| Color | Brownish | Clay pellets | N/A |
| Inclusion abundance | 5 – 7 % | Carbonate mudstone | Present |
| Matrix | Ca | Flints | N/A |
| Inclusion size | Small | Other minerals | Quartz – Muscovite – Biotite – Secondary calcite - Pyroxene |
| Fossils trace | Present | | |

XRPD

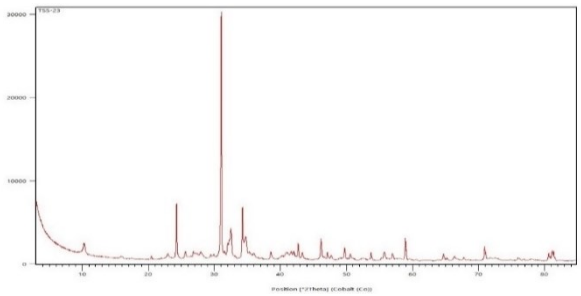

| Qz | Mus/Ill | Bt | Kfs | Pl | Hem | Px | Py | Gp | Mg-Cal | Cal | Arg | Geh | Zeo | Hyn | Sil | T°C |
|---|---|---|---|---|---|---|---|---|---|---|---|---|---|---|---|---|
| x | x | | x | x | | x | x | | x | x | | | | | | 850°-900° |

XRF

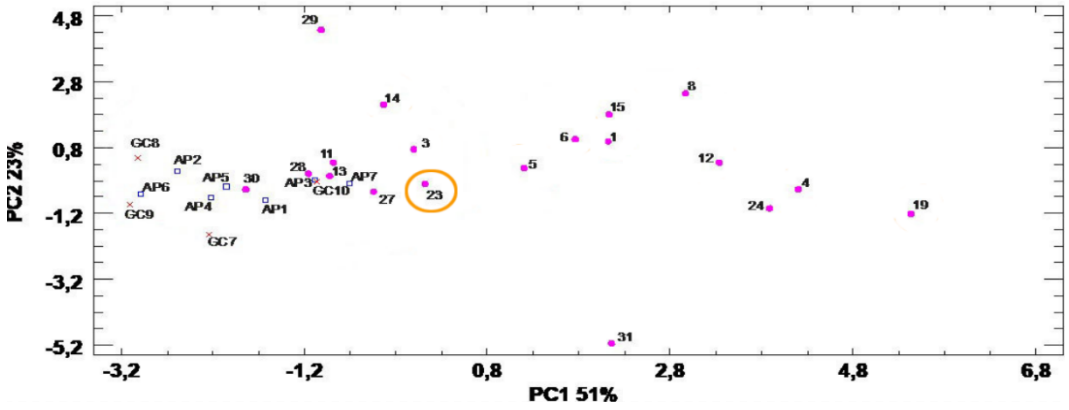

Sample: **TSS- 24** Site: Underwater, area B, US2 layer, TSS4

| Fragment | Type | Fresh-cut surface |
|---|---|---|


African type, 5mm thickness, orange beige color, high porosity less compact mixed texture, large inclusions are present on the surface.

| Thin section (x5, XPL) | Microscopic characteristics |
|---|---|

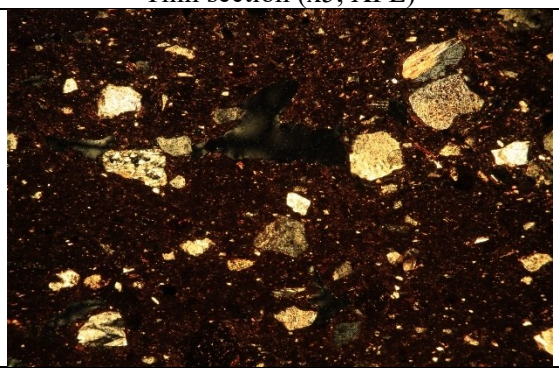

| | | | |
|---|---|---|---|
| Color | Reddish Brown | Clay pellets | Present |
| Inclusion abundance | 15 – 20% | Carbonate mudstone | N/A |
| Matrix | Fe | Flints | N/A |
| Inclusion size | Medium | Other minerals | Quartz – Muscovite – Biotite – Plagioclase – Pyroxene – Sillimanite |
| Fossils trace | N/A | | |

XRPD

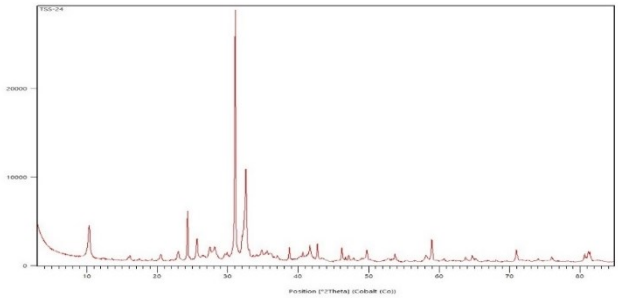

| Qz | Mus/Ill | Bt | Kfs | Pl | Hem | Px | Py | Gp | Mg-Cal | Cal | Arg | Geh | Zeo | Hyn | Sil | T°C |
|---|---|---|---|---|---|---|---|---|---|---|---|---|---|---|---|---|
| x | x | x | x | x | x | x | | | | x | | x | | | x | 850°-900° |

XRF

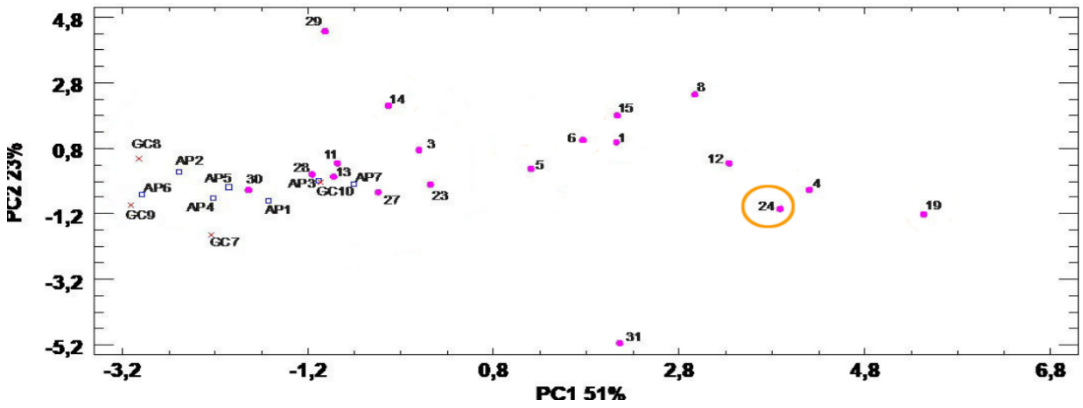

Sample: **TSS- 27** Site: Underwater, area B, US2 layer, TSS4

| Fragment | Type | Fresh-cut surface |
|---|---|---|

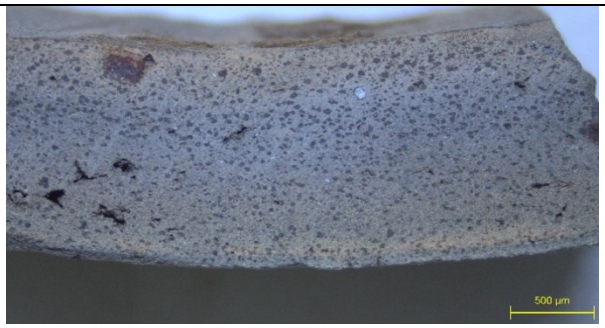


Ovoidal Adriatic type, 7mm thickness, grayish beige color, fine low porosity texture, presence of some inclusion on surface.

Thin section (x5, XPL)

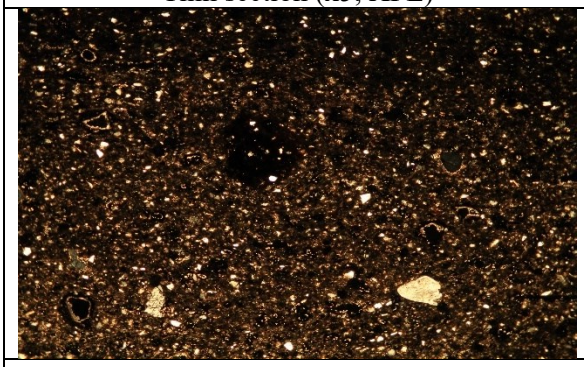

Microscopic characteristics

| | | | |
|---|---|---|---|
| Color | Brownish | Clay pellets | Present |
| Inclusion abundance | <5% | Carbonate mudstone | Present |
| Matrix | Ca | Flints | N/A |
| Inclusion size | Small | Other minerals | Quartz – Muscovite – Biotite – Secondary calcite – Plagioclase – K-Feldspar |
| Fossils trace | Present | | |

XRPD

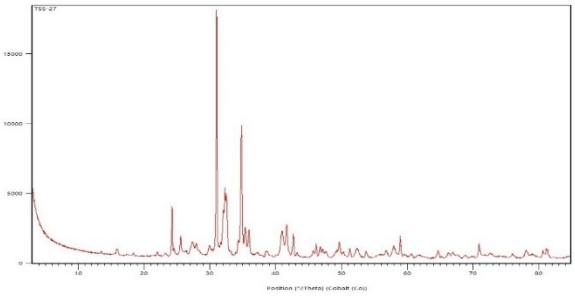

| Qz | Mus/Ill | Bt | Kfs | Pl | Hem | Px | Py | Gp | Mg-Cal | Cal | Arg | Geh | Zeo | Hyn | Sil | T°C |
|---|---|---|---|---|---|---|---|---|---|---|---|---|---|---|---|---|
| x | x | | x | x | | x | x | | x | x | | | | | | 900°-950° |

XRF

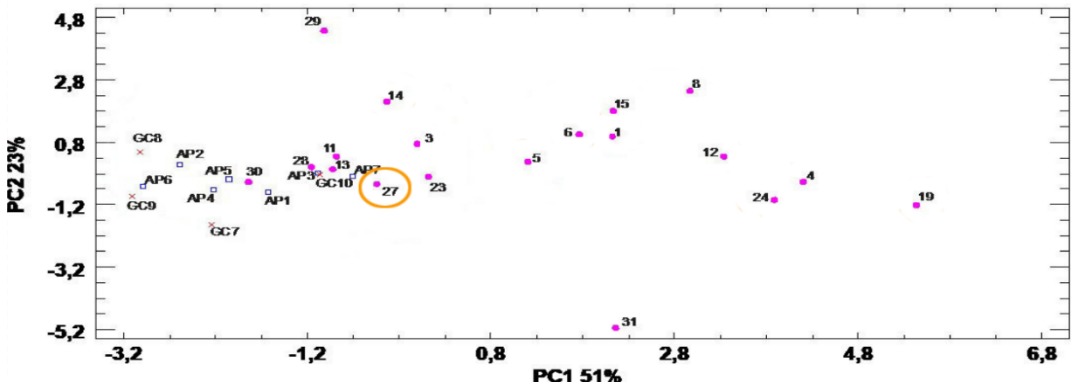

Sample: **TSS- 28** Site: Underwater, area B, US2 layer, TSS4

| Fragment | Type | Fresh-cut surface |
|---|---|---|

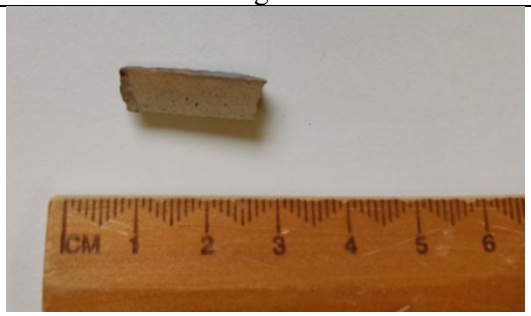

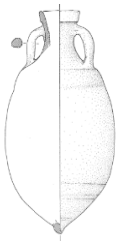


Ovoidal Adriatic type, 6mm thickness, beige color, fine low porosity texture, presence of inclusion on surface is rare.

Thin section (5x)

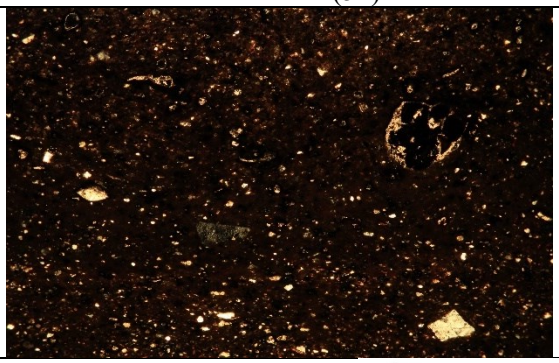

Microscopic characteristics

| | | | |
|---|---|---|---|
| Color | Reddish Brown | Clay pellets | Present |
| Inclusion abundance | 5% | Carbonate mudstone | Present |
| Matrix | Fe | Flints | N/A |
| Inclusion size | Small | Other minerals | Quartz – Muscovite – Biotite – Secondary calcite – Plagioclase K-Feldspar |
| Fossils trace | Present | | |

XRPD

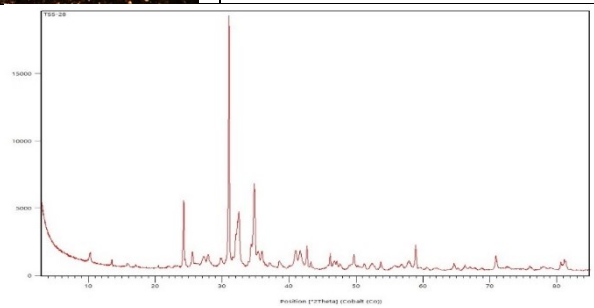

| Qz | Mus/Ill | Bt | Kfs | Pl | Hem | Px | Py | Gp | Mg-Cal | Cal | Arg | Geh | Zeo | Hyn | Sil | T°C |
|---|---|---|---|---|---|---|---|---|---|---|---|---|---|---|---|---|
| x | x | | x | x | x | x | | x | x | x | | | | | | 900°-950° |

XRF

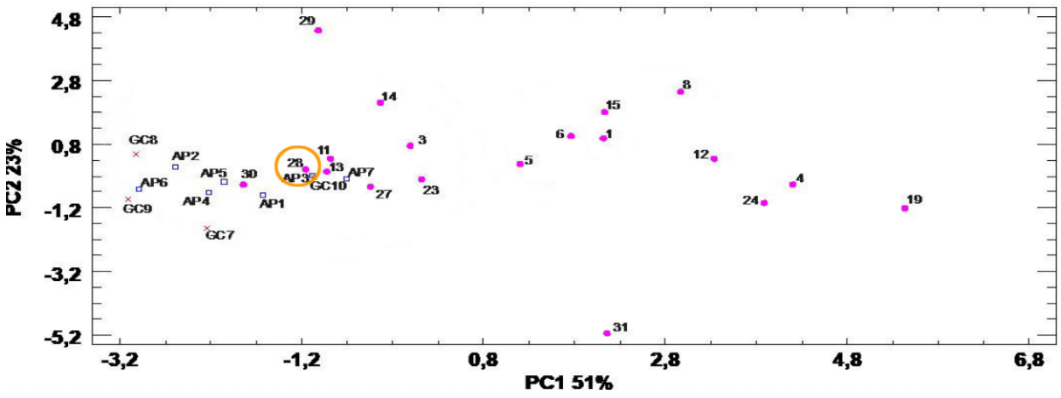

Sample: **TSS- 29** Site: Underwater, area B, US2 layer, TSS4

| Fragment | Type | Fresh-cut surface |
|---|---|---|

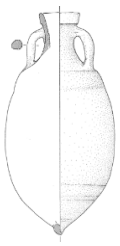


Ovoidal Adriatic type, 7mm thickness, grayish color, fine low porosity texture.

Thin section (x5, XPL)

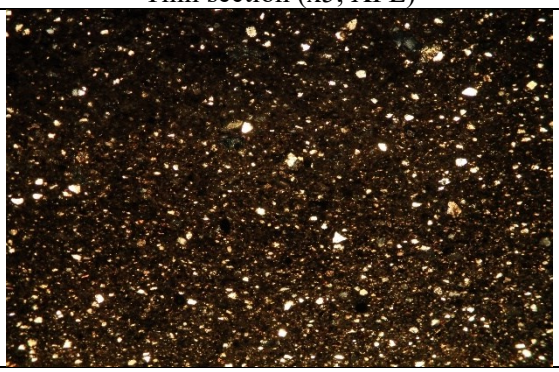

Microscopic characteristics

| | | | |
|---|---|---|---|
| Color | Brownish | Clay pellets | N/A |
| Inclusion abundance | 5% | Carbonate mudstone | Present |
| Matrix | Ca | Flints | N/A |
| Inclusion size | Small | Other minerals | Quartz – Muscovite – Biotite – Secondary calcite |
| Fossils trace | Present | | |

XRPD

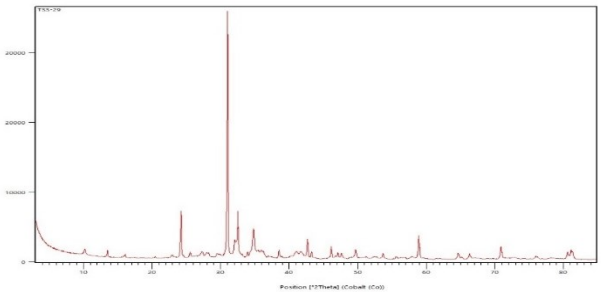

| Qz | Mus/Ill | Bt | Kfs | Pl | Hem | Px | Py | Gp | Mg-Cal | Cal | Arg | Geh | Zeo | Hyn | Sil | T°C |
|---|---|---|---|---|---|---|---|---|---|---|---|---|---|---|---|---|
| x | x | | x | x | | x | x | x | x | x | | | | | | 850°-900° |

XRF

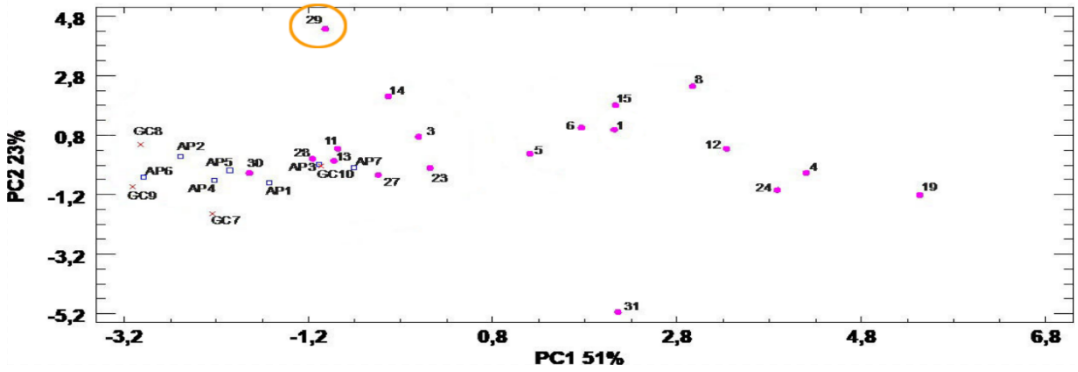

Sample: **TSS- 30** Site: Underwater, area B, US2 layer, TSS4

| Fragment | Type | Fresh-cut surface |
|---|---|---|

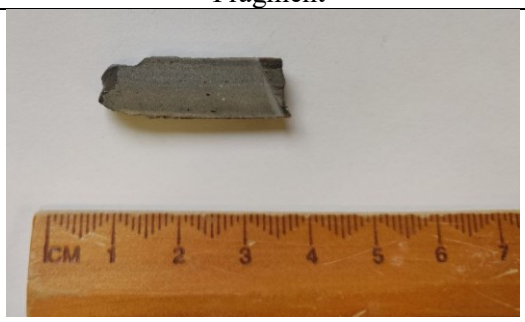

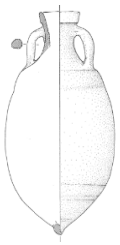

Ovoidal Adriatic type, 9mm thickness, grayish beige color, fine low porosity texture, tiny presence of quartz on surface.

Thin section (x5, XPL)

Microscopic characteristics

| | | | |
|---|---|---|---|
| Color | Brownish | Clay pellets | Present |
| Inclusion abundance | 7 – 10 % | Carbonate mudstone | Present |
| Matrix | Ca | Flints | Present |
| Inclusion size | Small | Other minerals | Quartz – Muscovite – Biotite – Secondary calcite - Plagioclase |
| Fossils trace | Present | | |

XRPD

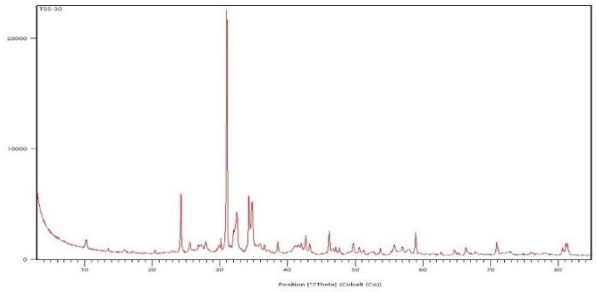

| Qz | Mus/Ill | Bt | Kfs | Pl | Hem | Px | Py | Gp | Mg-Cal | Cal | Arg | Geh | Zeo | Hyn | Sil | T°C |
|---|---|---|---|---|---|---|---|---|---|---|---|---|---|---|---|---|
| x | x | | x | x | x | x | x | | x | x | | x | | | | 900°-950° |

XRF

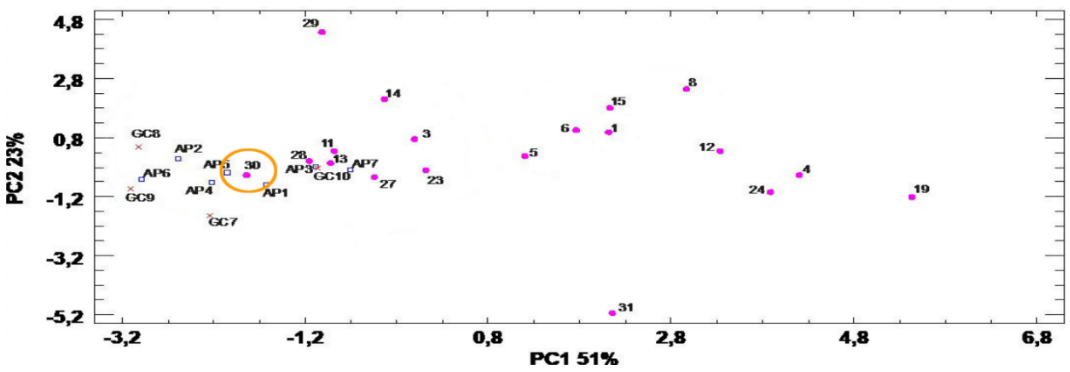

Sample: **TSS- 31** Site: Underwater, area B, US2 layer, TSS4

| Fragment | Type | Fresh-cut surface |
|---|---|---|

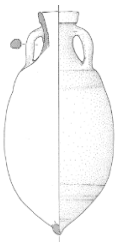


Ovoidal Adriatic type, 6mm thickness, gray and beige color, fine low porosity texture.

Thin section (x5, XPL)

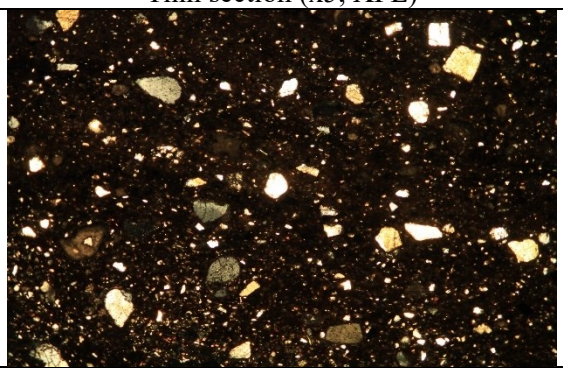

Microscopic characteristics

| | | | |
|---|---|---|---|
| Color | Brownish | Clay pellets | N/A |
| Inclusion abundance | 10 – 15 % | Carbonate mudstone | Present |
| Matrix | Ca | Flints | Present |
| Inclusion size | Small medium | Other minerals | Quartz – Muscovite – Biotite – Pyroxene |
| Fossils trace | Present | | |

XRPD

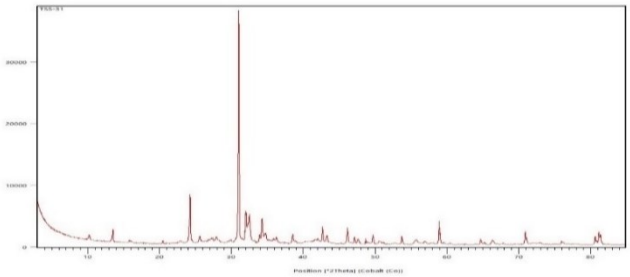

| Qz | Mus/Ill | Bt | Kfs | Pl | Hem | Px | Py | Gp | Mg-Cal | Cal | Arg | Geh | Zeo | Hyn | Sil | T°C |
|---|---|---|---|---|---|---|---|---|---|---|---|---|---|---|---|---|
| x | x | | x | x | | x | x | x | x | x | | | | | | 850°-900° |

XRF